Spectrum Sensing in Cognitive Radio Networks

by

Simin Bokharaiee

A Thesis submitted
to the Faculty of Graduate Studies of
The University of Manitoba
in partial fulfillment of the requirements of the degree of

Doctor of Philosophy

Department of Electrical and Computer Enginereeing
University of Manitoba
Winnipeg

Abstract

Given the ever-growing demand for radio spectrum, cognitive radio has recently emerged as an attractive wireless communication technology. To put cognitive radio technology into practice, the cognitive radios need to monitor the spectrum activities continuously to detect a suitable spectrum band for possible utilization. This dissertation is concerned with developing spectrum sensing algorithms in cognitive radio networks where a single or multiple cognitive radios assist in detecting licensed primary bands employed by single or multiple primary users.

First, given that orthogonal frequency-division multiplexing (OFDM) is an important wideband transmission technique, detection of OFDM signals in low-signal-to-noise-ratio scenario is studied. It is shown that the cyclic prefix correlation coefficient (CPCC)-based spectrum sensing algorithm, which was previously introduced as a simple and computationally efficient spectrum-sensing method for OFDM signals, is a special case of the constrained generalized likelihood ratio test (GLRT) in the absence of multipath. In addition to CPCC-based algorithm, a simple and low-complexity algorithm called the multipath-based constrained-GLRT (MP-based C-GLRT) algorithm is obtained by employing the inherent structure of OFDM signals and exploiting multipath correlation in the GLRT algorithm. Further performance improvement is achieved by combining both algorithms. A simple detection algorithm is also developed for unsynchronized OFDM signals, whose performance is only slightly degraded when compared with synchronized detection in a rich multipath environment.

In the second part of the dissertation, a cognitive radio network model with multiple CRs is considered in order to investigate the benefit of collaboration and diversity in improving the overall sensing performance. Specifically, the problem of decision fusion for cooperative spectrum sensing is studied when fading channels are present between the CRs and the fusion center (FC). The CRs perform spectrum sensing using inexpensive energy detectors and transmit their binary decisions to the FC for a final decision on the absence or presence of the primary user activity. Considering the limited resources in CR networks, which makes

it difficult to acquire the instantaneous channel-state information, noncoherent transmission schemes with on-off keying (OOK) and binary frequency-shift keying (BFSK) are employed to transmit the binary decisions to the FC. For each of the transmission schemes considered, energy- and decoding-based fusion rules are developed first. Then, the detection threshold at the CR nodes and at the FC, the combining weights (in the case of the energy-based fusion rule), and the sensing time are optimized to maximize the achievable secondary throughput of the CR network.

Finally, in order to reduce the required transmission bandwidth in the reporting phase of the CRs in a cooperative sensing scheme, the last part of the dissertation examines nonorthogonal transmission of local decisions by means of on-off keying. Proposed and analyzed is a novel decoding-based fusion rule that essentially performs in three steps: (1) estimating minimum mean-square error of the transmitted information from cognitive radios, (2) making hard decisions of the transmitted bits based on the estimated information, and (3) combining the hard decisions in a linear manner. Simulation results support the theoretical analysis and show that the added complexity of the decoding-based fusion rule leads to a considerable performance gain over the simpler energy-based fusion rule when the reporting links are reasonably strong.

Acknowledgments

It is a pleasure to take this opportunity to convey thanks to those who made this thesis possible with their kindness and support.

I would like to express my deepest appreciation and thanks to my advisor, Dr. Ha H. Nguyen for encouraging my research and for guiding me all the way through my Ph.D studies. Without him, this thesis would not have been completed. I also owe my sincere gratitude to my former co-advisor, Dr. Ed Shwedyk for his continued support of my research and thesis. Their knowledge, enthusiasm, assistance and guidance helped me all the time during my research and writing of this thesis.

I would also like to express my gratitude to the rest of my advisory committee, Dr. Miroslaw Pawlak, Dr. Zahra Moussavi and Dr. Hassan Soliman for reviewing this thesis and their insightful comments and suggestions throughout my research. I would also like to thank Dr. Xavier Fernando for accepting to serve as my external examiner and for reading and evaluating this thesis. My special thanks go to Amy Dario, Graduate Advisor of the Department of Electrical and Computer Engineering, for helping and supporting me at all critical moments.

I am grateful to the financial support of Natural Sciences and Engineering Research Council of Canada (NSERC), University of Manitoba International Graduate Students Scholarships, travel awards and University of Saskatchewan research grants and facilities.

My deepest love and thanks to my mother and father for supporting my studies with enthusiasm and encouragement. I would also like to thank my research group members for sharing their knowledge and invaluable assistance. You all made my defense an enjoyable moment.

Table of Contents

List of Abbreviations

AGM Arithmetic-to-geometric mean

AWGN Additive white gaussian noise

BAC Binary asymmetric channel

BFSK Binary frequency shift keying

BSC Binary symmetric channel

C-GLRT Constrained GLRT

CAV Covariance-based absolute value

CDMA Code-division multiple access

CFO Carrier frequency offset

CPCC Cyclic-prefix correlation coefficient

CPE Consumer premise equipment

CR Cognitive radio

DTV Digital TV

FC Fusion center

FCC Federal communications commission

FFT Fast Fourier transform

GLRT Generalized likelihood ratio test

I-Syn Imperfectly synchronized

ISI Inter-symbol interference

LLRT Log likelihood ratio test

LRT Likelihood ratio test

MLE Maximum likelihood estimation

MMSE Minimum mean-square error

OFDM Orthogonal frequency division multiplexing

OOK On-off keying

P-Syn Perfectly synchronized

PSD Power spectral density

QOS Quality of service

SNR Signal–to–noise ratio

SV Signature vector

TSC Total squared correlation

U-GLRT Unconstrained GLRT

UHF Ultra-high frequency

Unsyn Unsynchronized

WBE Welch-bound equality

WRAN Wireless regional area network

List of Tables

List of Figures

1. Introduction

1.1 Motivation

With the recent rapid growth in wireless communications systems and applications, the traditional use of radio frequency via spectrum allocation to the license holders causes spectrum scarcity. The restricted use of spectrum bands has lead to the overcrowding of the allocated spectrum bands with the increase in the variety of wireless services including voice, multimedia, web, short message, etc. This overcrowding has consequently resulted in low quality of service (QOS) for wireless applications [1].

On the other hand, measurements have verified that many frequency bands, such as television bands, amateur radio, and paging, are often under-utilized with large spectral holes. Therefore, cognitive radio systems have recently been proposed by the Federal Communications Commission (FCC) as a viable solution to overcome the problem of spectrum scarcity. The idea of cognitive radio is to opportunistically detect and use a vacant licensed band for transmission when it is not in use at a particular place or time, without causing any significant interference to the transmissions of the licensed user. In fact, FCC has developed policies for unlicensed wireless devices to opportunistically use the vacant frequency bands [2].

An example of cognitive radio (CR) technology is illustrated in Figure 1.1, in which a major source of primary transmission coexists with a cognitive radio network. A base station (BS) coordinates the cognitive radio users. Within the keep-out radius of the primary transmitter, the CRs are forced not to use the primary channel to keep the signal-to-interference ratio of the primary users above the acceptable limit [3].

In order to take advantage of CR technology, the cognitive radios need to monitor the primary user activities continuously to find a suitable spectrum band for possible utilization. To this end, the secondary users may access the same occupied channel simultaneously with the primary user (spectrum underlay) wherein the transmitted power of secondary users is constrained so that it does not exceed the noise floor of the primary user. In another scheme, which is more popular, the secondary users access only the spectrum white spaces in an noninstructive way (*s*pectrum overlay). In the latter scheme, which is also referred to as *opportunistic access*, the CRs are allowed to communicate over the unoccupied spectrum holes to avoid any possible interference to the primary users [4]. Since the primary users have the priority of service, at any moment when a primary user becomes active in the spectrum occupied by a cognitive user, the collision should be detected and the communication channels should be relocated.

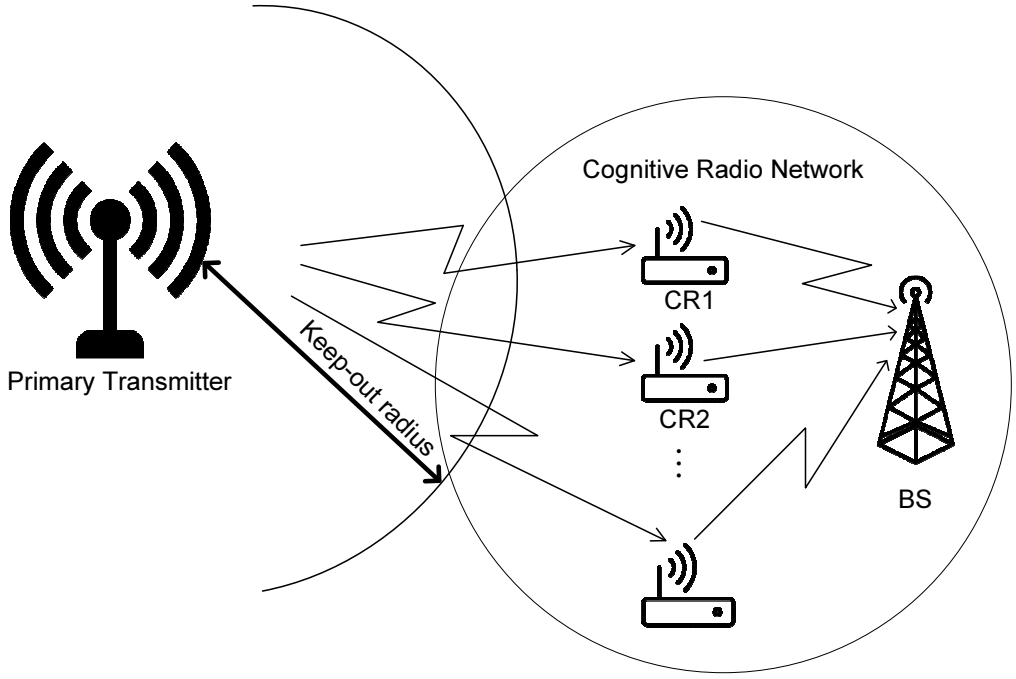

Figure 1.1 Example of a cognitive radio network.

From the above discussion, the ability of CRs to detect unoccupied spectrum holes is very crucial in the operation of a cognitive radio network. Such an ability depends on the *spectrum sensing* algorithm employed at the CRs. This research project is devoted to the

problem of spectrum sensing in cognitive radio networks, especially those with spectrum overlay access.

1.2 Overview of Spectrum Sensing

Spectrum sensing is a binary hypothesis testing problem. Let $\mathcal{H}_0$ and $\mathcal{H}_1$ denote the idle and active states of the primary user, respectively. In order to classify the observations into $\mathcal{H}_0$ or $\mathcal{H}_1$, a test statistics $\mathcal{T}$ is formed based on the received signal and a general test decision is as follows:

$$\begin{cases} \text{Decide} \quad \mathcal{H}_0, & \text{if } \mathcal{T} \leq \epsilon \\ \text{Decide} \quad \mathcal{H}_1, & \text{if } \mathcal{T} > \epsilon \end{cases} \tag{1.1}$$

where ϵ is a specified threshold value. Two probabilities of interest are: (i) the probability of detection, P_d, which is the probability that the primary user is correctly detected in its active mode, and (ii) the probability of false alarm, P_f, which is the probability that the primary user is detected (falsely) when it is in the idle state. Mathematically,

$$P_f = \Pr\left\{\mathcal{T} > \epsilon | \mathcal{H}_0\right\}, \tag{1.2}$$

and

$$P_d = \Pr\left\{\mathcal{T} > \epsilon | \mathcal{H}_1\right\}. \tag{1.3}$$

The probability that an active primary user is not identified by the CR user is called a missed detection probability and is given by $P_m = \Pr\left\{\mathcal{T} < \epsilon | \mathcal{H}_1\right\} = 1 - P_d$, which is the probability that the active primary user is not identified by the CR user. Keeping P_f below a certain value enables the CR user to efficiently utilize the available spectrum in order to maximize the achievable CR network throughput [5]. On the other hand, minimizing P_m ensures that the primary user is sufficiently protected, i.e., the amount of interference introduced to the primary users is maintained at a reasonable level.

The efficiency of the employed spectrum-sensing algorithm determines the amount of interference introduced into the primary users and the achievable CR network throughput.

Therefore, in order to design a spectrum sensing algorithm, the decision statistics as well as sensing parameters should be obtained to meet the requirements on the probability of detection and the probability of false alarm, as well as the achievable secondary throughput [5–7]. These requirements need a careful design of the time frame structure as an important sensing parameter. This is elaborated in the next section.

1.2.1 Time Frame Structure and Achievable Throughput

An important parameter in spectrum sensing is the sensing time interval. For cognitive radio applications, a frame structure is designed for periodic spectrum sensing and the secondary data transmissions. Figure 1.2 shows the time frame structure considered for periodic spectrum sensing. There are two main phases in each frame: a sensing phase (duration of τ), and a data transmission phase (duration of $T - \tau$). In Figure 1.2, the sensing time interval is specifically denoted by τ_s. Also a reporting delay, denoted by τ_r, is considered for the applications when the sensing results are reported to a central station. Commonly the sensing and reporting delay are summed up and denoted as one general sensing interval τ. Generally, the longer the sensing duration is, the more accurate the outcome of the spectrum-sensing algorithm becomes and, therefore, the lower the potential of interference to the primary users is. Using the given time frame structure, the achievable secondary throughput R_0, under the hypothesis $\mathcal{H}_0$ when the primary channel is vacant is defined as [5]

$$R_0 = C_0 \Pr(\mathcal{H}_0) \left(1 - \frac{\tau}{T}\right) [1 - P_f] , \tag{1.4}$$

where C_0 represents the throughput of the secondary network in the absence of the primary user. Theoretically, an increase in the sensing time results in a higher detection probability and lower false alarm probability, which in return leads to an improved utilization of the available unused spectrum [8, 9]. However, given a target probability of detection, the increase of the sensing time also results in a decrease of the data transmission time, hence the achievable throughput [5]. Therefore, an inherent tradeoff exists between the amount of interference introduced to the primary user and the achievable throughput of the cognitive radio network in terms of the length of the sensing duration of the frame structure [4,6,10–12].

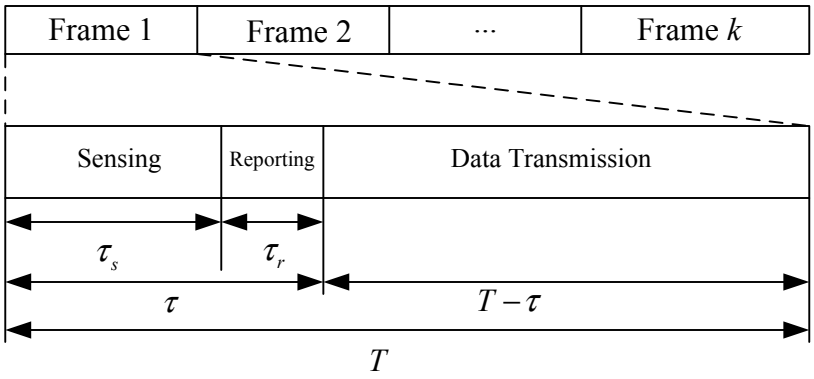

Figure 1.2 Time frame structure in a cognitive radio network.

In the next section, the most well-known spectrum sensing techniques that can be employed for an efficient spectrum detection are introduced.

1.2.2 Spectrum Sensing Techniques

The spectrum sensing techniques that have been proposed so far mainly include the energy detection [13], the likelihood ratio test (LRT) [8], and various feature detection algorithms [14–17]. Once the decision statistics are known, different sensing parameters such as the combining weights in a cooperative energy detection [18,19], decision threshold and sensing time [5,20] can be determined by optimizing various objective functions. Because energy detection is a simple and efficient algorithm and its performance can be analytically evaluated [18, 21], many recent works have developed algorithms to optimize sensing parameters for energy detection [5, 18–20, 22].

In [18], a joint sensing optimization problem for a multiband cognitive radio network is proposed to find the combining weights as well as the decision thresholds for each subband. Three objective functions were introduced with constraints on P_m and P_f: the opportunistic secondary throughput as a function of P_f, the aggregate interference to the primary user as a function of P_m and the modified deflection coefficient [18, 19]. Optimal and suboptimal solutions have been obtained for these objective functions. In [5], a single carrier cognitive radio system in additive white Gaussian noise (AWGN) channel is considered where the goal is to find the optimal sensing time via maximizing the achievable throughput for the sec-

ondary network. The approach is then extended to multi-slot cooperative spectrum sensing where proper weights are assigned to each time slot to maximize the achievable secondary throughput. In [20], the sensing time and power allocation are optimized for a multiband cognitive radio network.

It has to be noted that the optimization problems carried out in [5, 18–20, 22] requires some form of a priori knowledge of the received signal, including the exact noise power or/and the primary signal covariance matrix, channel state information, etc. However, in a cognitive radio network, perfect knowledge of fading channel or noise variance may not be available at the cognitive radio receiver. Therefore, there is a need to develop efficient wideband spectrum sensing algorithms which are robust to these uncertainties. In fact, a comprehensive work has been carried out to develop and evaluate new and efficient test statistics for specific types of cognitive radio systems (e.g. [13,15–17,23]), where a number of uncertainties has also been involved in developing the system model as well as the decision statistics. A few works have also been carried out to compare different spectrum sensing approaches (e.g. [1]). In the following, a review of the main detection methods for cognitive radio is presented and their requirements, advantages and disadvantages are discussed.

Energy Detection

Energy detection, by far, has been the most well known spectrum sensing method due to its low complexity and the fact that the structure of the primary signal is not required to be known. For the discussion in this section, the following signal model is adopted:

$$\mathbf{x}_n = \begin{cases} \mathbf{v}_n, & \mathcal{H}_0 \\ \widetilde{\mathbf{s}}_n + \mathbf{v}_n, & \mathcal{H}_1, \end{cases} \tag{1.5}$$

where $\widetilde{\mathbf{s}}_n$ is the received signal vector, which is distorted by the fading channel and $\mathbf{v}_n$ is the receiver noise vector at the time instance n. We also assume a Gaussian model for both the received signal and noise. If the length of the signal vector is denoted by L, over N time

samples, the energy detection rule will be:

$$\sum_{n=1}^{N} |\mathbf{x}_n|^2 \underset{\mathcal{H}_0}{\overset{\mathcal{H}_1}{\gtrless}} \epsilon. \tag{1.6}$$

The above rule applies equal weight combining over the signal vector components. Because different components of the signal undergo different fading channels, a more general detection rule considers weighted energy. That is [18]

$$\kappa = \sum_{k=0}^{L-1} g_k \kappa_k \underset{\mathcal{H}_0}{\overset{\mathcal{H}_1}{\gtrless}} \epsilon, \tag{1.7}$$

where κ_k is the energy over the kth component of the signal vector:

$$\kappa_k = \sum_{n=1}^{N} |x_n(k)|^2. \tag{1.8}$$

Figure 1.3 shows the block diagram of the weighted energy detection-based spectrum sensing. To find the weights, a set of objective functions involving the opportunistic secondary throughput as a function of P_f and the aggregate interference to the primary user as a function of P_m with a set of constraints are considered in [18]. Due to the high complexity and non-convex optimization problems that arise, a simpler solution based on a modified deflection coefficient [18, 19] has also been introduced. The modified deflection coefficient is defined as

$$d^2(\mathbf{g}) = \frac{\left(\mathrm{E}(\kappa|\mathcal{H}_1) - \mathrm{E}(\kappa|\mathcal{H}_0)\right)^2}{\mathrm{Var}(\kappa|\mathcal{H}_0)}, \tag{1.9}$$

where $\mathbf{g} = [g_1, g_2, \ldots, g_L]^\top$. It is observed that this measurement only depends on the first and second moments of the test statistics, therefore it is not required to find the distribution of the test statistics. The weight coefficients are chosen in order to achieve the maximum modified deflection coefficient for each subband under the given constraints.

For an energy detector, if there is no uncertainty on the noise variance, the performance is very good. However, in the presence of typical noise variance uncertainties around 0.5 dB [1], the performance of energy detection significantly degrades [13]. Therefore energy detection is considered a non-robust detector.

[1] The measurement is with respect to the actual noise variance.

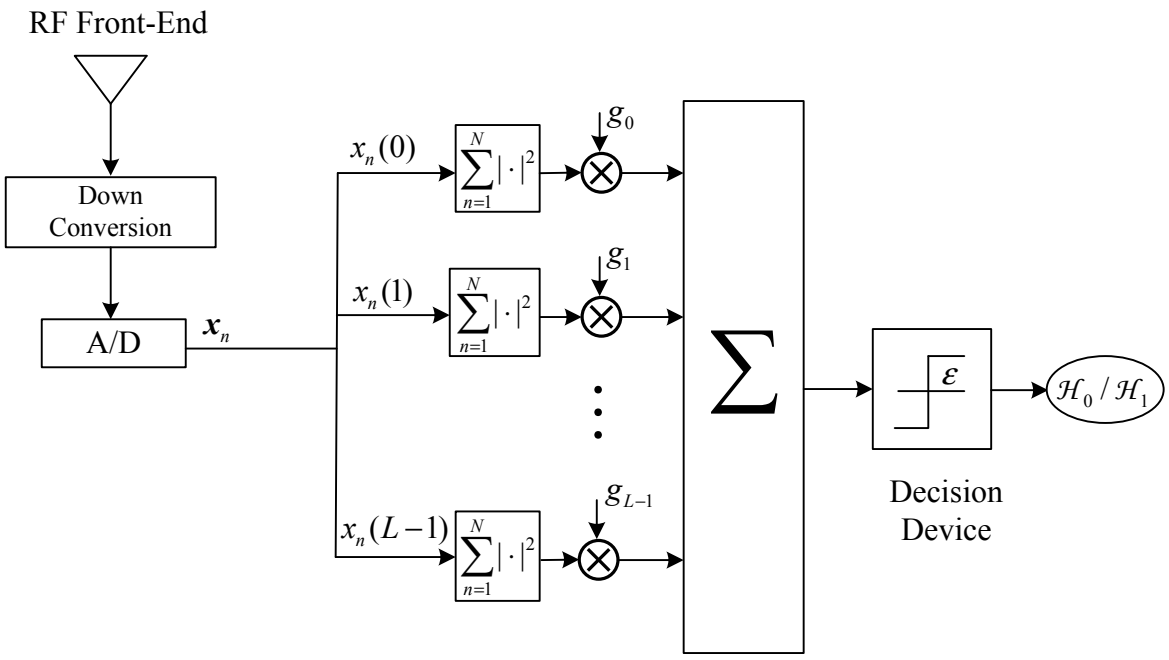

Figure 1.3 Multiband spectrum sensing scheme.

Likelihood Ratio Test

The Neyman-Pearson (NP) criterion [24] provides a powerful tool to find the optimal decision statistics for a binary hypothesis testing problem. The NP criterion maximizes the probability of detection for a given probability of false alarm. Using the NP criterion results in the following likelihood ratio test (LRT) [24]:

$$\mathcal{L}(\mathbf{x}_n) = \frac{f_{\mathbf{x}_n|\mathcal{H}_1}(\mathbf{x}_n|\mathcal{H}_1)}{f_{\mathbf{x}_n|\mathcal{H}_0}(\mathbf{x}_n|\mathcal{H}_0)} \underset{\mathcal{H}_0}{\overset{\mathcal{H}_1}{\gtrless}} \eta, \tag{1.10}$$

where η is the sensing threshold which is obtained based on the pre-selected probability of false alarm. For a sensing period equivalent to N time samples, one has

$$\mathcal{L}(\mathbf{x}) = \frac{f_{\mathbf{x}|\mathcal{H}_1}(\mathbf{x}|\mathcal{H}_1)}{f_{\mathbf{x}|\mathcal{H}_0}(\mathbf{x}|\mathcal{H}_0)}, \tag{1.11}$$

where $\mathbf{x} = [\mathbf{x}_1, \ldots, \mathbf{x}_N]$ denotes a block of N time samples. Because the noise is a white Gaussian random process, the distribution of $\mathbf{x}$ under $\mathcal{H}_0$ is

$$f_{\mathbf{x}|\mathcal{H}_0}(\mathbf{x}|\mathcal{H}_0) = \prod_{n=1}^{N} \frac{1}{(2\pi\sigma_v^2)^{L/2}} \exp\left[-\frac{1}{2\sigma_v^2}\|\mathbf{x}_n\|^2\right], \tag{1.12}$$

On the other hand, the distribution of $\mathbf{x}$ under $\mathcal{H}_1$ is

$$f_{\mathbf{x}|\mathcal{H}_1}(\mathbf{x}|\mathcal{H}_1) = \prod_{n=1}^{N} \frac{1}{(2\pi)^{L/2}\det^{1/2}(\mathbf{R}_{\mathbf{x}})} \exp\left[-\mathbf{x}_n^H \mathbf{R}_{\mathbf{x}}^{-1} \mathbf{x}_n\right], \tag{1.13}$$

where $\mathbf{R}_{\mathbf{x}} = E\left\{\mathbf{x}_n \mathbf{x}_n^H\right\}$.

When the primary signal components are independent and identically distributed (i.i.d), $\mathbf{R}_{\mathbf{x}}$ under $\mathcal{H}_1$ is a scaled identity matrix. It follows that the LRT reduces to an energy detection algorithm. Thus for i.i.d primary signals, energy detection is the optimal spectrum sensing method according to the NP criterion. However, if the received signal components are not i.i.d, the energy detection performance degrades. This is the reason why in a cooperative sensing scheme in which the received signals from multiple sources are not i.i.d, many approaches were proposed to find the optimal weights for cooperative energy detection (e.g. [5, 20, 22]).

Observing the signal model given in (1.5), it is obvious that for an AWGN channel, the received signals become i.i.d and the energy detector will be the optimal detector. However, if the multipath channel remains static over the short period of the spectrum sensing, the received signal is correlated due to multipath effect and the energy detection is not optimal. In particular, using the result in [25], the LRT decision statistics for the given binary hypothesis test in (1.5) is obtained as

$$\mathcal{T}_{\mathrm{LRT}}(\mathbf{x}) = \sum_{n=1}^{N} \mathbf{x}_n^H \left[\mathbf{R}_{\widetilde{\mathbf{s}}}(\mathbf{R}_{\widetilde{\mathbf{s}}} + \sigma_v^2 \mathbf{I})^{-1}\right] \mathbf{x}_n, \tag{1.14}$$

where $\mathbf{R}_{\widetilde{\mathbf{s}}} = E\left\{\widetilde{\mathbf{s}}_n \widetilde{\mathbf{s}}_n^H\right\}$.

It can be seen from (1.14) that the weighting coefficients of LRT requires the a priori knowledge of noise power and primary signal covariance matrix. In an actual cognitive radio scenario, such information might not be available at cognitive radios. Therefore, it is of great importance to develop spectrum sensing algorithms which do not require the precise knowledge of channel taps and noise variance. Such algorithms are expected to be able to extract and use some specific features of the received primary signal. In fact, a large number of techniques has been proposed and evaluated, among them are the statistical covariance

algorithm [17], eigenvalue-based algorithm (e.g. [15] and [16]) and cyclostationary algorithm (e.g. [26]). These algorithms are briefly introduced in the context of wideband spectrum sensing in the next section.

1.3 Wideband Spectrum Sensing

Wideband spectrum sensing algorithms involve detecting the presence or absence of licensed signals in low SNR environments. As such, it is necessary to develop algorithms which are practical and reliable in low SNR scenarios and robust to other uncertainties. On the other hand, orthogonal frequency division multiplexing (OFDM) is a multi-carrier modulation technique that has been recognized as a potential transmission technology for CR systems due to its numerous advantages for high bit-rate communications as well as its capability to dynamically allocate unused spectrum among CR users. As a suitable wideband modulation technique, OFDM can overcome the time dispersion of the channel which causes inter-symbol interference (ISI). Other advantages of OFDM include high spectral efficiency, robustness against narrow band interference (NBI), scalability, and easy implementation using the fast Fourier transform (FFT). The flexibility of OFDM provides opportunities to use advanced techniques, such as adaptive loading, transmit and receive diversity, to improve transmission efficiency [1, 27, 28]. After presenting the OFDM signal model in this section, a review of the main detection methods for cognitive radio is presented and their requirements, advantages and disadvantages are discussed.

1.3.1 Cognitive Radio Network with OFDM

The OFDM frame structure considered in this work is the same as that in [29] and [26] and it is shown in Figure 1.4. It is assumed that both the CR and primary OFDM systems employ L subcarriers and can be perfectly synchronized through pilot signals. Let $\{S_{n,k}\}_{k=0}^{L-1}$, with $E\{|S_{n,k}|^2\} = \sigma_S^2$, be the complex symbols to be transmitted in the nth OFDM block. Then the baseband OFDM modulated signal can be expressed as

$$s_n(m) = \frac{1}{\sqrt{L}} \sum_{k=0}^{L-1} S_{n,k} \mathrm{e}^{\frac{j2\pi mk}{L}};\ m = 0, \ldots, L-1. \tag{1.15}$$

For a large number of subcarriers L (i.e., the size of DFT/IDFT), $s_n(m)$ can be approximately modeled as a zero-mean circularly symmetric complex Gaussian random variable of variance σ_S^2, i.e., $s_n(m) \sim \mathcal{CN}(0, \sigma_S^2)$.

Represent the length-$(L + L_p)$ vector of the nth transmitted OFDM block as

$$\mathbf{s}_n^+ = [s_n(L-1),\ s_n(L-2), \ldots, s_n(0),\ \underbrace{s_n(L-1), \ldots, s_n(L-L_p)}_{\text{Cyclic Prefix}}]^\top, \tag{1.16}$$

where L_p denotes the number of samples in the guard interval, i.e., the length of the cyclic prefix (CP). The corresponding received signal and noise vectors are denoted by

$$\mathbf{x}_n = [x_n(L-1),\ x_n(L-2), \ldots, x_n(0),\ x_n(-1), \ldots, x_n(-L_p)]^\top, \tag{1.17}$$

$$\mathbf{v}_n = [v_n(L-1),\ v_n(L-2), \ldots, v_n(0),\ v_n(-1), \ldots, v_n(-L_p)]^\top, \tag{1.18}$$

where the noise samples $v_n(l)$'s are i.i.d. $\mathcal{CN}(0, \sigma_v^2)$ random variables.

The primary user signal is received through a wireless multipath fading channel whose discrete-time baseband model is represented by channel filter taps h_i, $i = 1, \ldots, L_c$, where L_c denotes the number of multipath components. If the multipath channel taps are unknown constants, this implies that the received OFDM signal samples are correlated during the period of spectrum sensing. As such, spectrum sensing methods that employ correlation features of the signals, such as the multipath-induced correlation and the cyclic-based correlation can be implemented in a cognitive radio network for an efficient detection of the primary OFDM signals. A review of such methods is presented next.

1.3.2 Robust Spectrum Sensing Algorithms for OFDM Signal

Robust spectrum sensing algorithms do not need to know the noise variance and primary signal covariance matrix. They exploit the primary signal's features or some side information [30] to identify signal from noise, hence, they are very practical in cognitive radio networks. Previously proposed robust detection algorithms that can be applied to OFDM-based cognitive radio systems can be mainly divided into three groups, namely the cyclostationary-based detection, covariance-based algorithms and the generalized likelihood ratio test (GLRT).

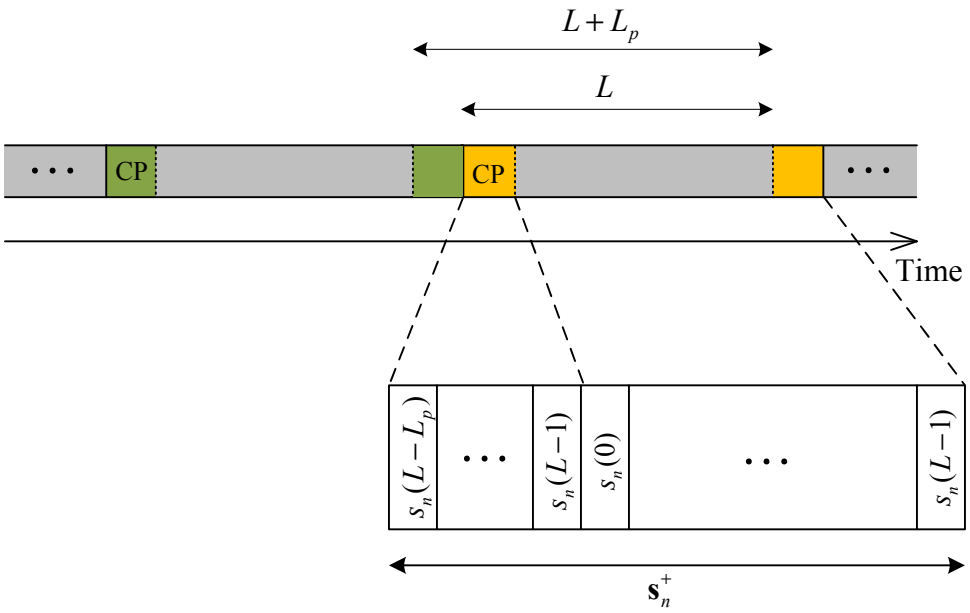

Figure 1.4 OFDM frame structure.

Cyclostationary-Based Detection

Due to the presence of a cyclic prefix (CP), an OFDM signal has a nonzero autocorrelation coefficient at multiple delays of L OFDM samples. This property of the OFDM signal can be exploited in the time domain to design an autocorrelation based detector. This approach is very useful in a single user OFDM based system under an AWGN channel. For the multipath channel, as it is shown in [31], there is a degradation in the expected performance of the detector depending on the number of multipath channel taps.

For an AWGN channel, the binary hypothesis testing problem can be expressed as

$$x_n(k) = \begin{cases} v_n(k), & \mathcal{H}_0 \\ h_1 s_n(k) + v_n(k), & \mathcal{H}_1 \end{cases}$$
$$k = -L_p, \ldots, L-1; \quad n = 1, \ldots, N \tag{1.19}$$

where $v_n(k)$ is the kth received noise sample of the nth OFDM symbol and $s_n(k)$ is the kth sample of nth OFDM symbol. Let $\rho = \frac{\mathrm{E}(x_n(k)x_n^*(k\pm L))}{\mathrm{E}(x_n(k)x_n^*(k))}$ be the autocorrelation coefficient for

lags of $\pm L$ samples. Under the two hypotheses one has:

$$\begin{aligned} \rho = 0 &: (\text{given } \mathcal{H}_0), \\ \rho = \alpha &: (\text{given } \mathcal{H}_1). \end{aligned} \tag{1.20}$$

If the CP length is not known, it is shown in [26] that:

$$\alpha = \frac{L_p}{L_p + L} \frac{\mathrm{E}(|h_1|^2)\sigma_s^2}{\mathrm{E}(|h_1|^2)\sigma_s^2 + \sigma_v^2} = \frac{L_p}{L_p + L} \frac{\mathrm{SNR}}{1 + \mathrm{SNR}}. \tag{1.21}$$

However, if the CP length is known a priori, then the expectation is only taken over the L_p samples in the head and tail of the OFDM signal and therefore $\alpha = \frac{\mathrm{SNR}}{1+\mathrm{SNR}}$ [26]. Let $\widehat{\rho}$ be an estimate of the autocorrelation coefficient ρ from the finite received samples, given as,

$$\widehat{\rho} = \frac{\sum_{n=1}^{N} \sum_{k=L}^{L+L_p-1} 2\mathrm{Re}(x_n(k)^* x_n(k-L))}{\sum_{n=1}^{N} \sum_{k=L}^{L+L_p-1} (|x_n(k)|^2 + |x_n(k-L)|^2)}. \tag{1.22}$$

Then the decision rule is as follows [26], [31]:

$$\widehat{\rho} \underset{\mathcal{H}_0}{\overset{\mathcal{H}_1}{\gtrless}} \epsilon, \tag{1.23}$$

In [26], it is shown that the sample autocorrelation test given in (1.23) is approximately the log likelihood ratio test (LLRT) statistic for an AWGN channel when the SNR is low.

Covariance-Based Detection

Under $\mathcal{H}_0$, the received signal covariance matrix is a scaled identity matrix which represents the noise covariance matrix. If the primary signal is not an i.i.d random process, the received signal covariance matrix under $\mathcal{H}_1$ is no longer a scaled identity matrix. Hence, many researchers have developed spectrum sensing algorithms based on the statistics of the received signal covariance matrix which is different from that of the noise. After receiving the signal samples, the test statistic is derived from the received signal sample covariance matrix. In what follows, different covariance-based spectrum sensing algorithms with their application to OFDM-based cognitive radios are outlined.

Spectrum Sensing based on the Minimum and Maximum Eigenvalues of the Sample Covariance Matrix

For the binary hypothesis testing problem given in (1.5), denote the sample covariance matrix by $\bar{\mathbf{R}}_{\mathbf{x}} = \frac{1}{N}\sum_{n=1}^{N} \mathbf{x}_n \mathbf{x}_n^H$. Under $\mathcal{H}_0$, the normalized sample covariance matrix $\bar{\mathbf{R}}'_{\mathbf{x}} = \frac{N}{\sigma_v^2}\bar{\mathbf{R}}_{\mathbf{x}}$ is a complex white Wishart matrix. Its eigenvalues fall within a *finite* support called the Marchenko-Pastur support. Whereas under $\mathcal{H}_1$ the largest eigenvalue increases outside the Marchenko-Pastur support [16]. Therefore it is suggested in [16] to employ

$$\frac{l_{\max}}{l_{\min}} = \frac{\lambda_{\max}}{\lambda_{\min}} \tag{1.24}$$

as the decision test, where $l_{\max}$ and $l_{\min}$ denote the largest and smallest eigenvalues of $\bar{\mathbf{R}}'_{\mathbf{x}}$ and $\lambda_{\max}$ and $\lambda_{\min}$ denote the largest and smallest eigenvalues of $\bar{\mathbf{R}}_{\mathbf{x}}$. It is shown in [16] that under $\mathcal{H}_0$, $l_{\max}$ and $l_{\min}$ converge as follows:

$$\begin{aligned} l_{\max} &\overset{\text{a.s.}}{\to} b = (N^{\frac{1}{2}} + L^{\frac{1}{2}})^{\frac{1}{2}} \\ l_{\min} &\overset{\text{a.s.}}{\to} a = (N^{\frac{1}{2}} - L^{\frac{1}{2}})^{\frac{1}{2}} \end{aligned} \tag{1.25}$$

in the limit

$$N, L \to \infty \ \text{ with } \frac{L}{N} \to \bar{c} \tag{1.26}$$

where $\bar{c} \in (0, 1)$ is a constant. Under $\mathcal{H}_1$, it is known that $\bar{\mathbf{R}}'_{\mathbf{x}}$ belongs to the class of *spiked population models* and its largest eigenvalue converges almost surely to a value $b' > b$. The authors of [16] have found a quite accurate expression for the limiting eigenvalue ratio distribution under $\mathcal{H}_0$ using the properties of the Wishart matrices. The result is then employed to calculate the decision sensing threshold as a function of a target probability of false alarm.

Spectrum Sensing based on the Covariance Absolute Values (CAV)

Using the fact that the off diagonal elements of $\mathbf{R}_{\mathbf{x}}$ are nonzero in the presence of the primary signal, the covariance-based absolute value (CAV) detection algorithm is proposed in [15]. Let $\bar{r}_{kj}$, $k, j = 1, \ldots, L$, denote the elements of the sample covariance matrix $\bar{\mathbf{R}}_{\mathbf{x}}$ for

the duration of spectrum sensing. The CAV algorithm is proposed for real-valued $\bar{r}_{kj}$'s and computes two decision values, T_1 and T_2, as

$$T_1 = \sum_{k=1}^{L} \sum_{j=1}^{L} |\bar{r}_{k,j}|, \tag{1.27}$$

$$T_2 = \sum_{k=1}^{L} |\bar{r}_{k,k}|. \tag{1.28}$$

For the general case of complex $\bar{r}_{kj}$'s, the above decision values are extended to

$$T_1 = \sum_{k=1}^{L} \sum_{j=1}^{L} \left(|\mathrm{Re}(\bar{r}_{k,j})| + |\mathrm{Im}(\bar{r}_{k,j})| \right), \tag{1.29}$$

$$T_2 = \sum_{k=1}^{L} \left(|\mathrm{Re}(\bar{r}_{k,k})| + |\mathrm{Im}(\bar{r}_{k,k})| \right), \tag{1.30}$$

where $\mathrm{Re}(x)$ and $\mathrm{Im}(x)$ denote the real and imaginary components of x. The presence of the signal is determined based on T_1 and T_2, and a threshold ϵ. The detection algorithm decides $\mathcal{H}_1$, if $\frac{T_1}{T_2} > \epsilon$ [17]. Since the probability of false alarm is a function of the sensing threshold and does not depend on the primary signal information, the sensing threshhold can be obtained given a target probability of false alarm. In [17], for the CAV algorithm, the probabilities of false alarm and detection are also obtained in closed-form expressions using the central limit theorem and some approximations. However, theoretical curves are not very much in agreement with simulation results.

Because the CAV algorithm does not depend on the knowledge of noise variance, it shows a reliable performance in the presence of noise uncertainty compared to the energy detection. Simulation results verify this fact in [17].

Generalized Likelihood Ratio Test

If any of the two hypotheses describing a binary hypothesis testing problem involves some unknown parameters, the hypothesis is called a composite hypothesis [24]. For a composite hypothesis, one approach is to perform the maximum likelihood estimation (MLE) of the unknown parameters. The estimated parameters are then used in the likelihood ratio test as if they are correct values. The result is then called the *generalized likelihood*

ratio test (GLRT) [24]. This approach enables the cognitive radio receiver to incorporate the uncertainties in calculating the test statistics. Spectrum sensing based on GLRT was presented in [25] for single antenna CR user and in [32,33] for multi-antenna CR receiver. The decision tests have been obtained under different number of unknown parameters, e.g., noise variance and/or signal covariance matrix. For the general case when both noise variance and signal covariance matrix are unknown, exploiting the GLRT algorithm gives the arithmetic-to-geometric mean (AGM) method. Denote the eigenvalues of the sample covariance matrix, $\bar{\mathbf{R}}_{\mathbf{x}}$, by λ_i, $i = 1, \ldots, L$. The AGM test statistic is given as

$$\mathcal{T}_{\mathrm{AGM}}(\boldsymbol{\lambda}) = \frac{\frac{1}{L}\sum_{i=1}^{L}\lambda_i}{\prod_{i=1}^{L}\lambda_i^{\frac{1}{L}}}, \tag{1.31}$$

where $\boldsymbol{\lambda} = (\lambda_1, \ldots, \lambda_L)$. If some information such as noise variance or the rank of signal covariance matrix is available, this additional information can be incorporated into the test statistics to give a modified test statistics as a function of the eigenvalues [25].

The key advantage of the GLRT approach is that by concentrating on a certain portion of the observation, one can exploit structural properties of the covariance matrix to improve its estimation in the GLRT. The decision statistic is then obtained as a function of the signal observations. This is presented in detail in [31] and outlined in Chapter 2 for an OFDM-based CR system.

Based on the discussion in this section, robust spectrum sensing algorithms which rely on important features in the received signal, such as multipath structure, cyclic prefix or receive diversity can be developed for efficient spectrum sensing. Moreover, utilizing multiple CRs in a collaborative manner can further improve the sensing performance. In the next section, the motivation, benefits and methods of implementing a cooperative cognitive radio network are presented.

1.4 Cooperative Spectrum Sensing

Cooperative spectrum sensing exploits multiple cognitive radio users to improve the performance of the sensing network in the detection of a primary user. The reason for imple-

menting a cooperative network lies in the importance of the accuracy of spectrum sensing since the interference resulting from the coexistence of cognitive radio and primary users in the same spectrum band severely degrades the performance of the primary user. In the presence of a fading channel, the spatial diversity gain obtained from cooperative CRs helps to overcome the destructive effects such as multipath fading and/or shadowing.

With cooperative sensing, the local sensing data from multiple CR users which are distributed over the sensing area are transmitted to a fusion center (FC) to be combined. By the combination of the results, the CR achieves a diversity gain which helps to improve the reliability of the final sensing decision. The decision fusion can be performed as a soft fusion scheme where each CR sends its observation to FC, or as the hard fusion scheme, where local hard decisions are gathered at the fusion center to achieve the final decision. Depending on the scenario in which the spectrum sensing is performed, soft decisions may outperform the hard decision fusion, whereas hard decision fusion requires less signaling overhead [34–36].

Two phases, sensing and reporting, can be considered for cooperative sensing in a cognitive radio network. In the sensing phase, each CR node listens and collects data from the primary user. After processing the collected data at each CR node, the measurement is transmitted through dedicated control channels to a fusion center. Two transmission schemes, namely orthogonal and nonorthogonal can be considered to transmit the results to the fusion center. In the orthogonal transmission scheme as shown in Figure 1.5, each CR node transmits the data to the FC over the orthogonal sub-channels or time slots (TS1,TS2, ...) equally divided in the time domain (TDMA manner). Therefore every CR node communicates with the fusion center in a distinct orthogonal channel without interference.

Contrary to the orthogonal transmission, in the nonorthogonal transmission scheme shown in Figure 1.6, all the CR signal vectors are simultaneously transmitted to the fusion center [37]. Therefore a better bandwidth efficiency is acquired since fewer reporting channels, hence less spectrum resource is consumed for the transmission phase. Due to the introduced interference in the non-orthogonal scheme, cooperative sensing with orthogonal transmission typically outperforms the one with non-orthogonal transmission at the cost of

requiring more resources. The observation is particularly true when the reporting channels are strong and interference is the main cause of degrading the fusion rather than the added noise at the fusion center. However in an orthogonal scheme, when the reliability of local

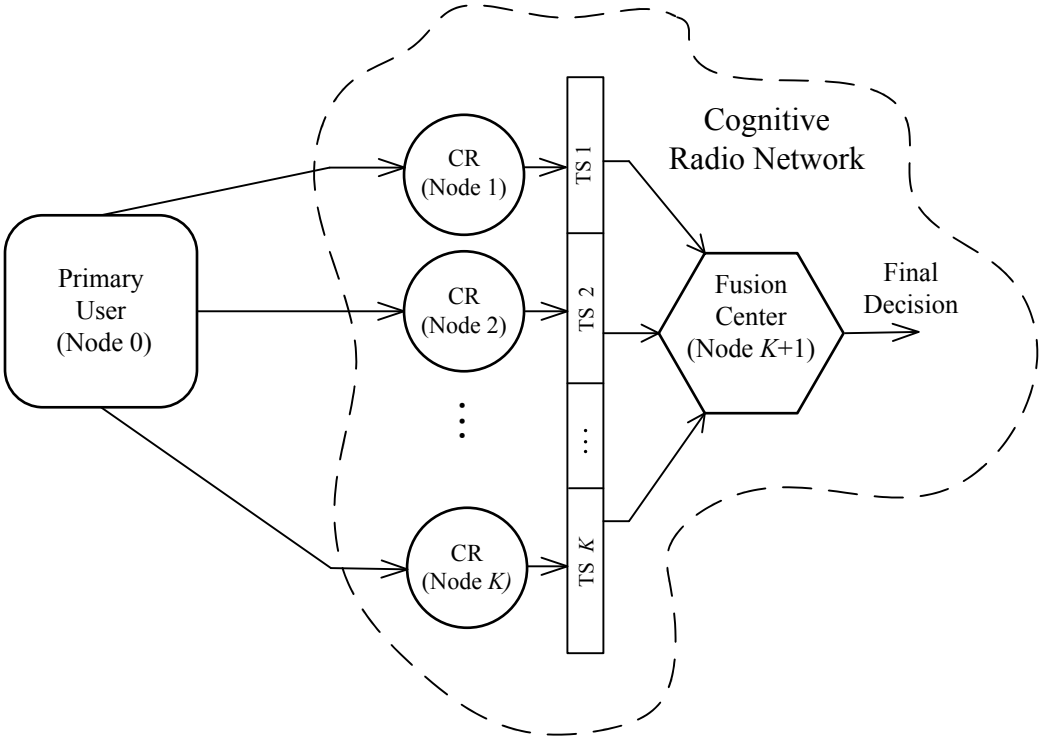

Figure 1.5 Orthogonal transmission of local decisions in a cognitive radio network.

sensing results may vary due to the different fading/shadowing channels, assigning the same weight to all different local sensing results for data combining at the fusion center limits the efficiency of the cooperative sensing. For more efficient combining, the schemes in [38] and [39] apply different weights to local sensing results in proportion to their reliability. On the other hand, in the situation when the reliability of the individual sensing result changes frequently, it takes additional time and spectrum resources to update the weights at the fusion center. This drawback may negatively affect the sensing time requirement in detecting the primary user as well as the bandwidth efficiency of the cognitive radio system. The examples of these systems include the CR systems with mobile CR users (mobile CR systems) and the CR systems where the primary user can appear at an arbitrary location.

Based on the above discussion, careful design consideration is required with regard to the tradeoff between the spectrum expenditure and the sensing performance of the cooperative network.

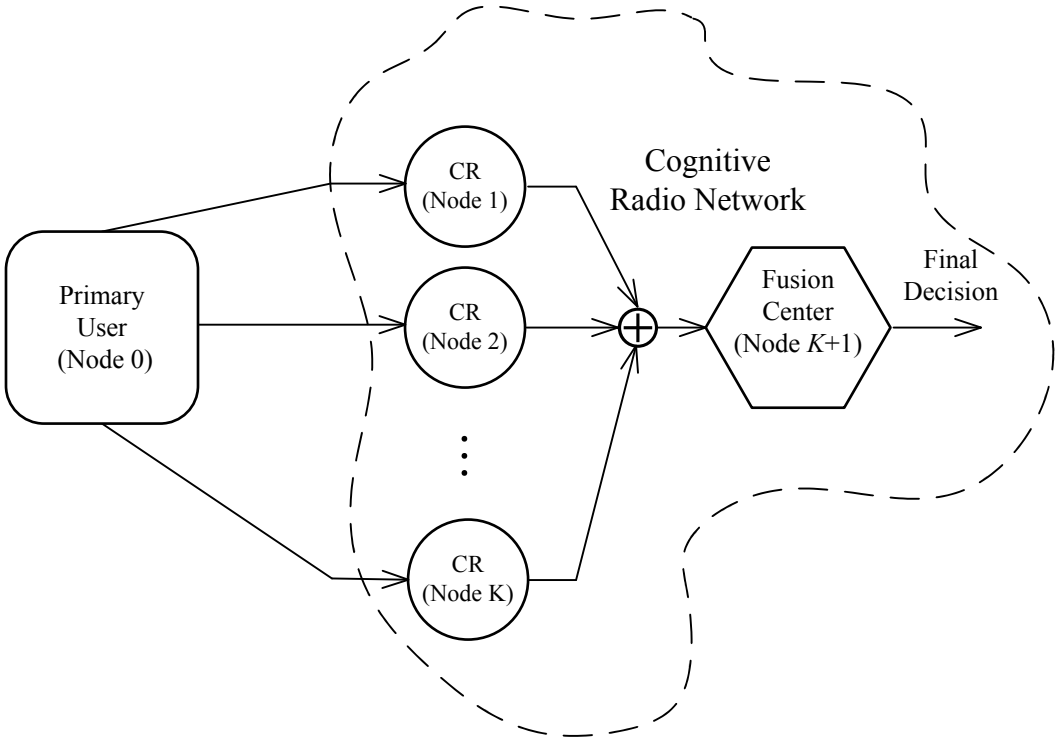

Figure 1.6 Non-orthogonal transmission of local decisions in a cognitive radio network.

1.5 Organization and Contribution of the Thesis

This dissertation is organized in five chapters as follows. After the introduction (this chapter), in Chapter 2, a GLRT algorithm is proposed for detecting the primary OFDM signals to monitor the licensed bandwidth. It is first shown that the GLRT algorithm can exploit both multipath and cyclic correlations to yield a novel blind spectrum sensing algorithm. It is then verified that the cyclic-prefix correlation coefficient (CPCC)-based detection algorithm is a special case of the constrained GLRT algorithm in the absence of multipath fading channel. It is further shown that when multipath fading is present, which is the case for OFDM applications, performance of the detection based on the cyclic-prefix correlation

coefficient degrades. Furthermore, by exploiting the known structure of the OFDM channel matrix in a constrained GLRT algorithm, a detection algorithm is obtained which is solely based on the multipath correlation coefficients. By combining the CPCC-based and multipath correlation coefficients-based algorithms, an even more reliable spectrum sensing method can be realized. The spectrum sensing algorithms developed in the first part of Chapter 2 assume that perfect synchronization can be obtained at the cognitive radio receiver. As such, the detection performance of sensing algorithms in this case serves as an upper bound for situations where synchronization has to be actually performed at the cognitive radio receiver. An efficient blind synchronization of time and carrier frequency offsets has been proposed to improve the sensing algorithm. However certain drawbacks still exist, including but not limited to the complexity and the delay added to the sensing task and the weak synchronization performance in the low SNR region These drawbacks motivate us to develop a simple GLRT-based algorithm that does not require timing synchronization to be established between the primary and secondary users.

In Chapter 3, the problem of decision fusion for cooperative spectrum sensing in cognitive radio networks is studied. The CRs perform spectrum sensing using energy detection and transmit their binary decisions over the *orthogonal* reporting channels to the FC for a final decision on the absence or presence of the primary user activity. Considering the limited resources in cognitive radio networks, which makes it difficult to acquire the instantaneous reporting channel state information, noncoherent transmission schemes with on-off keying (OOK) and binary frequency shift keying (BFSK) are employed to transmit the binary decisions to the fusion center. For each of the transmission schemes considered, energy-based and decoding-based fusion rules are first developed. Then the detection threshold at the CR nodes as well as at the FC, the combining weights (in the case of energy-based fusion rule) and the sensing time are optimized to maximize the achievable secondary throughput of the cognitive radio network. A performance comparison between energy-based fusion rule and the decoding-based fusion rule is made for different signal-to-noise ratios (SNRs) of the reporting channels. Also it is shown that BFSK achieves a higher secondary throughput than OOK at the expense of a larger transmission bandwidth.

In Chapter 4, cooperative spectrum sensing in cognitive radio (CR) networks is studied in which nonorthogonal transmission of local CR decisions is considered toward the fusion center (FC) in order to reduce the required transmission bandwidth in the reporting phase. To further reduce the transmission bandwidth, the transmission of local decisions by means of on-off keying (OOK) is examined at each cognitive radio. The problem of interest is how to efficiently report and combine the local decisions to/at the fusion center under fading channels. To this end two main fusion rules, namely energy-detection as well as decoding-based fusion rules are developed. Performance analysis of these fusion rules is carried out and used to design the required sensing parameters. Simulation results support the theoretical analysis and show that the added complexity of decoding-based fusion rule leads to a considerable performance gain over the simpler energy-based fusion rule when the reporting links are reasonably strong. It is also shown that in some situations the simpler energy-based fusion rule can perform almost as well as the decoding-based fusion rule.

Finally Chapter 5 draws conclusions and gives suggestions for future study.

2. Blind Spectrum Sensing for OFDM-Based Cognitive Radio Systems

2.1 Introduction

Orthogonal frequency division multiplexing (OFDM) has been known to be one of the most effective multicarrier techniques for broadband wireless communications. The main reason lies in its inherent capability to combat multipath fading and avoid inter-symbol interference. OFDM has attracted significant attention in the development of CR technology [1, 27]. In an OFDM-based communication system, CR spectrum sensing can be performed either in the time or frequency domain. In the frequency domain, subcarrier-wise detection can be performed [18, 40], which becomes attractive when the available bandwidth is divided into subbands which are allocated to different primary users. In [18], a frequency-domain spectrum sensing method has been proposed which optimizes sensing parameters over each subcarrier, whereas the algorithm in [40] is proposed to detect available portions of the spectrum. Although some OFDM-based technologies, such as digital audio broadcasting (DAB) or IEEE 802.16 wireless MAN, employ data multiplexing for different primary users, single-transmission OFDM systems are also common in practice. Among them are digital video broadcasting (DVB), IEEE 802.11 wireless LAN and IEEE 802.16e mobile WiMAX. For such wireless systems, the CR receiver needs to detect the primary OFDM signals to monitor the licensed bandwidth [1].

The likelihood ratio test (LRT) is known to be the optimal algorithm for spectrum sensing [8] if the exact knowledge of channel state information and noise variance can be made

[1] The contribution in this chapter is published in [31].

available at the receiver. Unfortunately, such knowledge is generally difficult to obtain at the cognitive radio receiver. On the other hand, the energy detection algorithm does not require channel information and performs well if the noise variance is known. However, even a slight uncertainty, around 0.5 dB in noise variance, causes its performance to severely drop below the performance with known noise variance [13]. It should also be pointed out that the energy detector is the optimal spectrum sensing method for independent and identically distributed (i.i.d) primary signals and its performance is degraded if the received primary signals are correlated [41]. Therefore, it is of great importance to develop efficient spectrum sensing algorithms for the detection of signals which are not necessarily i.i.d distributed. To alleviate the requirement on the precise knowledge of channel and noise variance which are generally unavailable at the cognitive radio receiver, a suitable detection algorithm is expected to extract and use some particular features of the received primary signals. In fact, a number of techniques have been proposed and evaluated, among them are the statistical covariance algorithm [17], eigenvalue-based algorithm [15, 16] and cyclostationary algorithm [26, 42].

As OFDM is an effective technique to combat multipath fading, it is expected that OFDM is employed in rich scattering environments. With advanced compression techniques, the information signals (in discrete-time complex basedband representation) can be considered as independent and identically distributed (i.i.d) random variables. However, when these signals are passed through a multipath fading channel, the received signals at the receiver are correlated versions of the transmitted signals, which typically have different statistics from the background noise. On the other hand, a very important feature of OFDM transmission is the use of cyclic prefix, which results in nonzero correlation of the received primary signal samples at certain delays. In [26], a method has been proposed based on the cyclic feature of OFDM blocks in the time domain. Though the algorithm shows a good performance, the signal correlation induced by multipath propagation is not exploited in such an algorithm.

The aim of a detection algorithm is to decide between the two hypotheses of whether the primary signal is present or absent. In the case when some parameters (e.g., channel state information and noise variance) are not known, the hypothesis is called a composite hypothesis [24]. For a composite hypothesis, one approach is to obtain estimate of the un-

known parameters (typically the maximum likelihood estimates). The estimated parameters are then used in the likelihood ratio test as if they are the correct values. This results in the so-called the *generalized* likelihood ratio test (GLRT) [8, 24]. GLRT has been widely employed in many hypothesis testing problems, e.g. [42–44], including spectrum sensing applications [25, 30].

In this chapter, it is first shown that the GLRT algorithm can exploit both multipath and cyclic correlations to yield a novel blind spectrum sensing algorithm. It is then verified that the cyclic-prefix correlation coefficient (CPCC)-based detection algorithm is a special case of the constrained GLRT algorithm in the absence of multipath fading channel. It is further shown that when multipath fading is present, which is the case for OFDM applications, performance of the detection based on the cyclic-prefix correlation coefficient degrades. Furthermore, by exploiting the known structure of the OFDM channel matrix in a constrained GLRT algorithm, a detection algorithm is obtained which is solely based on the multipath correlation coefficients. By combining the CPCC-based and multipath correlation coefficients-based algorithms, an even more reliable spectrum sensing method can be realized.

The spectrum sensing algorithms developed in the first part of this chapter (Sections 2.4 and 2.5) assume that perfect synchronization can be obtained at the cognitive radio receiver. As such, the detection performance of sensing algorithms in this case serves as an upper bound for situations where synchronization has to be actually performed at the cognitive radio receiver. In [45], a blind synchronization algorithm was proposed for maximum-likelihood estimations of time and carrier frequency offsets of OFDM signals. While such a blind synchronization algorithm can be conveniently incorporated in the spectrum sensing framework considered in this chapter, there are two main drawbacks: (i) using a synchronization algorithm adds more complexity and may cause delay to the sensing task, (ii) in the low SNR region where the cognitive radio is operating, the synchronization performance is far from perfect, hence the sensing performance is significantly degraded when compared to the case of perfect synchronization. These drawbacks motivate us to develop a simple GLRT-based algorithm in Section 2.6 that does not require timing synchronization to be

established between the primary and secondary users.

This chapter is organized as follows. Section 2.2 describes the system model and formulates the spectrum sensing problem. Section 2.3 presents a general framework of the GLRT detection scheme and shows how to exploit cyclic prefix and multipath correlation features. In Sections 2.4 and 2.5, two constrained GLRT algorithms are presented, where the data and cyclic parts of the OFDM signal are considered separately to exploit the structure of the covariance matrix in enhancing the performance of the GLRT algorithm. It is shown in both cases that the constrained GLRT algorithms lead to detection algorithms which solely depend on the sample correlation coefficients. A combined detection scheme is also proposed. The spectrum sensing algorithm for unsynchronized OFDM signals is proposed in Section 2.6. Simulation results are presented in Section 2.7 and Section 2.8 concludes the paper.

For convenience, the main mathematical symbols used in this chapter and their meanings are summarized in Table 2.1.

2.2 System Model

The OFDM signal model considered in this chapter is the same as that in [26] and [29], which assumes that the primary OFDM system employs L subcarriers and the cognitive radio and primary users can be perfectly synchronized. The case of no timing synchronization is discussed and treated separately in Section 2.6. Let $\{S_{n,k}\}_{k=0}^{L-1}$, with $E\{|S_{n,k}|^2\} = \sigma_S^2$, be the complex symbols to be transmitted in the nth OFDM block. Then the baseband OFDM modulated signal can be expressed as

$$s_n(m) = \frac{1}{\sqrt{L}} \sum_{k=0}^{L-1} S_{n,k} \mathrm{e}^{\frac{j2\pi mk}{L}};\ m = 0, \ldots, L-1. \tag{2.1}$$

For a large number of subcarriers L (i.e., the size of DFT/IDFT), $s_n(m)$ can be approximately modeled as a zero-mean circularly symmetric complex Gaussian random variable of variance σ_S^2, i.e., $s_n(m) \sim \mathcal{CN}(0, \sigma_S^2)$.

Table 2.1 Mathematical symbols used in Chapter 2.

Symbol	Description
$\mathbf{s}_n$, σ_S^2	L-length vector of the nth OFDM symbol, and variance of elements of $\mathbf{s}_n$
$\mathbf{s}_n^+$	$(L+L_p)$-length vector of the nth transmitted OFDM block
$\mathbf{x}_n$, σ_x^2	Received OFDM signal vector, and variance of elements of $\mathbf{x}_n$
$\mathbf{v}_n$, σ_v^2	Received noise vectors, and variance of elements of $\mathbf{v}_n$
$\mathbf{y}_n$, $\mathbf{R}_\mathbf{y}$	M-length vector of the nth received signal block, and its covariance matrix
$\mathbf{z}_n$, σ_z^2	M-length column vector of the noise samples, the noise variance
$S_{n,k}$	kth complex symbol of the nth OFDM block
L	Total number of subcarriers in an OFDM symbol
N, M	Number of received blocks, and length of received vector
L_p	Number of samples in the guard interval of an OFDM block
L_c	Number of channel filter taps
ρ	Cyclostationary correlation coefficient of the OFDM block
$\mathbb{h}$	Toeplitz matrix constructed from the channel filter taps
$\mathcal{H}_0$	Idle state of the primary user
$\mathcal{H}_1$	Active state of the primary user
P_d	Probability that the primary user is correctly detected in its active mode
P_f	Probability of a false detection of the primary user when it is in the idle state

Represent the length-$(L+L_p)$ vector of the nth transmitted OFDM block as

$$\mathbf{s}_n^+ = [s_n(L-1)\dots s_n(0)\underbrace{s_n(L-1)\dots s_n(L-L_p)}_{\text{Cyclic Prefix}}]^\top, \tag{2.2}$$

where L_p denotes the number of samples in the guard interval, i.e., the length of the cyclic prefix (CP). The corresponding received signal and noise vectors are denoted by

$$\mathbf{x}_n = [x_n(L-1)\ x_n(L-2)\dots x_n(0)x_n(-1)\dots x_n(-L_p)]^\top, \tag{2.3}$$

$$\mathbf{v}_n = [v_n(L-1)\ v_n(L-2)\dots v_n(0)v_n(-1)\dots v_n(-L_p)]^\top, \tag{2.4}$$

where the noise samples $v_n(l)$'s are i.i.d. $\mathcal{CN}(0,\sigma_v^2)$ random variables.

The primary user signal is received through a wireless multipath fading channel whose discrete-time baseband model is represented by channel filter taps h_i, $i=1,\dots,L_c$, where

L_c denotes the number of multipath components. It is also assumed that the fading process remains static during the interval of spectrum sensing. This implies that the channel filter taps can be treated as unknown constants during the period of spectrum sensing. The relationship of $\mathbf{x}_n$, $\mathbf{s}_n$ and $\mathbf{v}_n$ can be expressed in a matrix form as follows:

$$\mathbf{x}_n = \mathbb{h}\bar{\mathbf{s}}_n + \mathbf{v}_n, \tag{2.5}$$

where $\bar{\mathbf{s}}_n = [\mathbf{s}_n^\top, s_{n-1}(L-1), \ldots, s_{n-1}(L-L_c+1)]^\top$ and $\mathbb{h}$ is $(L+L_p) \times (L+L_p+L_c-1)$ Toeplitz matrix constructed from the channel filter taps as

$$\mathbb{h} = \begin{bmatrix} h_1 & \ldots & h_{L_c} & 0 & \ldots & \ldots & \ldots & 0 \\ 0 & h_1 & \ldots & h_{L_c} & 0 & \ldots & \ldots & 0 \\ \vdots & & \ddots & & \ddots & & & \vdots \\ \vdots & \ldots & 0 & h_1 & \ldots & h_{L_c} & 0 & 0 \\ \vdots & & & \ddots & \ddots & & \ddots & 0 \\ 0 & \ldots & \ldots & \ldots & 0 & h_1 & \ldots & h_{L_c} \end{bmatrix} \tag{2.6}$$

Note that the last L_p samples of $\mathbf{x}_n$ is the inter-symbol interference (ISI) part. Since $x_n(l)$'s are linear combinations of zero-mean complex Gaussian random variables, they are also zero-mean complex Gaussian random variables. Based on (2.5), the variance of $x_n(l)$ is $\sigma_x^2 = \sigma_S^2 \sum_{i=1}^{L_c} |h_i|^2 + \sigma_v^2$ when the primary user's signal is present, otherwise $\sigma_x^2 = \sigma_v^2$. It is also of interest to define the signal-to-noise ratio (SNR) in the presence of the primary user's signal as $\text{SNR} = \sigma_S^2 \sum_{i=1}^{L_c} |h_i|^2 / \sigma_v^2$.

Two binary hypotheses $\mathcal{H}_0$ and $\mathcal{H}_1$ are defined in spectrum sensing, in which $\mathcal{H}_0$ denotes the idle state of the primary user and $\mathcal{H}_1$ represents the active state of the primary user. In order to classify the observations into $\mathcal{H}_0$ or $\mathcal{H}_1$, a test statistic $\mathcal{T}$ is formulated and a general test decision is as follows:

$$\begin{cases} \text{Decide} \ \ \mathcal{H}_0, & \text{if } \mathcal{T} \leq \epsilon \\ \text{Decide} \ \ \mathcal{H}_1, & \text{if } \mathcal{T} > \epsilon \end{cases} \tag{2.7}$$

where ϵ is some threshold value. Two probabilities of interest are: (i) the probability of detection, P_d, which is the probability that the primary user is correctly detected in its

active mode, and (ii) the probability of false alarm, P_f, which represents the probability of a false detection of the primary user when it is in the idle state. Mathematically,

$$P_f = \Pr\left\{\mathcal{T} > \epsilon | \mathcal{H}_0\right\}, \tag{2.8}$$

$$P_d = \Pr\left\{\mathcal{T} > \epsilon | \mathcal{H}_1\right\}. \tag{2.9}$$

2.3 Generalized Likelihood Ratio Test (GLRT)

As mentioned before, spectrum sensing based on GLRT has been presented in [25] in which different tests are obtained under different parameter assumptions, i.e., unknown noise variance and/or signal covariance matrix. In the sequel, the GLRT is reviewed in its general form, and it will be employed for the detection of OFDM signals in the following sections. Let $\mathbf{y}_n \sim \mathcal{CN}(0, \mathbf{R}_\mathbf{y})$ denote the length-M column vector of the nth received signal block and $\mathbf{z}_n \sim \mathcal{CN}(0, \sigma_z^2\mathbf{I})$ denote the length-M column vector containing the noise samples. In the scenario that the noise variance, σ_z^2, and signal covariance matrix, $\mathbf{R}_\mathbf{y}$, are unknown, the GLRT is as follows [25]:

$$\mathcal{L}_\mathrm{G}(\mathbf{y}) = \frac{f_{\mathbf{y}|\mathcal{H}_1,\widehat{\mathbf{R}}_\mathbf{y}}(\mathbf{y}|\mathcal{H}_1, \widehat{\mathbf{R}}_\mathbf{y})}{f_{\mathbf{y}|\mathcal{H}_0,\widehat{\sigma}_z^2}(\mathbf{y}|\mathcal{H}_0, \widehat{\sigma}_z^2)} \underset{\mathcal{H}_0}{\overset{\mathcal{H}_1}{\gtrless}} \eta, \tag{2.10}$$

in which $\mathbf{y} = [\mathbf{y}_1, \ldots, \mathbf{y}_N]$ is a collection of N received blocks. In the preceding test, $\widehat{\mathbf{R}}_\mathbf{y}$ and $\widehat{\sigma}_z^2$ are the maximum likelihood estimates of $\mathbf{R}_\mathbf{y}$ and σ_z^2 under hypothesis $\mathcal{H}_1$ and $\mathcal{H}_0$, respectively.

The maximum likelihood estimate of σ_z^2 can be obtained as:

$$\widehat{\sigma}_z^2 = \max_{\sigma_z^2} \left\{\ln f_{\mathbf{y}|\mathcal{H}_0,\sigma_z^2}(\mathbf{y}|\mathcal{H}_0, \sigma_z^2)\right\}, \tag{2.11}$$

where

$$f_{\mathbf{y}|\mathcal{H}_0,\sigma_z^2}(\mathbf{y}|\mathcal{H}_0, \sigma_z^2) = \prod_{n=1}^{N} \frac{1}{(\pi\sigma_z^2)^M} \exp\left(-\frac{1}{\sigma_z^2}\|\mathbf{y}_n\|^2\right), \tag{2.12}$$

and $\|\cdot\|$ denotes the vector Euclidean norm. It follows that [25]

$$\widehat{\sigma}_z^2 = \frac{1}{NM}\mathrm{tr}(\mathbf{y}\mathbf{y}^H) = \frac{1}{M}\mathrm{tr}(\bar{\mathbf{R}}_\mathbf{y}). \tag{2.13}$$

where $\bar{\mathbf{R}}_{\mathbf{y}} = \mathbf{y}\mathbf{y}^H/N$ denotes the *sample* covariance matrix and H represents the Hermitian transpose.

On the other hand, the maximum likelihood estimate of $\mathbf{R}_{\mathbf{y}}$ can be obtained as:

$$\widehat{\mathbf{R}}_{\mathbf{y}} = \max_{\mathbf{R}_{\mathbf{y}} \in \mathcal{S}_{\mathbf{R}_{\mathbf{y}}}} \ln f_{\mathbf{y}|\mathcal{H}_1,\mathbf{R}_{\mathbf{y}}}(\mathbf{y}|\mathcal{H}_1, \mathbf{R}_{\mathbf{y}}), \tag{2.14}$$

where $\mathcal{S}_{\mathbf{R}_{\mathbf{y}}}$ specifies the set of $\mathbf{R}_{\mathbf{y}}$ having certain structures, and

$$f_{\mathbf{y}|\mathcal{H}_1,\mathbf{R}_{\mathbf{y}}}(\mathbf{y}|\mathcal{H}_1, \mathbf{R}_{\mathbf{y}}) = \prod_{n=1}^{N} \frac{1}{\pi^M \det(\mathbf{R}_{\mathbf{y}})} \exp\left(-\mathbf{y}_n^H \mathbf{R}_{\mathbf{y}}^{-1} \mathbf{y}_n\right). \tag{2.15}$$

To obtain a more explicit expression of the test in (2.10), first rewrite $f_{\mathbf{y}|\mathcal{H}_0,\sigma_z^2}(\mathbf{y}|\mathcal{H}_0, \sigma_z^2)$ and $f_{\mathbf{y}|\mathcal{H}_1,\mathbf{R}_{\mathbf{y}}}(\mathbf{y}|\mathcal{H}_1, \mathbf{R}_{\mathbf{y}})$ as follows:

$$\begin{aligned} f_{\mathbf{y}|\mathcal{H}_0,\sigma_z^2}(\mathbf{y}|\mathcal{H}_0, \sigma_z^2) &= \left[\frac{1}{(\pi\sigma_z^2)^M}\right]^N \exp\left(-\frac{1}{\sigma_z^2}\sum_{n=1}^{N} \|\mathbf{y}_n\|^2\right) \\ &= \left[\frac{1}{(\pi\sigma_z^2)^M}\right]^N \exp\left(-\frac{1}{\sigma_z^2}\mathrm{tr}\left(\mathbf{y}\mathbf{y}^H\right)\right) \\ &= \left[\frac{1}{\pi\sigma_z^2}\exp\left(-\frac{\widehat{\sigma}_z^2}{\sigma_z^2}\right)\right]^{NM}, \end{aligned} \tag{2.16}$$

and

$$\begin{aligned} f_{\mathbf{y}|\mathcal{H}_1,\mathbf{R}_{\mathbf{y}}}(\mathbf{y}|\mathcal{H}_1, \mathbf{R}_{\mathbf{y}}) &= \left[\frac{1}{\pi^M \det(\mathbf{R}_{\mathbf{y}})}\right]^N \prod_{n=1}^{N} \exp\left(-\mathbf{y}_n^H \mathbf{R}_{\mathbf{y}}^{-1} \mathbf{y}_n\right) \\ &= \left[\frac{1}{\pi^M \det(\mathbf{R}_{\mathbf{y}})}\right]^N \exp\left(-\mathrm{tr}\left(\mathbf{y}^H \mathbf{R}_{\mathbf{y}}^{-1} \mathbf{y}\right)\right) \\ &= \left[\frac{1}{\pi^M \det(\mathbf{R}_{\mathbf{y}})}\right]^N \exp\left(-\mathrm{tr}\left(\mathbf{R}_{\mathbf{y}}^{-1} \mathbf{y}\mathbf{y}^H\right)\right) \\ &\overset{\mathbf{y}\mathbf{y}^H = N\bar{\mathbf{R}}_{\mathbf{y}}}{=} \left[\frac{1}{\pi^M \det(\mathbf{R}_{\mathbf{y}})}\right]^N \exp\left(-N\mathrm{tr}\left(\mathbf{R}_{\mathbf{y}}^{-1} \bar{\mathbf{R}}_{\mathbf{y}}\right)\right) \\ &= \left[\frac{1}{(\pi)\det^{\frac{1}{M}}(\mathbf{R}_{\mathbf{y}})} \exp\left(-\frac{1}{M}\mathrm{tr}\left(\mathbf{R}_{\mathbf{y}}^{-1} \bar{\mathbf{R}}_{\mathbf{y}}\right)\right)\right]^{NM}. \end{aligned} \tag{2.17}$$

By substituting $\widehat{\mathbf{R}}_{\mathbf{y}}$ and $\widehat{\sigma}_z^2$ into (2.16) and (2.17), one has

$$f_{\mathbf{y}|\mathcal{H}_0,\widehat{\sigma}_z^2}(\mathbf{y}|\mathcal{H}_0, \widehat{\sigma}_z^2) = \left[\frac{1}{\pi\widehat{\sigma}_z^2}\exp(-1)\right]^{NM} = \left[\frac{1}{\frac{\pi}{M}\mathrm{tr}(\bar{\mathbf{R}}_{\mathbf{y}})}\exp(-1)\right]^{NM}, \tag{2.18}$$

and

$$f_{\mathbf{y}|\mathcal{H}_1,\widehat{\mathbf{R}}_\mathbf{y}}(\mathbf{y}|\mathcal{H}_1,\widehat{\mathbf{R}}_\mathbf{y}) = \left[\frac{1}{\pi \det^{\frac{1}{M}}(\widehat{\mathbf{R}}_\mathbf{y})}\exp\left(-\frac{1}{M}\mathrm{tr}\left(\widehat{\mathbf{R}}_\mathbf{y}^{-1}\bar{\mathbf{R}}_\mathbf{y}\right)\right)\right]^{NM}. \tag{2.19}$$

Finally, substituting (2.18) and (2.19) into (2.10) yields the following GLRT algorithm:

$$\mathcal{T}_{\mathrm{G}}(\mathbf{y}) = \{\mathcal{L}_{\mathrm{G}}(\mathbf{y})\}^{\frac{1}{MN}} = \frac{\frac{1}{M}\mathrm{tr}(\bar{\mathbf{R}}_\mathbf{y})}{\det^{\frac{1}{M}}(\widehat{\mathbf{R}}_\mathbf{y})}\beta(\widehat{\mathbf{R}}_\mathbf{y}) \underset{\mathcal{H}_0}{\overset{\mathcal{H}_1}{\gtrless}} \epsilon, \tag{2.20}$$

where

$$\beta(\widehat{\mathbf{R}}_\mathbf{y}) = \frac{\exp\left(-\frac{1}{M}\mathrm{tr}(\widehat{\mathbf{R}}_\mathbf{y}^{-1}\bar{\mathbf{R}}_\mathbf{y})\right)}{\exp(-1)}. \tag{2.21}$$

and $\epsilon = \eta^{\frac{1}{MN}}$ is a fixed threshold value selected to meet a requirement on the probability of false alarm, and it is independent of the received primary signal characteristics.

It is important to point out that the form in (2.20) is still very general and encompasses a large class of GLRT. What it says is that the test itself and hence its performance depends on how one estimates the covariance matrix of the received signal block under $\mathcal{H}_1$. According to [46], under the mild condition that both $\mathbf{R}_\mathbf{y}$ and its variation, $\delta(\mathbf{R}_\mathbf{y})$, have the same structure (e.g., $\mathbf{R}_\mathbf{y}$ does not have any constant entries), the structured maximum likelihood estimate of $\mathbf{R}_\mathbf{y}$ satisfies $\mathrm{tr}(\widehat{\mathbf{R}}_\mathbf{y}^{-1}\bar{\mathbf{R}}_\mathbf{y}) = M$. This implies that $\beta(\widehat{\mathbf{R}}_\mathbf{y}) = 1$ and the test becomes

$$\mathcal{T}_{\mathrm{G}}(\mathbf{y}) = \frac{\frac{1}{M}\mathrm{tr}(\bar{\mathbf{R}}_\mathbf{y})}{\det^{\frac{1}{M}}(\widehat{\mathbf{R}}_\mathbf{y})} = \frac{\frac{1}{MN}\mathrm{tr}(\mathbf{y}\mathbf{y}^H)}{\det^{\frac{1}{M}}(\widehat{\mathbf{R}}_\mathbf{y})} \underset{\mathcal{H}_0}{\overset{\mathcal{H}_1}{\gtrless}} \epsilon. \tag{2.22}$$

Since the covariance matrices involved in our study meet the aforementioned structural condition, the test in (2.22) shall be employed for spectrum sensing in this chapter.

On the other hand, for the special case when there is no constraint on the structure of the covariance matrix, the maximum likelihood estimate of $\mathbf{R}_\mathbf{y}$ is $\widehat{\mathbf{R}}_\mathbf{y} = \bar{\mathbf{R}}_\mathbf{y}$ and the test is the same as the one developed in [25] and has the following form:

$$\bar{\mathcal{T}}_{\mathrm{G}}(\mathbf{y}) = \frac{\frac{1}{M}\mathrm{tr}(\bar{\mathbf{R}}_\mathbf{y})}{\det^{\frac{1}{M}}(\bar{\mathbf{R}}_\mathbf{y})} \underset{\mathcal{H}_0}{\overset{\mathcal{H}_1}{\gtrless}} \epsilon. \tag{2.23}$$

The preceding *unconstrained* GLRT (U-GLRT) is described for a general observation $\mathbf{y} = [\mathbf{y}_1, \ldots, \mathbf{y}_N]$, where $\mathbf{y}_n \sim \mathcal{CN}(0, \mathbf{R}_\mathbf{y})$, $n = 1, \ldots, N$. When applied to the OFDM-based

cognitive radio system in Section 4.2, one can simply replace $\mathbf{y}_n$ by $\mathbf{x}_n$ of (2.5). Furthermore, it is also possible to use only a portion of the complete observation $\mathbf{y}$ in the GLRT algorithm. Although this appears to be counterproductive, the key advantage is that by concentrating on a certain part of the observation, one can exploit structural properties of the covariance matrix to improve its estimation in the GLRT. This is presented in detail in the next sections for an OFDM-based CR system.

2.4 GLRT Based on Cyclic Prefix Correlation

One way to exploit a strong structural correlation property of the observation is to use only the head and tail of each received OFDM block in the GLRT algorithm. To this end, define

$$\dot{\mathbf{x}}_n = [x_n(L-1)\dots x_n(L-L_p), x_n(0)\dots x_n(-L_p)]^\top, \tag{2.24}$$

as the vector containing $2L_p$ samples, L_p samples in the first part and L_p samples in the last part, of the nth OFDM block. The corresponding transmitted signal and additive white Gaussian noise vectors are defined as

$$\begin{aligned}\dot{\mathbf{s}}_n =&[s_n(L-1)\dots s_n(L-(L_p+L_c-1))s_n(L-1)\dots \\ &s_n(L-L_p)s_{n-1}(L-1)\dots s_{n-1}(L-L_c+1)]^\top, \\ \dot{\mathbf{v}}_n =&[v_n(L-1)\dots v_n(L-L_p), v_n(-1)\dots v_n(-L_p)]^\top.\end{aligned}$$

Then, one has

$$\dot{\mathbf{x}}_n = \dot{\mathbb{h}}\dot{\mathbf{s}}_n + \dot{\mathbf{v}}_n, \tag{2.25}$$

where $\dot{\mathbb{h}}$ is the following $2L_p \times 2(L_p + L_c - 1)$ block diagonal channel matrix:

$$\dot{\mathbb{h}} = \begin{bmatrix} \dot{\mathbb{h}}_A & 0 \\ 0 & \dot{\mathbb{h}}_A \end{bmatrix},$$

and

$$\dot{\mathbb{h}}_A = \begin{bmatrix} h_1 & \dots & \dots & h_{L_c} & 0 & \dots & 0 \\ 0 & h_1 & \dots & \dots & h_{L_c} & \ddots & 0 \\ & & \ddots & & & \ddots & 0 \\ 0 & \dots & 0 & h_1 & \dots & & h_{L_c} \end{bmatrix}_{L_p \times (L_p + L_c - 1)} \tag{2.26}$$

Let $\dot{\mathbf{x}} = [\dot{\mathbf{x}}_1 \dots \dot{\mathbf{x}}_N]$ and $\dot{\mathbf{s}} = [\dot{\mathbf{s}}_1 \dots \dot{\mathbf{s}}_N]$. The covariance matrix $\mathbf{R}_{\dot{\mathbf{x}}} = E\{\dot{\mathbf{x}}_n \dot{\mathbf{x}}_n^H\}$ under $\mathcal{H}_1$ can be shown to be:

$$\mathbf{R}_{\dot{\mathbf{x}}} = \dot{\mathbb{h}} \mathbf{R}_{\dot{\mathbf{s}}} \dot{\mathbb{h}}^H + \sigma_v^2 \mathbf{I}_{L_p} = \begin{bmatrix} \dot{\mathbb{h}}_A \dot{\mathbb{h}}_A^H & \dot{\mathbb{h}}_B \dot{\mathbb{h}}_B^H \\ \dot{\mathbb{h}}_B \dot{\mathbb{h}}_B^H & \dot{\mathbb{h}}_A \dot{\mathbb{h}}_A^H \end{bmatrix} \sigma_S^2 + \sigma_v^2 \mathbf{I}_{L_p}, \tag{2.27}$$

where $\dot{\mathbb{h}}_B$ is the first $L_p \times L_p$ block of matrix $\dot{\mathbb{h}}_A$ and $\mathbf{I}_{L_p}$ denotes the identity matrix of size L_p.

A cyclic prefix correlation coefficient (CPCC)-based spectrum sensing algorithm was in fact proposed in [26] with the focus on additive white Gaussian noise (AWGN) channels. Next it is shown that this CPCC-based sensing algorithm is exactly the constrained version of the GLRT algorithm based on observation $\dot{\mathbf{x}}$ and in the absence of multipath environment. It will be shown in Section 2.7 that the constrained GLRT algorithm provides a substantial performance improvement over the U-GLRT algorithm when only the observation $\dot{\mathbf{x}}$ is used. Furthermore, since the CPCC-based algorithm is only equivalent to the constrained GLRT (C-GLRT) algorithm when there is no multipath, it shall also be explicitly shown that its performance is degraded in a multipath environment.

2.4.1 No-Multipath Propagation

In the absence of the multipath propagation effect, $L_c = 1$, and the covariance matrix $\mathbf{R}_{\dot{\mathbf{x}}}$ in (2.27) has the following simpler form:

$$\mathbf{R}_{\dot{\mathbf{x}}} = \sigma_x^2 \begin{bmatrix} \mathbf{I}_{L_p} & \rho \mathbf{I}_{L_p} \\ \rho \mathbf{I}_{L_p} & \mathbf{I}_{L_p} \end{bmatrix}, \tag{2.28}$$

where $\rho = \frac{\mathrm{E}\{x_n(k)x_n^*(k\pm L)\}}{\mathrm{E}\{x_n(k)x_n^*(k)\}}$, $k = L-1,\ldots,L-L_p$, is the correlation coefficient among the corresponding L_p samples in the head and tail of the OFDM block. It is simple to show that this correlation coefficient is given as:

$$\rho = \begin{cases} 0, & \mathcal{H}_0 \\ \frac{\sigma_S^2|h_1|^2}{\sigma_S^2|h_1|^2+\sigma_v^2} = \frac{\mathrm{SNR}}{1+\mathrm{SNR}}, & \mathcal{H}_1 \end{cases} \tag{2.29}$$

Given the structure of the covariance matrix in (2.28), estimating $\mathbf{R}_{\dot{\mathbf{x}}}$ is equivalent to estimating ρ and σ_x^2. Their maximum likelihood estimates are given as follows:

$$(\widehat{\rho},\widehat{\sigma}_x^2) = \max_{\rho,\sigma_x^2} \ \ln f_{\dot{\mathbf{x}}|\mathcal{H}_1,\rho,\sigma_x^2}(\dot{\mathbf{x}}|\mathcal{H}_1,\rho,\sigma_x^2). \tag{2.30}$$

Substituting $\mathbf{y} = \dot{\mathbf{x}}$, $M = 2L_p$ and $\mathbf{R}_{\mathbf{y}} = \mathbf{R}_{\dot{\mathbf{x}}}$ in (2.15) gives:

$$\ln f_{\dot{\mathbf{x}}|\mathcal{H}_1,\mathbf{R}_{\dot{\mathbf{x}}}}(\dot{\mathbf{x}}|\mathcal{H}_1,\mathbf{R}_{\dot{\mathbf{x}}}) = -NL\ln(2\pi) - N\ln\left(\det(\mathbf{R}_{\dot{\mathbf{x}}})\right) - \sum_{n=1}^{N} \dot{\mathbf{x}}_n^H \mathbf{R}_{\dot{\mathbf{x}}}^{-1}\dot{\mathbf{x}}_n. \tag{2.31}$$

Using the identities $\det(r\mathbf{A}_{M\times M}) = (r^M)\det(\mathbf{A}_{M\times M})$ and $\det\begin{bmatrix} \mathbf{A} & \mathbf{B} \\ \mathbf{C} & \mathbf{D} \end{bmatrix} = \det(\mathbf{A} - \mathbf{BD}^{-1}\mathbf{C})$, one has $\det(\mathbf{R}_{\dot{\mathbf{x}}}) = (\sigma_x^2)^{2L_p}(1-\rho^2)^{L_p}$. In addition, $\mathbf{R}_{\dot{\mathbf{x}}}^{-1} = \frac{1}{\sigma_x^2(1-\rho^2)}\begin{bmatrix} \mathbf{I}_{L_p} & -\rho\mathbf{I}_{L_p} \\ -\rho\mathbf{I}_{L_p} & \mathbf{I}_{L_p} \end{bmatrix}$. Substituting these expressions in (2.31) evaluates to:

$$\begin{aligned} &\ln f_{\dot{\mathbf{x}}|\mathcal{H}_1,\rho,\sigma_x^2}\left(\dot{\mathbf{x}}|\mathcal{H}_1,\rho,\sigma_x^2\right) \\ &\quad = -NL\ln(2\pi) - N\ln((\sigma_x^2)^{2L_p}(1-\rho^2)^{L_p}) \\ &\quad = -\frac{1}{\sigma_x^2(1-\rho^2)}(g_1(\dot{\mathbf{x}}) - \rho g_2(\dot{\mathbf{x}})), \end{aligned} \tag{2.32}$$

where $g_1(\dot{\mathbf{x}}) = \sum_{n=1}^{N}(\dot{\mathbf{x}}_{1,n}^H\dot{\mathbf{x}}_{1,n} + \dot{\mathbf{x}}_{2,n}^H\dot{\mathbf{x}}_{2,n})$ and $g_2(\dot{\mathbf{x}}) = \sum_{n=1}^{N}(\dot{\mathbf{x}}_{1,n}^H\dot{\mathbf{x}}_{2,n} + \dot{\mathbf{x}}_{2,n}^H\dot{\mathbf{x}}_{1,n})$ and $\dot{\mathbf{x}}_{1,n}$ and $\dot{\mathbf{x}}_{2,n}$ are the vectors containing the first and last L_p components of $\dot{\mathbf{x}}_n$, respectively.

Let $a = 1/\sigma_x^2$. Then (2.31) can be rewritten as:

$$f(\rho,a) = -NL\ln(2\pi) + 2NL_p\ln(a) - NL_p\ln(1-\rho^2) - \frac{a}{(1-\rho^2)}\left(g_1(\dot{\mathbf{x}}) - \rho g_2(\dot{\mathbf{x}})\right). \tag{2.33}$$

The first derivatives of (2.33) with respect to ρ and a can be obtained as:

$$\frac{\partial f(\rho,a)}{\partial a} = \frac{2NL_p}{a} - \frac{1}{(1-\rho^2)}\left(g_1(\dot{\mathbf{x}}) - \rho g_2(\dot{\mathbf{x}})\right), \tag{2.34}$$

$$\frac{\partial f(\rho,a)}{\partial \rho} = \frac{2NL_p\rho}{1-\rho^2} - \frac{2a\rho}{(1-\rho^2)^2}\left(g_1(\dot{\mathbf{x}}) - \rho g_2(\dot{\mathbf{x}})\right) + \frac{\rho a g_2(\dot{\mathbf{x}})}{1-\rho^2}. \tag{2.35}$$

By simultaneously solving $\frac{\partial f(\rho,a)}{\partial a} = 0$ and $\frac{\partial f(\rho,a)}{\partial \rho} = 0$, one obtains:

$$\widehat{\sigma}_x^2 = \frac{1}{\widehat{a}} = \frac{g_1(\dot{\mathbf{x}})}{2NL_p} = \frac{\sum_{n=1}^{N}(\dot{\mathbf{x}}_{1,n}^H\dot{\mathbf{x}}_{1,n} + \dot{\mathbf{x}}_{2,n}^H\dot{\mathbf{x}}_{2,n})}{2NL_p}, \tag{2.36}$$

$$\widehat{\rho} = \frac{g_1(\dot{\mathbf{x}})}{g_2(\dot{\mathbf{x}})} = \frac{\sum_{n=1}^{N}(\dot{\mathbf{x}}_{1,n}^H\dot{\mathbf{x}}_{2,n} + \dot{\mathbf{x}}_{2,n}^H\dot{\mathbf{x}}_{1,n})}{\sum_{n=1}^{N}(\dot{\mathbf{x}}_{1,n}^H\dot{\mathbf{x}}_{1,n} + \dot{\mathbf{x}}_{2,n}^H\dot{\mathbf{x}}_{2,n})}. \tag{2.37}$$

which are exactly the sample variance and sample correlation coefficient, respectively.

Next, (2.22) can be employed to obtain the test statistics by setting $M = 2L_p$ and $\mathbf{R}_{\mathbf{y}} = \widehat{\mathbf{R}}_{\dot{\mathbf{x}}}$. With the aid of (2.28), the test is:

$$\mathcal{T}_{\mathrm{G}}(\dot{\mathbf{x}}) = \frac{\frac{1}{2NL_p}\mathrm{tr}(\dot{\mathbf{x}}\dot{\mathbf{x}}^H)}{\det^{\frac{1}{2L_p}}(\widehat{\mathbf{R}}_{\dot{\mathbf{x}}})} = \frac{1}{\sqrt{1-\widehat{\rho}^2}} \underset{\mathcal{H}_0}{\overset{\mathcal{H}_1}{\gtrless}} \dot{\epsilon}, \tag{2.38}$$

or equivalently

$$\widehat{\rho} \underset{\mathcal{H}_0}{\overset{\mathcal{H}_1}{\lessgtr}} \frac{\sqrt{\dot{\epsilon}^2-1}}{\dot{\epsilon}}. \tag{2.39}$$

As can be seen, the test statistics in (2.39) simply compares the cyclic correlation coefficient with a threshold. It is therefore identical to the detection algorithm proposed in [26].

2.4.2 Multipath Channel Propagation

In this part, the asymptotic behavior of $\widehat{\rho}$ under $\mathcal{H}_1$ is analyzed in order to illustrate the performance degradation of the test in (2.39) in the multipath scenario. First, observe that in an AWGN channel one has the following limit:

$$\lim_{N\longrightarrow\infty}\widehat{\rho} = \frac{\mathrm{SNR}}{1+\mathrm{SNR}}. \tag{2.40}$$

The sample covariance matrix $\bar{\mathbf{R}}_{\dot{\mathbf{x}}}$ can be decomposed into four $L_p \times L_p$ block matrices as follows:

$$\bar{\mathbf{R}}_{\dot{\mathbf{x}}} = \begin{bmatrix} \bar{\mathbf{R}}_{\dot{\mathbf{x}},11} & \bar{\mathbf{R}}_{\dot{\mathbf{x}},12} \\ \bar{\mathbf{R}}_{\dot{\mathbf{x}},21} & \bar{\mathbf{R}}_{\dot{\mathbf{x}},22} \end{bmatrix}, \tag{2.41}$$

where $\bar{\mathbf{R}}_{\dot{\mathbf{x}},21} = \bar{\mathbf{R}}^H_{\dot{\mathbf{x}},12}$. Thus, (2.37) can be expressed as:

$$\widehat{\rho} = \frac{\mathrm{tr}(\bar{\mathbf{R}}_{\dot{\mathbf{x}},12} + \bar{\mathbf{R}}_{\dot{\mathbf{x}},21})}{\mathrm{tr}(\bar{\mathbf{R}}_{\dot{\mathbf{x}},11} + \bar{\mathbf{R}}_{\dot{\mathbf{x}},22})}. \tag{2.42}$$

Employing (2.27), the denominator of (2.42) has the following asymptotic behavior under $\mathcal{H}_1$:

$$\begin{aligned}\mathcal{D}_{\mathbf{h}} =& \lim_{N\longrightarrow\infty} \mathrm{tr}(\bar{\mathbf{R}}_{\dot{\mathbf{x}},11} + \bar{\mathbf{R}}_{\dot{\mathbf{x}},22}) = 2\left(\mathrm{tr}(\dot{\mathbb{h}}_A \dot{\mathbb{h}}_A^H)\sigma_S^2 + L_p\sigma_v^2\right) \\ =& 2L_p\left[\sum_{i=1}^{L_c} |h_i|^2\sigma_S^2 + \sigma_v^2\right] = 2L_p\sigma_v^2(1+\mathrm{SNR}).\end{aligned} \tag{2.43}$$

For the numerator of (2.42), we have:

$$\begin{aligned}\mathcal{N}_{\mathbf{h}} =& \lim_{N\longrightarrow\infty} \mathrm{tr}(\bar{\mathbf{R}}_{\bar{\mathbf{x}},12} + \bar{\mathbf{R}}_{\bar{\mathbf{x}},21}) = 2\mathrm{tr}(\dot{\mathbb{h}}_B \dot{\mathbb{h}}_B^H)\sigma_S^2 = 2\sigma_S^2 \sum_{j=1}^{L_p}\sum_{i=1}^{j} |h_i|^2 \\ <& 2\sigma_S^2 \sum_{j=1}^{L_p}\sum_{i=1}^{L_c} |h_i|^2 = 2L_p\sigma_S^2 \sum_{i=1}^{L_c} |h_i|^2 = 2L_c\sigma_v^2\mathrm{SNR}.\end{aligned} \tag{2.44}$$

It then follows that the CP correlation coefficient in the multipath channel, $\tilde{\rho}_{\mathbf{h}}$, is equal to:

$$\mathcal{H}_1 : \tilde{\rho}_{\mathbf{h}} = \lim_{N\longrightarrow\infty} \widehat{\rho} = \frac{\mathcal{N}_{\mathbf{h}}}{\mathcal{D}_{\mathbf{h}}} = \frac{\sum_{j=1}^{L_p}\sum_{i=1}^{j} |h_i|^2\sigma_S^2}{L_p\left[\sum_{i=1}^{L_c} |h_i|^2\sigma_S^2 + \sigma_v^2\right]} < \frac{\mathrm{SNR}}{1+\mathrm{SNR}} = \rho, \tag{2.45}$$

where the subscript $\mathbf{h}$ indicates the dependency on channel realization $\mathbf{h} = [h_1, \ldots, h_{L_c}]^T$. Note that for a given P_f, the threshold in (2.39) is fixed and does not depend on the correlation coefficient. Therefore, (2.40) and (2.45) can be compared to observe the degradation of the detection performance of CPCC-based detection algorithm in the presence of multipath propagation. In order to understand the role of L_p and L_c in the detection performance, one simple way is to obtain the expected value of $\tilde{\rho}_{\mathbf{h}}$ with respect to all channel realizations with a fixed SNR. In Appendix A.1, it is shown that:

$$\begin{aligned}\mathcal{H}_1 : \tilde{\rho} = \mathrm{E}\{\tilde{\rho}_{\mathbf{h}}\} &= \frac{\mathrm{SNR}}{1+\mathrm{SNR}}\left[\frac{2L_p - L_c + 1}{2L_p}\right] \\ &= \rho\left[\frac{2L_p - L_c + 1}{2L_p}\right].\end{aligned} \tag{2.46}$$

From (2.46), it is clearly seen that for a fixed L_p and SNR, the average CP correlation coefficient decreases with an increase in the number of multipath delay components.

2.5 Generalized Likelihood Ratio Test Algorithm Based on Multipath Correlation

As shown in the previous section, the CPCC-based detection algorithm suffers a performance degradation in a multipath channel. On the one hand, this is expected, because the CPCC-based algorithm only uses observation in the head and tail of an OFDM block to exploit the correlation structure, which results from the use of the cyclic prefix. On the other hand, multipath also introduces strong correlation to the received OFDM samples, which could also be exploited in the constrained GLRT algorithm. This is precisely the motivation and objective of this section. The developed algorithm shall use the portion of the received OFDM symbol that does not include the ISI part. In this way, the known structure of the observation can be taken into account to improve the estimation of the signal covariance matrix. Furthermore, a simplified test statistic is derived as a function of the received signal correlation coefficients.

2.5.1 Constrained GLRT Algorithm

The portion of the received OFDM block without the ISI part and the corresponding transmitted signal and noise vectors can be represented, respectively, as $\ddot{\mathbf{x}}_n = [x_n(L-1)\dots x_n(0)]^\top$, $\ddot{\mathbf{s}}_n = [s_n(L-1)\dots s_n(0)]^\top$ and $\ddot{\mathbf{v}}_n = [v_n(L-1)\dots v_n(0)]^\top$. They are related according to

$$\ddot{\mathbf{x}}_n = \ddot{\mathbb{h}}\ddot{\mathbf{s}}_n + \ddot{\mathbf{v}}_n, \tag{2.47}$$

where $\ddot{\mathbb{h}}$ is the $L \times L$ circulant channel matrix whose first row is $[h_1 \ \cdots \ h_{L_c-1} \ h_{L_c} \ 0 \cdots \ 0]$.

Let $\mathbf{R}_{\ddot{\mathbf{x}}} \equiv [r_{k,j}]_{k,j=1,\dots,L} = \mathrm{E}\{\ddot{\mathbf{x}}_n \ddot{\mathbf{x}}_n^H\}$ be the signal covariance matrix. Using (2.47), under $\mathcal{H}_1$ one has

$$\mathbf{R}_{\ddot{\mathbf{x}}} = \ddot{\mathbb{h}}\ddot{\mathbb{h}}^H \sigma_S^2 + \sigma_v^2 \mathbf{I}. \tag{2.48}$$

The matrix $\mathbf{R}_{\ddot{\mathbf{x}}}$ has the following properties:

(i) $\mathbf{R}_{\ddot{\mathbf{x}}}$ is Hermitian: $r_{k,j} = r_{j,k}^*$.

(ii) All the diagonal elements are equal: $r_{k,k} = \sum_{i=1}^{L_c} |h_i|^2 \sigma_S^2 + \sigma_v^2$, $k = 0, \dots, L-1$

(iii) Since $\ddot{\mathbb{h}}\ddot{\mathbb{h}}^H$ is circularly symmetric, $\mathbf{R}_{\ddot{\mathbf{x}}}$ is also circularly symmetric. This last property is specific to OFDM transmission.

From the above properties, one has the following proposition.

Proposition: Let L_p denote the length of the cyclic prefix. To obtain an estimate of the covariance matrix $\mathbf{R}_{\ddot{\mathbf{x}}}$, it is sufficient to estimate L_p values.

Proof: Since $L_c \leq L_p$, the circulant channel matrix $\ddot{\mathbb{h}}$ has at most L_p nonzero values in each row. Therefore $\ddot{\mathbb{h}}\ddot{\mathbb{h}}^H$ has at most $2L_p - 1$ nonzero values in each row that also appear in all the other rows of $\ddot{\mathbb{h}}\ddot{\mathbb{h}}^H$ due to its circularity. Since $\ddot{\mathbb{h}}\ddot{\mathbb{h}}^H$ is also a Hermitian matrix, there are $L_p - 1$ conjugate pairs in each row, excluding the diagonal element. Therefore only L_p values are needed to completely define $\mathbf{R}_{\ddot{\mathbf{x}}}$. □

The first row of the covariance matrix can be expressed as

$$[r_{1,0} r_{1,1} \dots r_{1,L-1}] = \left[\begin{array}{ccccccccccc} \gamma_0 & \gamma_1 & \dots & \gamma_{L_p-1} & 0 & \dots & 0 & \gamma^*_{L_p-1} & \dots & \gamma^*_1 \end{array} \right]. \tag{2.49}$$

The consecutive rows are obtained through a right circular shift of the previous row. To employ the GLRT algorithm, the vector $\boldsymbol{\gamma} = [\gamma_0, \gamma_1, \dots, \gamma_{L_p-1}]$ can be estimated based on the criterion in (2.14), which is equivalent to

$$\widehat{\boldsymbol{\gamma}} = \max_{\boldsymbol{\gamma}} \ \ln f_{\ddot{\mathbf{x}}|\mathcal{H}_1,\boldsymbol{\gamma}}(\ddot{\mathbf{x}}|\mathcal{H}_1, \boldsymbol{\gamma}). \tag{2.50}$$

Solving the preceding problem is quite challenging since the term $\mathbf{R}^{-1}_{\ddot{\mathbf{x}}}$ can not be easily differentiated with respect to $\boldsymbol{\gamma}$. Instead an equivalent optimization problem shall be considered and it is described next.

Since $\mathbf{R}_{\ddot{\mathbf{x}}}$ is a circulant matrix, all the vectors $\mathbf{w}_k = \frac{1}{\sqrt{L}}[1, \mathrm{e}^{-j2\pi k/L}, \dots, \mathrm{e}^{-j2\pi k(L-1)/L}]^\top$, $k = 0, \dots, L-1$, are its eigenvectors with the corresponding eigenvalues:

$$\lambda_k = \sum_{i=0}^{L-1} r_{1,i} \mathrm{e}^{-\frac{j2\pi ki}{L}} = \gamma_0 + \sum_{m=1}^{L_p-1} \mathrm{Re}\left\{ \gamma_m \mathrm{e}^{-\frac{j2\pi km}{L}} \right\}. \tag{2.51}$$

Let $\mathbf{W} = [\mathbf{w}_0, \dots, \mathbf{w}_{L-1}]$ denote the matrix of eigenvectors (which is also an IDFT matrix) and $\boldsymbol{\Lambda} = \mathrm{diag}(\lambda_k)$ the diagonal matrix of the eigenvalues. Then $\mathbf{R}_{\ddot{\mathbf{x}}} = \mathbf{W}^H \boldsymbol{\Lambda} \mathbf{W}$ is the

eigenvalue decomposition of $\mathbf{R}_{\ddot{\mathbf{x}}}$ and one has

$$\mathbf{W}^H \mathbf{R}_{\ddot{\mathbf{x}}} \mathbf{W} = \mathbf{W}^H \mathbf{W} \mathbf{\Lambda} \mathbf{W}^H \mathbf{W} = \mathbf{\Lambda}. \tag{2.52}$$

Let $\mathbf{X}_n = \mathbf{W}^H \ddot{\mathbf{x}}_n = [X_{0,n}, \ldots, X_{L-1,n}]^\top$ be the DFT of $\ddot{\mathbf{x}}_n$. It is obvious that

$$\mathbf{R}_{\mathbf{X}} = \mathrm{E}\{\mathbf{X}_n \mathbf{X}_n^H\} = \mathrm{E}\{\mathbf{W}^H \ddot{\mathbf{x}}_n \ddot{\mathbf{x}}_n^H \mathbf{W}\} = \mathbf{W}^H \mathrm{E}\{\ddot{\mathbf{x}}_n \ddot{\mathbf{x}}_n^H\} \mathbf{W} = \mathbf{\Lambda}. \tag{2.53}$$

The preceding means that λ_k's represent the average energy per each subcarrier, and hence, they are positive. From (2.51), it is observed that

$$\gamma_m = \frac{1}{L} \sum_{k=0}^{L-1} \lambda_k \mathrm{e}^{\frac{j2\pi km}{L}}, \quad m = 0, \ldots, L_p - 1. \tag{2.54}$$

Therefore, if one can find the maximum likelihood estimate of λ_k's by solving

$$\widehat{\lambda}_k = \max_{\lambda_k} \ \ln f_{\ddot{\mathbf{x}}|\mathcal{H}_1, \mathbf{R}_{\ddot{\mathbf{x}}}}(\ddot{\mathbf{x}}|\mathcal{H}_1, \mathbf{R}_{\ddot{\mathbf{x}}}), \tag{2.55}$$

then the maximum likelihood estimate of γ_m's can be obtained as

$$\widehat{\gamma}_m = \frac{1}{L} \sum_{k=0}^{L-1} \widehat{\lambda}_k \mathrm{e}^{\frac{j2\pi km}{L}}, \quad m = 0, \ldots, L_p - 1. \tag{2.56}$$

To express $\ln f_{\ddot{\mathbf{x}}|\mathcal{H}_1, \mathbf{R}_{\ddot{\mathbf{x}}}}(\ddot{\mathbf{x}}|\mathcal{H}_1, \mathbf{R}_{\ddot{\mathbf{x}}})$ as a function of λ_k's, first, substitute $\mathbf{y} = \ddot{\mathbf{x}}$ and $M = L$ in (2.15) to yield

$$\ln f_{\ddot{\mathbf{x}}|\mathcal{H}_1, \mathbf{R}_{\ddot{\mathbf{x}}}}(\ddot{\mathbf{x}}|\mathcal{H}_1, \mathbf{R}_{\ddot{\mathbf{x}}}) = -NL\ln(2\pi) - N\ln\det(\mathbf{R}_{\ddot{\mathbf{x}}}) - \sum_{n=1}^{N} \ddot{\mathbf{x}}_n^H \mathbf{R}_{\ddot{\mathbf{x}}}^{-1} \ddot{\mathbf{x}}_n. \tag{2.57}$$

With the aid of (2.53) it is observed that

$$\ddot{\mathbf{x}}_n^H \mathbf{R}_{\ddot{\mathbf{x}}}^{-1} \ddot{\mathbf{x}}_n = \ddot{\mathbf{x}}_n^H \mathbf{W} \mathbf{\Lambda}^{-1} \mathbf{W}^H \ddot{\mathbf{x}}_n = \mathbf{X}_n^H \mathbf{\Lambda}^{-1} \mathbf{X}_n = \sum_{k=0}^{L-1} \frac{|X_{n,k}|^2}{\lambda_k}, \tag{2.58}$$

and

$$\det(\mathbf{R}_{\ddot{\mathbf{x}}}) = \prod_{k=0}^{L-1} \lambda_k. \tag{2.59}$$

Using (2.58) and (2.59), (2.57) can be equivalently expressed as:

$$\psi(\lambda_0, \ldots, \lambda_{L-1}) = -NL\ln(2\pi) - N\ln \prod_{k=0}^{L-1} \lambda_k - \sum_{n=1}^{N} \sum_{k=0}^{L-1} \frac{|X_{n,k}|^2}{\lambda_k}. \tag{2.60}$$

For convenience, define $\alpha_k = \frac{1}{\lambda_k} > 0$ and rewrite (2.60) as

$$\phi(\alpha_0, \ldots, \alpha_{L-1}) = -NL\ln(2\pi) + N\ln \prod_{k=0}^{L-1} \alpha_k - \sum_{n=1}^{N}\sum_{k=0}^{L-1} \alpha_k |X_{n,k}|^2. \tag{2.61}$$

It is simple to verify that

$$\frac{\partial \phi(\alpha_0, \ldots, \alpha_{L-1})}{\partial \alpha_k} = \frac{N}{\alpha_k} - \sum_{n=1}^{N} |X_{n,k}|^2, \tag{2.62}$$

$$\frac{\partial^2 \phi(\alpha_0, \ldots, \alpha_{L-1})}{\partial \alpha_k^2} = -\frac{N}{\alpha_k^2} < 0. \tag{2.63}$$

Therefore $\phi(\alpha_0, \ldots, \alpha_{L-1})$ is a concave function of $\alpha_0, \ldots, \alpha_{L-1}$. Setting (2.62) to zero yields

$$\widehat{\lambda}_k = \frac{1}{\widehat{\alpha}_k} = \frac{1}{N}\sum_{n=1}^{N} |X_{n,k}|^2. \tag{2.64}$$

Employing (2.64) in (2.56) gives

$$\begin{aligned}
\widehat{\gamma}_m =& \frac{1}{NL}\sum_{k=0}^{L-1}\sum_{n=1}^{N} |X_{n,k}|^2 \mathrm{e}^{\frac{j2\pi km}{L}} \\
=& \frac{1}{NL}\sum_{k=0}^{L-1}\sum_{n=1}^{N} X_{n,k}^* \mathrm{e}^{\frac{j2\pi km}{L}} \frac{1}{\sqrt{L}}\sum_{i=0}^{L-1} x_n(i)\mathrm{e}^{-\frac{j2\pi ki}{L}} \\
=& \frac{1}{NL}\sum_{n=1}^{N}\sum_{i=0}^{L-1} x_n(i) \frac{1}{\sqrt{L}}\sum_{k=0}^{L-1} X_{n,k}^* \mathrm{e}^{-\frac{j2\pi(i-m)k}{L}} \\
=& \frac{1}{NL}\sum_{n=1}^{N}\sum_{i=0}^{L-1} x_n(i) \left[\frac{1}{\sqrt{L}}\sum_{k=0}^{L-1} X_{n,k} \mathrm{e}^{\frac{j2\pi(i-m)k}{L}}\right]^* \\
=& \frac{1}{NL}\sum_{n=1}^{N}\sum_{i=0}^{L-1} x_n(i) x_n^*\left([i-m] \bmod L\right), \quad m = 0, \ldots, L_p - 1,
\end{aligned} \tag{2.65}$$

which represent the sample correlation values up to the maximum delay of $L_p - 1$ samples.

Next, the covariance matrix estimate, $\widehat{\mathbf{R}}_{\ddot{\mathbf{x}}}$, can be constructed from the sample correlation values obtained in (2.65). The resulting test statistics can then be established by exploiting (2.22) with $\mathbf{y} = \ddot{\mathbf{x}}$, $\widehat{\mathbf{R}}_{\mathbf{y}} = \widehat{\mathbf{R}}_{\ddot{\mathbf{x}}}$ and $M = L$. In the time domain, one has:

$$\mathcal{T}_{\mathrm{G}}(\ddot{\mathbf{x}}) = \frac{\frac{1}{LN}\mathrm{tr}(\ddot{\mathbf{x}}\ddot{\mathbf{x}}^H)}{\det^{\frac{1}{L}}(\widehat{\mathbf{R}}_{\ddot{\mathbf{x}}})} \underset{\mathcal{H}_0}{\overset{\mathcal{H}_1}{\gtrless}} \ddot{\epsilon}. \tag{2.66}$$

2.5.2 MPCC-Based Test

The spectrum sensing framework elaborated so far in this section makes use of the correlation property of the primary signal to identify it from the background noise. It is of interest to establish an approximated, but simpler test that can still capture the multipath correlation of the primary signal. Some recent works [47, 48] have also intuitively developed test statistics as functions of the received signal in the time domain by exploiting the multipath correlation property. Appendix A.2 shows that by making an appropriate approximation in the low SNR region, the test in (2.66) can also be simplified as a function of the sample correlation coefficients. In particular, the simplified test is:

$$\widetilde{\mathcal{T}}(\ddot{\mathbf{x}}) = \sum_{m=1}^{L_p-1} |\widehat{\varrho}_m|^2, \tag{2.67}$$

where $\widehat{\varrho}_m$ represents the sample correlation coefficient corresponding to a delay of m samples, given as:

$$\widehat{\varrho}_m = \frac{\sum_{n=1}^{N}\sum_{i=0}^{L-1} x_n(i)x_n^*\left((i-m) \bmod L\right)}{\sum_{n=1}^{N}\sum_{i=0}^{L-1} |x_n(i)|^2}. \tag{2.68}$$

It is demonstrated in Section 2.7 that the performance of the above simplified test is very close to that of the constrained GLRT in Section 2.5.1.

2.5.3 Combination of CPCC-Based and MPCC-Based Detection Algorithms

As discussed at the end of Section 2.3, the full multipath and cyclic correlations can be jointly considered in one covariance matrix. However, the success of the constrained GLRT algorithms introduced in Sections 2.4 and 2.5 with a finite sample size and at low SNR value lies in the structural constraints of their covariance matrices. A simple but effective approach to combine multipath and cyclic correlations is to decide $\mathcal{H}_1$ whenever one of the two constrained GLRT algorithms detects the presence of the primary user. The combined test always yields the best performance between the two detection algorithms in each channel realization. It should be noted that the threshold values have to be selected in such a way that the overall probability of false alarm meets the required constraint.

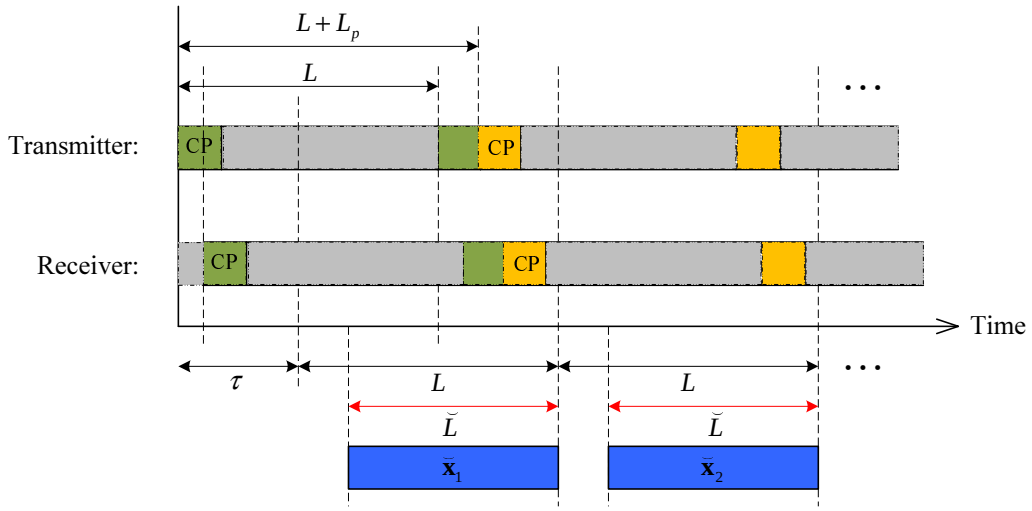

Figure 2.1 Timing relation between transmitter and receiver in the unsynchronized case.

2.6 Detection Algorithm for Unsynchronized Orthogonal Frequency Division Multiplexing Signals

As pointed out before, the spectrum sensing algorithms presented in Sections 2.4 and 2.5 require symbol timing synchronization between the secondary and primary users. In the absence of symbol timing synchronization, the cyclic correlation is taken into account by considering samples located within the lags of $\pm L$ [26]. The consequence of this approach is a decrease of the correlation coefficient to $\breve{\rho} = \frac{L_p}{L+L_p}\rho$ [26], which causes a drop in the performance of the detection algorithm.

At the secondary user's receiver, the received signal samples are divided into blocks of L samples each. This means that the corresponding samples in adjacent blocks are correlated due to the CP [26]. Compared with the received signal model in the synchronized case (see, e.g., (2.5)), the receiver in the unsynchronized case does not know when an OFDM block will start. As such, the timing index in this section is with reference to the time the secondary user's receiver starts to collect the receive signal samples. In general, the timing origin at the secondary user's receiver can be lead or lag over the timing origin at the transmitter by τ samples, as illustrated in Fig. 2.1. For N transmitted OFDM blocks, the number of sample blocks processed by the receiver is $\breve{N} = \left\lfloor \frac{N(L+L_p-\tau)}{L} \right\rfloor$.

To develop an efficient GLRT-based detection algorithm for unsynchronized OFDM signals, consider only the last portion of $\breve{L} = L - L_p + 1$ samples in each block of L samples (see Fig. 2.1), which can be represented as:

$$\breve{\mathbf{x}}_n = [\breve{x}_n(L-1), \ldots, \breve{x}_n(L_p-1)]^\top = \breve{\mathbb{h}}\breve{\mathbf{s}}_n + \breve{\mathbf{v}}_n, \quad n = 1, \ldots, \breve{N}. \tag{2.69}$$

In the preceding expression, $\breve{\mathbb{h}}$ is the $\breve{L} \times L$ Toeplitz channel matrix with the first row $[h_1, \ldots, h_{L_c}, 0, \ldots, 0]$ and first column $[h_1, 0, \ldots, 0]^\top$. The corresponding length-L transmitted signal vector is denoted by $\breve{\mathbf{s}}_n = [\breve{s}_n(L-1), \ldots, \breve{s}_n(0)]^\top$, $n = 1, \ldots, \breve{N}$. It is important to emphasize that, due to unsynchronization, $\breve{\mathbf{s}}_n$ does not necessarily align with the transmitted OFDM blocks and it generally contains data symbols from two consecutive transmitted OFDM blocks. It also has to be noted that the reason for employing the signal model in (2.69) in the analysis is to efficiently exploit the correlation among the transmitted signals due to the presence of CP. Based on this model, all the corresponding samples in the neighboring transmitted vectors, i.e., $\breve{\mathbf{s}}_n$ and $\breve{\mathbf{s}}_{n-1}$ are correlated with the *average* correlation coefficient $\vartheta = \mathrm{E}\{\breve{s}_n(i)\breve{s}^*_{n-1}(i)\}/\mathrm{E}\{|\breve{s}_n(i)|^2\} = L_p/L + L_p$. Consequently, the corresponding samples in the neighboring received vectors, i.e., $\breve{\mathbf{x}}_n$ and $\breve{\mathbf{x}}_{n-1}$, are correlated with the correlation coefficient $\breve{\rho} = \mathrm{E}\{\breve{x}_n(i)\breve{x}^*_{n-1}(i)\}/\mathrm{E}\{|\breve{x}_n(i)|^2\} = \vartheta(\sigma_S^2 \sum_{i=1}^{L_c} |h_i|^2/\sigma_S^2 \sum_{i=1}^{L_c} |h_i|^2 + \sigma_v^2) = \vartheta(\mathrm{SNR}/\mathrm{SNR}+1)$.

To take the correlation between the neighboring vectors $\breve{\mathbf{x}}_n$ into account, define the length-$2\breve{L}$ vectors $\tilde{\mathbf{x}}_n = [\breve{\mathbf{x}}_n^\top, \breve{\mathbf{x}}_{n-1}^\top]^\top$, $n = 2, \ldots, \breve{N}$. The covariance matrix of $\tilde{\mathbf{x}}_n$ is expressed and approximated as:

$$\begin{aligned}\mathbf{R}_{\tilde{\mathbf{x}}} = \mathrm{E}\{\tilde{\mathbf{x}}_n\tilde{\mathbf{x}}_n^H\} &= \breve{\mathbb{h}}\sigma_S^2 \begin{bmatrix} \mathbf{I}_L & \vartheta\mathbf{I}_L \\ \vartheta\mathbf{I}_L & \mathbf{I}_L \end{bmatrix} \breve{\mathbb{h}}^H + \sigma_v^2\mathbf{I}_{2L} \\ &\cong \begin{bmatrix} \mathbf{R}_{\breve{\mathbf{x}}} & \breve{\rho}\mathbf{R}_{\breve{\mathbf{x}}} \\ \breve{\rho}\mathbf{R}_{\breve{\mathbf{x}}} & \mathbf{R}_{\breve{\mathbf{x}}} \end{bmatrix}. \end{aligned} \tag{2.70}$$

The matrix $\mathbf{R}_{\breve{\mathbf{x}}}$ is an $\breve{L} \times \breve{L}$ Hermitian Toeplitz matrix and it can be described by its first row $[\breve{\gamma}_0, \ldots, \breve{\gamma}_{L_p-1},\ 0, \ldots, 0]$ and its first column $[\breve{\gamma}_0^*,\ \breve{\gamma}_1^*, \ldots, \breve{\gamma}_{L_p-1}^*,\ 0, \ldots 0]^\top$. Let

$\tilde{\mathbf{x}} = [\tilde{\mathbf{x}}_2, \ldots, \tilde{\mathbf{x}}_{\breve{N}}]$ and $\breve{\mathbf{x}} = [\breve{\mathbf{x}}_1, \ldots, \breve{\mathbf{x}}_{\breve{N}}]$. To facilitate matrix manipulations and parameter estimations, the correlation among adjacent $\tilde{\mathbf{x}}_n$'s is ignored. This allows one to apply the general GLRT test in (2.23) to the observation $\tilde{\mathbf{x}}$ by substituting $\mathbf{y} = \tilde{\mathbf{x}}$, $M = 2\breve{L}$ and $N = \breve{N} - 1$. The resulting test is:

$$\breve{\mathcal{T}}_{\mathrm{G}}(\tilde{\mathbf{x}}) \cong \frac{\frac{1}{2\breve{L}(\breve{N}-1)}\mathrm{tr}(\tilde{\mathbf{x}}\tilde{\mathbf{x}}^H)}{\det^{\frac{1}{2\breve{L}}}(\widehat{\mathbf{R}}_{\tilde{\mathbf{x}}})} = \frac{\frac{1}{\breve{L}\breve{N}}\mathrm{tr}(\breve{\mathbf{x}}\breve{\mathbf{x}}^H)}{\sqrt{(1-\widehat{\breve{\rho}}^2)}\det^{1/\breve{L}}(\widehat{\mathbf{R}}_{\breve{\mathbf{x}}})} \underset{\mathcal{H}_0}{\overset{\mathcal{H}_1}{\gtrless}} \breve{\epsilon}. \tag{2.71}$$

where $\widehat{\mathbf{R}}_{\tilde{\mathbf{x}}}$, $\widehat{\mathbf{R}}_{\breve{\mathbf{x}}}$ and $\widehat{\breve{\rho}}$ are estimates of $\mathbf{R}_{\tilde{\mathbf{x}}}$, $\mathbf{R}_{\breve{\mathbf{x}}}$ and $\breve{\rho}$ respectively. From the expression in (2.71), it is seen that both $\mathbf{R}_{\breve{\mathbf{x}}}$ and $\breve{\rho}$ need to be estimated.

Since obtaining the ML estimate of $\mathbf{R}_{\breve{\mathbf{x}}}$ appears to be very cumbersome, the entries of $\mathbf{R}_{\breve{\mathbf{x}}}$ shall be estimated by the sample correlation coefficients as follows:

$$\widehat{\breve{\gamma}}_m = \frac{1}{\breve{N}\breve{L}}\left[\sum_{n=1}^{\breve{N}}\sum_{i=m}^{L}\breve{x}_n(i)\breve{x}_n^*(i-m) + \sum_{n=1}^{\breve{N}-1}\sum_{i=1}^{m-1}\breve{x}_n(i)\breve{x}_{n-1}^*(L+i-m)\right],\ m = 0, \ldots, L_p - 1. \tag{2.72}$$

To obtain the ML estimate of $\breve{\rho}$, the log-likelihood function of $\tilde{\mathbf{x}}$ is approximately expressed as:

$$\ln f_{\tilde{\mathbf{x}}|\mathcal{H}_1,\mathbf{R}_{\tilde{\mathbf{x}}}}(\tilde{\mathbf{x}}|\mathcal{H}_1, \mathbf{R}_{\tilde{\mathbf{x}}}) \cong -(\breve{N}-1)\cdot\breve{L}\cdot\ln(2\pi) - (\breve{N}-1)\cdot\breve{L}\cdot\ln(\det(\mathbf{R}_{\tilde{\mathbf{x}}})) - \sum_{n=1}^{\breve{N}}\tilde{\mathbf{x}}_n^H\mathbf{R}_{\tilde{\mathbf{x}}}^{-1}\tilde{\mathbf{x}}_n. \tag{2.73}$$

It can be easily verified that:

$$\mathbf{R}_{\tilde{\mathbf{x}}}^{-1} = \frac{1}{1-\breve{\rho}^2}\begin{bmatrix} \mathbf{R}_{\breve{\mathbf{x}}}^{-1} & -\breve{\rho}\mathbf{R}_{\breve{\mathbf{x}}}^{-1} \\ -\breve{\rho}\mathbf{R}_{\breve{\mathbf{x}}}^{-1} & \mathbf{R}_{\breve{\mathbf{x}}}^{-1} \end{bmatrix}. \tag{2.74}$$

Using the above and $\det(\mathbf{R}_{\tilde{\mathbf{x}}}) = (1-\breve{\rho}^2)^{\breve{L}}\det^2(\mathbf{R}_{\breve{\mathbf{x}}})$, (2.73) can be equivalently expressed as:

$$\begin{aligned}\breve{\psi}(\breve{\rho}, \mathbf{R}_{\breve{\mathbf{x}}}) =& -(\breve{N}-1)\breve{L}\ln(2\pi) - (\breve{N}-1)\breve{L}\ln(1-\breve{\rho}^2) - 2(\breve{N}-1)\ln(\mathbf{R}_{\breve{\mathbf{x}}}) \\ & - \frac{1}{1-\breve{\rho}^2}\cdot\sum_{n=2}^{\breve{N}-1}\left[\breve{\mathbf{x}}_n^H\mathbf{R}_{\breve{\mathbf{x}}}^{-1}\breve{\mathbf{x}}_n - \breve{\rho}\breve{\mathbf{x}}_{n-1}^H\mathbf{R}_{\breve{\mathbf{x}}}^{-1}\breve{\mathbf{x}}_n - \breve{\mathbf{x}}_n^H\mathbf{R}_{\breve{\mathbf{x}}}^{-1}\breve{\mathbf{x}}_{n-1}\breve{\mathbf{x}}_{n-1}^H\mathbf{R}_{\breve{\mathbf{x}}}^{-1}\breve{\mathbf{x}}_{n-1}\right].\end{aligned} \tag{2.75}$$

Solving $\frac{\partial\breve{\psi}(\breve{\rho},\mathbf{R}_{\breve{\mathbf{x}}})}{\partial\breve{\rho}}=0$ gives:

$$\frac{2\breve{\rho}(\breve{N}-1)\breve{L}}{(1-\breve{\rho}^2)}-\frac{2\breve{\rho}}{(1-\breve{\rho}^2)^2}\sum_{n=2}^{\breve{N}}\left[\breve{\mathbf{x}}_n^H\mathbf{R}_{\breve{\mathbf{x}}}^{-1}\breve{\mathbf{x}}_n-\breve{\rho}\breve{\mathbf{x}}_{n-1}^H\mathbf{R}_{\breve{\mathbf{x}}}^{-1}\breve{\mathbf{x}}_n-\breve{\rho}\breve{\mathbf{x}}_n^H\mathbf{R}_{\breve{\mathbf{x}}}^{-1}\breve{\mathbf{x}}_{n-1}+\breve{\mathbf{x}}_{n-1}^H\mathbf{R}_{\breve{\mathbf{x}}}^{-1}\breve{\mathbf{x}}_{n-1}\right]$$
$$+\frac{1}{(1-\breve{\rho}^2)}\sum_{n=2}^{\breve{N}}\left[\breve{\mathbf{x}}_{n-1}^H\mathbf{R}_{\breve{\mathbf{x}}}^{-1}\breve{\mathbf{x}}_n+\breve{\mathbf{x}}_n^H\mathbf{R}_{\breve{\mathbf{x}}}^{-1}\breve{\mathbf{x}}_{n-1}\right]=0. \tag{2.76}$$

To simplify (2.76), one can make use of the following approximation under the assumption of sufficiently large $\breve{N}$:

$$\begin{aligned}&\frac{1}{2(\breve{N}-1)\breve{L}}\left[\sum_{n=2}^{\breve{N}}\breve{\mathbf{x}}_n^H\mathbf{R}_{\breve{\mathbf{x}}}^{-1}\breve{\mathbf{x}}_n+\breve{\mathbf{x}}_{n-1}^H\mathbf{R}_{\breve{\mathbf{x}}}^{-1}\breve{\mathbf{x}}_{n-1}\right]\\ =&\frac{1}{2(\breve{N}-1)\breve{L}}\mathrm{tr}\left(\mathbf{R}_{\breve{\mathbf{x}}}^{-1}\left[\sum_{n=2}^{\breve{N}}\breve{\mathbf{x}}_n\breve{\mathbf{x}}_n^H+\sum_{n=2}^{\breve{N}}\breve{\mathbf{x}}_{n-1}\breve{\mathbf{x}}_{n-1}^H\right]\right)\\ =&\frac{1}{\breve{L}}\mathrm{tr}\left(\mathbf{R}_{\breve{\mathbf{x}}}^{-1}\bar{\mathbf{R}}_{\breve{\mathbf{x}}}\right)\cong 1.\end{aligned} \tag{2.77}$$

where $\bar{\mathbf{R}}_{\breve{\mathbf{x}}}=\frac{1}{2(\breve{N}-1)}\left(\sum_{n=2}^{\breve{N}}\breve{\mathbf{x}}_n\breve{\mathbf{x}}_n^H+\sum_{n=2}^{\breve{N}}\breve{\mathbf{x}}_{n-1}\breve{\mathbf{x}}_{n-1}^H\right)$ represents the sample covariance matrix of $\breve{\mathbf{x}}$'s. Using (2.77), (2.76) can be simplified to:

$$\breve{\rho}+\frac{2\breve{\rho}}{(1-\breve{\rho}^2)}\left(-1+\frac{\breve{\rho}}{2(\breve{N}-1)\breve{L}}\sum_{n=2}^{\breve{N}}\left[\breve{\mathbf{x}}_{n-1}^H\mathbf{R}_{\breve{\mathbf{x}}}^{-1}\breve{\mathbf{x}}_n+\breve{\mathbf{x}}_n^H\mathbf{R}_{\breve{\mathbf{x}}}^{-1}\breve{\mathbf{x}}_{n-1}\right]\right)$$
$$+\frac{1}{2(\breve{N}-1)\breve{L}}\sum_{n=2}^{\breve{N}}\left[\breve{\mathbf{x}}_{n-1}^H\mathbf{R}_{\breve{\mathbf{x}}}^{-1}\breve{\mathbf{x}}_n+\breve{\mathbf{x}}_n^H\mathbf{R}_{\breve{\mathbf{x}}}^{-1}\breve{\mathbf{x}}_{n-1}\right]\cong 0. \tag{2.78}$$

It can be shown that the following solution satisfies (2.78):

$$\widehat{\breve{\rho}}=\frac{1}{2(\breve{N}-1)\breve{L}}\sum_{n=2}^{\breve{N}}\left[\widehat{\breve{\mathbf{x}}}_{n-1}^H\mathbf{R}_{\breve{\mathbf{x}}}^{-1}\widehat{\breve{\mathbf{x}}}_n+\widehat{\breve{\mathbf{x}}}_n^H\mathbf{R}_{\breve{\mathbf{x}}}^{-1}\widehat{\breve{\mathbf{x}}}_{n-1}\right]. \tag{2.79}$$

In summary, after finding $\widehat{\mathbf{R}}_{\breve{\mathbf{x}}}$ based on (2.72), $\widehat{\breve{\rho}}$ can be obtained from (2.79). The results are then used in (2.71) to realize the test.

2.7 Simulation Results

The simulation parameters are chosen similarly to those in [26]. In particular, the primary user's OFDM system has $L = 32$ subcarriers and transmits i.i.d 16-QAM symbols with normalized unit power. The detection period is taken to be equal to $N = 100$ OFDM blocks and the results are averaged over 1000 random realizations of a Rayleigh multipath fading channel. Except for Fig. 2.9, the channel coefficients are i.i.d. complex Gaussian random variables. The case of correlated channels is considered for Fig. 2.9. Note that for an OFDM system having bandwidth of 5 MHz, 32 subcarriers and a cyclic prefix length of 8 (similar to [26]), the sensing time is roughly $((32+8)/5 \times 10^6) \times 100 = 8 \times 10^{-4}$ s, or 0.8 ms. The performance of different spectrum sensing algorithms is evaluated and compared via the probability of detection, P_d, for a constant false alarm rate of $P_f = 0.05$.

First, Fig. 2.2 compares the detection performance of the energy detector (ED) and three spectrum sensing algorithms developed and analyzed in this chapter under perfect synchronization assumption, namely CPCC-based algorithm (Section 2.5.1 and reference [26]), multi-

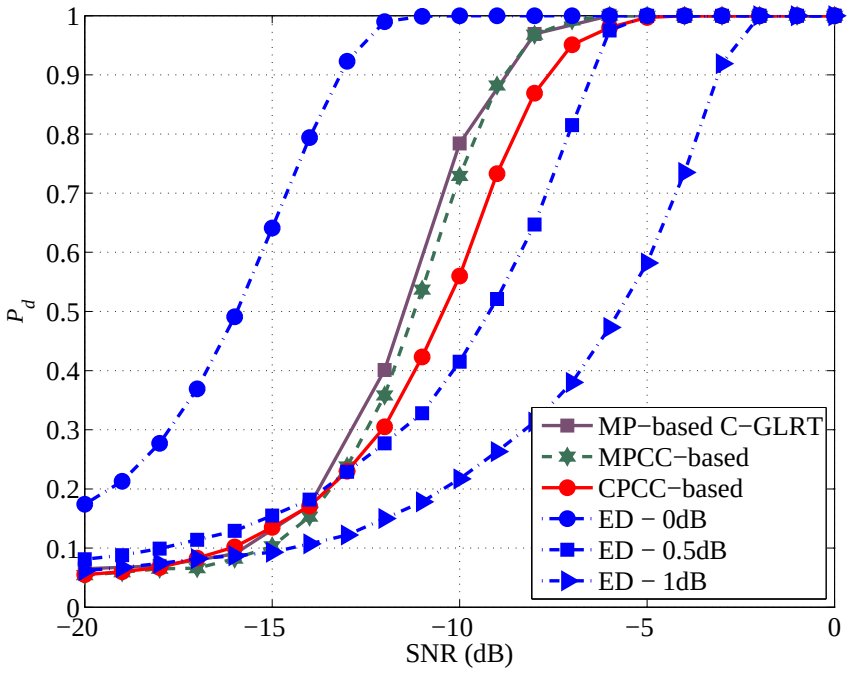

Figure 2.2 Performance comparison of constrained-GLRT and unconstrained-GLRT spectrum sensing algorithms, $L_c = L_p = 8$.

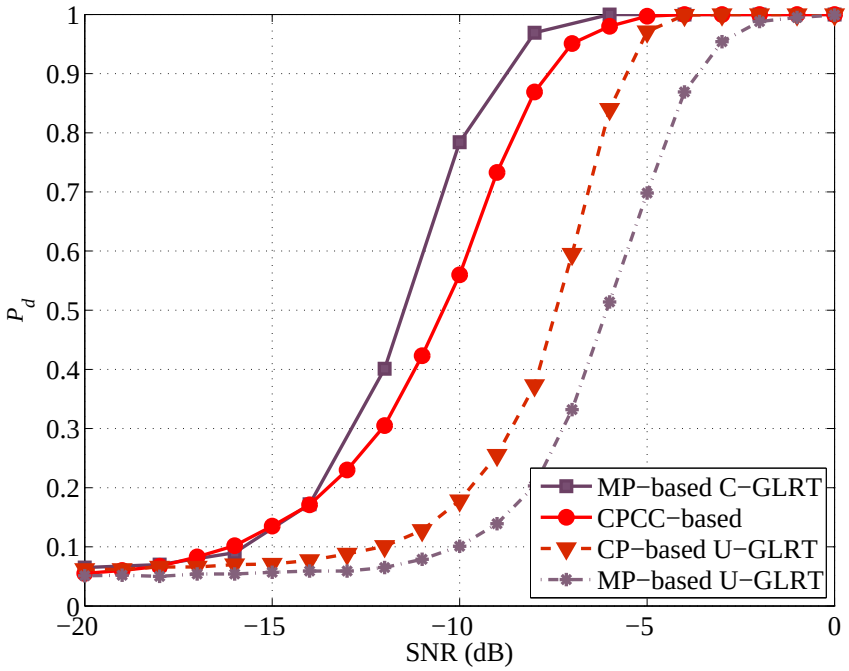

Figure 2.3 Performance comparison of constrained-GLRT and unconstrained-GLRT spectrum sensing algorithms, $L_c = L_p = 8$.

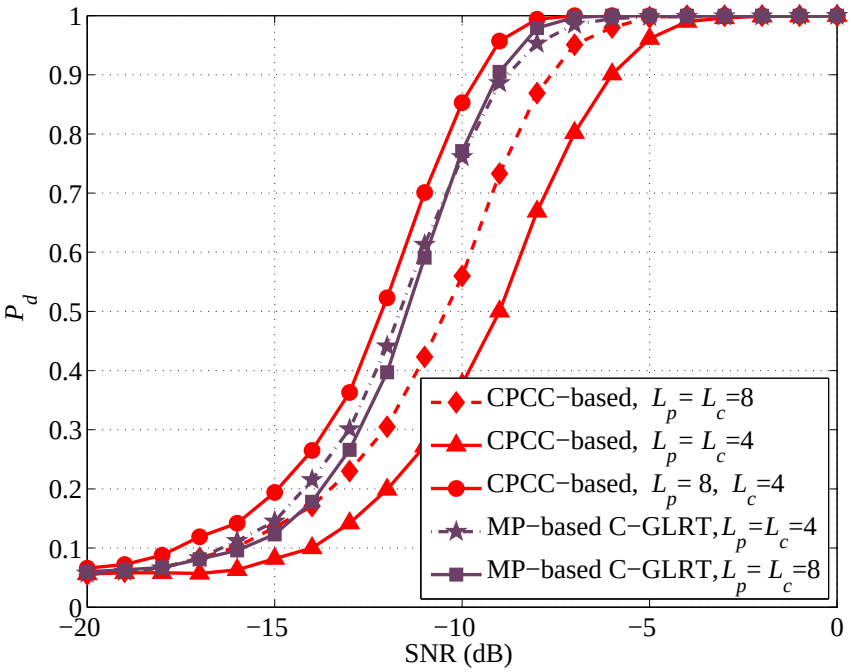

Figure 2.4 Effect of L_p and L_c on the performance of spectrum sensing algorithms.

path correlation-based constrained GLRT (MP-based C-GLRT algorithm, Section 2.5.1) and the simpler MPCC-based algorithm (Section 2.5.2). For this particular figure, $L_p = L_c = 8$ is used. As pointed out before, the ED algorithm requires a precise knowledge of the noise variance and a small noise uncertainty, e.g., 0.5 dB or 1.0 dB, causes a huge performance degradation as can be seen from the figure. In contrast, the three other algorithms are completely blind, and their performances are impressive. Note that the simplified MPCC-based algorithm performs closely with the MP-based C-GLRT algorithm, and both of them clearly outperform the CPCC-based algorithm. This superior performance is expected since, with a large number of channel taps ($L_c = 8$), it would be more beneficial to exploit multipath correlation than CP correlation.

Next, Fig. 2.3 shows performance improvement of the constrained GLRT algorithms over their unconstrained counterparts, both with multipath correlation and CP correlation. For this figure L_p and L_c are also set to be $L_p = L_c = 8$. Recall that the U-GLRT algorithm is basically (2.23), but using only cyclic prefix portions of the observations in the CP-based algorithm, or ISI-free portions of the observations in the multipath-based algorithm. In both cases, the improvements in detection performance are very large.

Fig. 2.4 shows the detection performance of both MP- and CPCC-based C-GLRT algorithms under different values of L_p and L_c. Observe that the performance of MP-based C-GLRT changes very little between $L_p = L_c = 4$ and $L_p = L_c = 8$. This can be explained as follows: While a bigger value of L_c is desirable in terms of having stronger correlation property, there is a larger number of quantities to estimate with the same size of observations. These opposing effects appear to cancel out in the scenarios considered in Fig. 2.4. In contrast, the performance of CPCC-based algorithm can be significantly improved by increasing the length of the CP (comparing the settings of $L_p = L_c = 4$ with $L_p = 8,\ L_c = 4$). Such a performance improvement is obviously expected, but comes at the expense of additional resources since, as far as ISI avoidance is concerned it is desirable to use the minimum CP length of $L_p = L_c = 4$. Furthermore, performance degradation of the CPCC-based C-GLRT algorithm in environment with a higher channel taps (rich multipath environment) can also be observed by comparing the curves with $L_p = 8,\ L_c = 4$ and $L_p = L_c = 8$. Such an

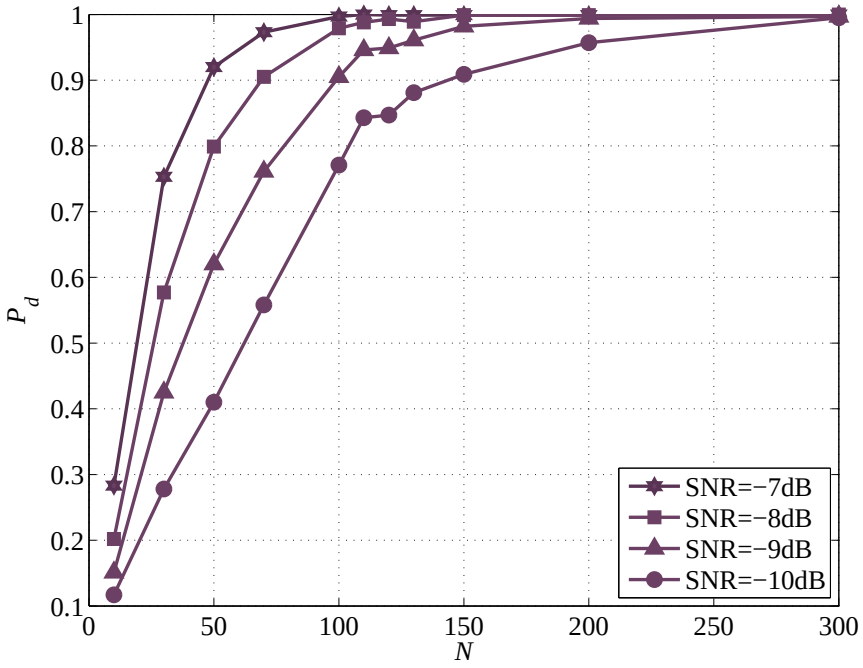

Figure 2.5 Performance of MP-based C-GLRT algorithm with respect to observation size, N.

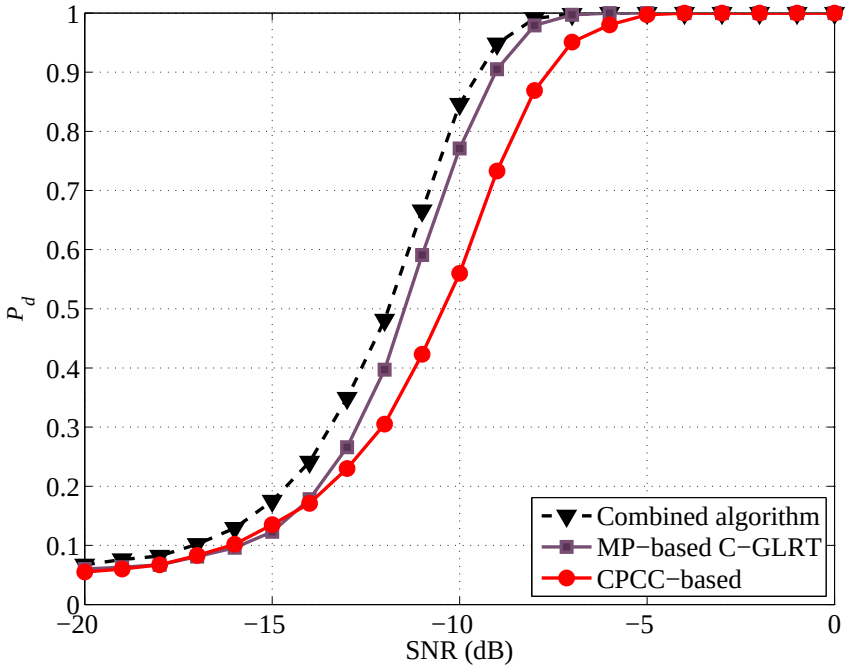

Figure 2.6 Performance of the combined algorithm, $L_p = L_c = 8$.

observation agrees with the analysis in (2.46). Recall that this was theoretically proved in Section 2.4.2.

Fig. 2.5 shows the convergence behavior of the probability of detection of the proposed MP-based C-GLRT algorithm as a function of N. As can be seen from the figure, for every SNR value, the probability of detection can be made arbitrarily close to 1 by allowing sufficient observations.

Fig. 2.6 shows the performance of the combined algorithm (discussed in Section 2.5.3) for the case $L_c = L_p = 8$. It is seen that the combined sensing algorithm outperforms both the MP-based and CPCC-based C-GLRT algorithms. Such a result is as expected since the combined algorithm takes into account all the observations (both ISI-free and CP portions of received blocks) and at the same time benefits from the covariance structures exploited in MP-based and CPCC-based algorithms.

Fig. 2.7 shows the performance of the MP-based C-GLRT and CPCC-based algorithms when the synchronization algorithm in [45] is performed first over the sensing interval. The normalized residual carrier frequency offset (CFO) is set to 0.5, which is the worst case. Note that the types of sensing algorithm are distinguished by different line styles, while the combinations of imperfect/perfect timing synchronization (indicated as "I-Syn" and "P-Syn") and CFO values are identified by different markers. The carrier frequency offset introduces a phase shift to the time domain samples of an OFDM signal [45]. Nevertheless, the circularity of the received signal covariance matrix is preserved in this case and the MP-based C-GLRT algorithm is not affected by a CFO. However, the CP correlation coefficient becomes a complex value when frequency offset is present. The effect of CFO on the CPCC-based spectrum sensing algorithm can be compensated by considering the magnitude of the sample correlation coefficient in the CPCC-based algorithm [45]. As can be seen from Fig. 2.7, the performance of sensing algorithms remains unchanged in the presence of CFO. On the other hand, it is seen that the imperfect symbol timing causes performance degradation in both algorithms. For the MP-based C-GLRT in the presence of timing offset, the degradation is due to the fact that the ISI part cannot be perfectly removed; therefore, the covariance

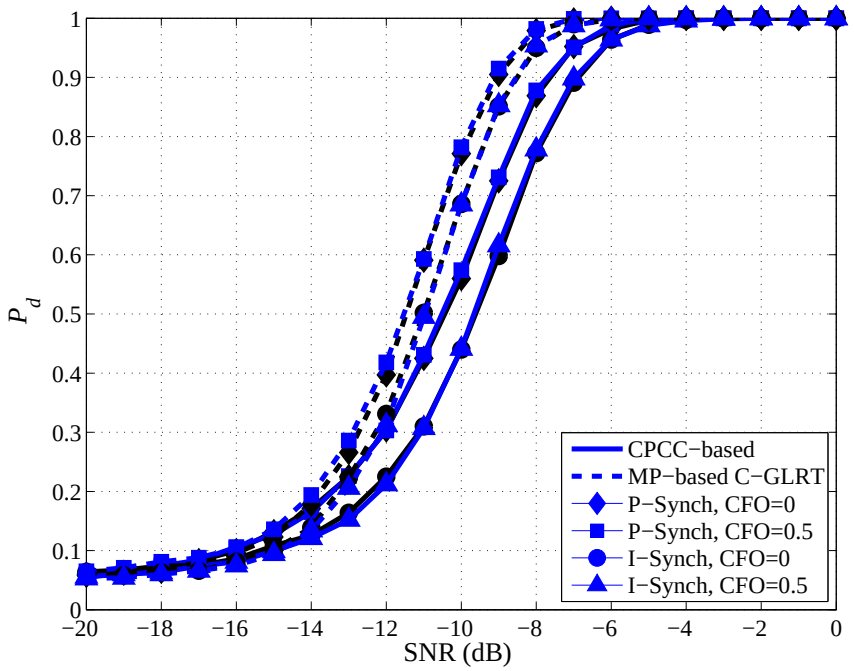

Figure 2.7 Performance of the spectrum sensing algorithms in the presence of residual time and carrier frequency offsets, $L_c = L_p = 8$. Note that the types of sensing algorithm are distinguished by different line styles, while the combinations of imperfect/perfect timing synchronization (indicated as "I-Synch" and "P-Synch") and CFO values are identified by different markers.

matrix of the received signal is not truly circulant. The time offset also degrades the performance of CPCC-based algorithm, since the identical head and tail of the OFDM signal cannot be perfectly retrieved at the receiver.

Fig. 2.8 compares performance of the proposed sensing algorithms for perfectly synchronized, imperfectly synchronized, and unsynchronized OFDM signals, which are labeled in the figure as "P-Syn", "I-Syn" and "Unsyn", respectively. In particular, the combined algorithm in Section 2.5.3 is compared against the algorithm in (2.71) for two different numbers of channel taps, namely $L_c = 8$ and $L_c = 1$ as well as when the CP length is set to $L_p = 8$. Observe the opposite performance behaviors when the number of channel taps reduces from $L_c = 8$ to $L_c = 1$; the performance gets better for the synchronized and imperfectly syn-

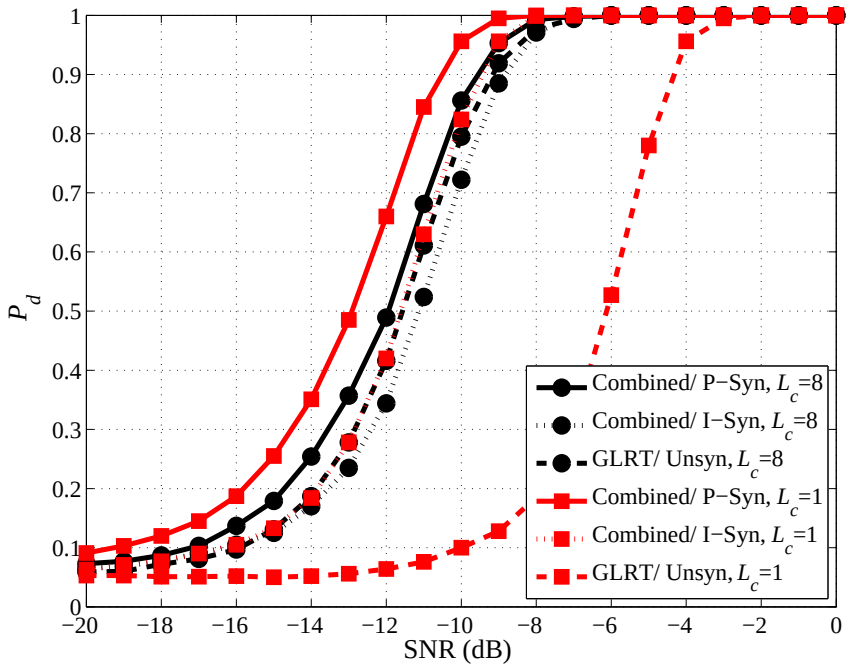

Figure 2.8 Performance comparison of spectrum sensing algorithms in synchronized, imperfectly synchronized and unsynchronized transmission scenarios.

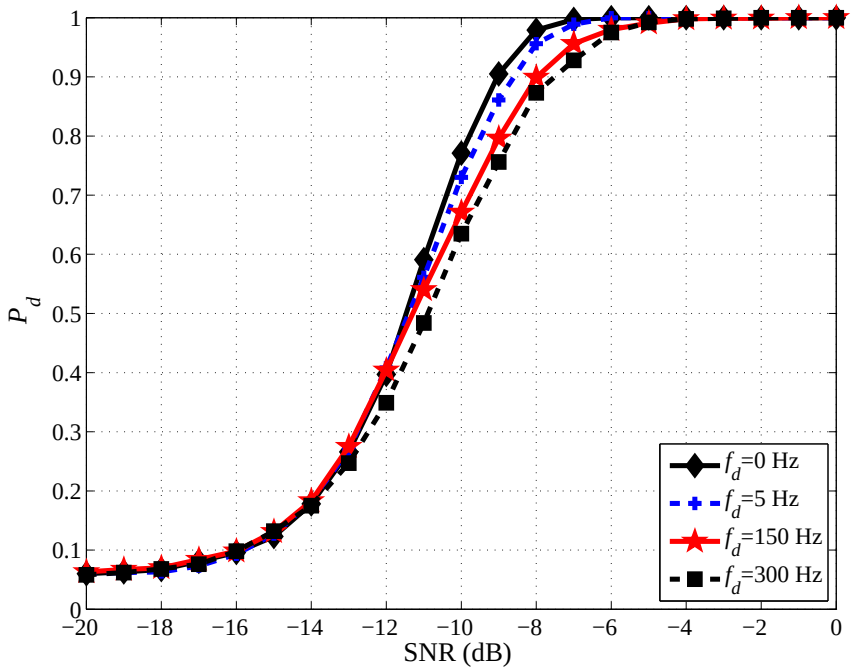

Figure 2.9 Performance comparison of MP-based C-GLRT in a time-varying Rayleigh fading channel, $L_c = L_p = 8$.

chronized case, whereas it gets worse for the unsynchronized case. The latter behavior is, in fact, expected since performance degradation of the proposed detection algorithm for unsynchronized OFDM signals is mainly due to the reduction in the cyclic correlation coefficient. Because the cyclic prefix correlation strongly determines the performance of the detection algorithm in a fading environment with a fewer channel taps, the unsynchronized detection algorithm performs quite poorly in such an environment. In contrast, in a rich multipath environment, for example, with $L_c = 8$, there is only a small performance loss when detecting unsynchronized OFDM signals. In addition, in such an environment, the imperfectly synchronized algorithm performs worse than the unsynchronized algorithm. Considering the added complexity due to performing synchronization, the algorithm developed for unsynchronized OFDM signals in Section 2.6 is a better candidate for spectrum sensing in a rich multipath environment.

Finally, Fig. 2.9 shows the performance of MP-based C-GLRT algorithm over time-varying Rayleigh fading channels when the doppler frequency, f_d, is set to different values. Typical doppler shifts correspond to the mobile velocities of about 3–60 km/h. If the system is operated in frequency bands of 2–4 GHz (e.g., IEEE 802.11, IEEE 802.16 and IEEE 802.20), the doppler shifts are about 5–200 Hz. From the maximum Doppler frequency f_d, the coherence time τ_c can be approximated as $\tau_c = \frac{1}{4f_d}$ [49]. The coherence time τ_c, when $f_d = 200$ Hz is thus obtained to be 1.25 ms. It can be seen that, for typical Doppler frequencies, the coherence time is greater than the sensing time of 0.8 ms and multipath correlation is still very beneficial. Since the change in the channel taps is small during the sensing time, the sensing performance is not substantially degraded, even for fast changes in channel taps.

2.8 Conclusions

In this chapter, a spectrum sensing method for OFDM-based cognitive radio systems has been developed based on the GLRT framework. The key feature in such development is to explicitly take into account the structure (constraint) of the covariance matrix of the underlying OFDM signal so that the ML estimations of unknown parameters are improved, which leads to robust and efficient spectrum sensing tests. In particular, it has been shown that

the CPCC-based test, which was recently proposed in [26], can be obtained as a constrained GLRT for an AWGN channel. It was also shown that the performance of CPCC-based test degrades in a multipath environment. Moreover, by exploiting the multipath correlation in the GLRT framework, an efficient test was obtained which can be sequentially updated with any new reception of OFDM symbols. A simplified MPCC-based test was also presented. Simulation results verify that both the CPCC-based and MP-based C-GLRT algorithms greatly outperform energy detection in an environment with noise uncertainty. The MP-based C-GLRT algorithm performs better than the CPCC-based algorithm in a rich multipath environment. Furthermore, a simple algorithm that combines both the CPCC-based and MP-based C-GLRT algorithms is suggested, which can further improve the detection performance in a multipath environment.

While the studies in this chapter mainly focused on detection of synchronized OFDM signals, the developed algorithms can be applied together with the synchronization algorithm in [45], and they experience only a small performance loss due to imperfect synchronization. Lastly, a simple GRLT-based algorithm was also proposed for the detection of unsynchronized OFDM signals from the primary user. Simulation results demonstrated satisfactory performance of such an algorithm in a rich multipath fading environment.

3. Cooperative Spectrum Sensing in Cognitive Radio Networks with Noncoherent Transmission

3.1 Introduction

As it is pointed out in the preceding chapters, dynamic spectrum sensing is the key in enabling cognitive radio (CR) technology, since it allows for opportunistic identification and use of the available spectrum bands from a licensed primary network. The detection performance of a spectrum sensing algorithm is affected by the wireless channel conditions between the primary user and cognitive radios (CRs). When the channel is in a deep fade, the sensing result can be completely unreliable. Moreover, as the received signal from the primary user is usually very weak, the sensing time may get prohibitively long. Robust spectrum sensing methods that can identify the available licensed spectrum over a reasonable amount of time are of great interest. Recent studies show that, cooperative spectrum sensing methods using energy-based detectors [18,21,50], which can be inexpensively implemented at each cooperative node, are good candidates to significantly improve the sensing performance of the CR network, particularly in a low signal–to–noise ratio (SNR) regime, which is very common in CR applications [47, 50–52] [1].

Accordingly, designing efficient cooperative networks and algorithms to achieve a proper tradeoff between complexity and performance has been the focus of ongoing research. Cooperative spectrum sensing is usually deployed in two successive phases: 1) sensing and 2) reporting. In the sensing phase, each CR performs spectrum sensing for a specific amount

[1] The contribution in this chapter is published in [39].

of time and acquires a decision based on its own observation. In the reporting phase, all the local sensing decisions are transmitted to a fusion center (FC) and then a final decision is made to indicate the absence (hypothesis $\mathcal{H}_0$) or presence (hypothesis $\mathcal{H}_1$) of the primary user [53]. Typically, the reporting link for each cognitive radio uses a control channel to report its sensing result to the FC [54]. Since the control channel bandwidth is limited, a summary of the node decision is reported using one or a few modulated bits [55], [56]. This type of cooperative sensing scheme is called decision fusion [57].

One of the key parameters that strongly affects the sensing performance is the sensing time. A longer sensing time will improve the detection performance. However, if the frame duration is fixed, a longer sensing time will reduce the data transmission time of the secondary users in the cognitive radio network. In [5], the sensing-throughput tradeoff problem has been formulated to find the optimal sensing time that maximizes the secondary users' throughput while providing adequate protection to the primary users. Recognizing that both the sensing time and cooperative fusion scheme affect the throughput of the secondary users, a joint optimization of the sensing time and cooperative fusion scheme was recently considered in [38]. In [38, 52, 58] the k-out-of-N fusion rule has been examined, where all the CRs' reporting links are considered *error free*. However, in practice, reporting channels are neither ideal nor perfectly known at the FC. Therefore, efficient cooperative schemes that consider sensing, transmission and fusion still need to be properly designed to achieve the maximum efficiency.

As aforementioned, because the control channels are band limited, estimating the instantaneous channel gains is impractical. To bypass the need of (instantaneous) channel estimation, simple noncoherent modulation schemes such as on-off keying (OOK) and binary frequency shift keying (BFSK) can be employed for the transmission of local decisions. In fact, [59] has developed sensing algorithms over different fading channels using OOK signaling. However, performance evaluation and optimization of the sensing parameters have not been carried out in [59]. The study in this chapter is similar to [59] in the sense that the spectrum sensing algorithm is developed under unknown Rayleigh fading channels. In addition to OOK signaling, BFSK is also studied. The obtained theoretical analysis and simulation

results will show that BFSK performs better than OOK. Furthermore, cooperative sensing parameters (including the sensing thresholds, combining weights and sensing time) are determined for each transmission scheme to achieve the maximum secondary throughput. In particular, it is verified that the throughput function is a concave function of the sensing time and has a unique solution. As such, efficient algorithms can be readily employed to obtain the optimal sensing time.

The rest of this chapter is organized as follows. Section 3.2 reviews the system model considered in this chapter and describes the spectrum sensing problem. In Section 3.3, the fusion of the local decisions that were transmitted over fading channels is addressed, in which the following two efficient fusion rules are developed: 1) the energy-based fusion rule and 2) the decoding-based fusion rule. Analytical evaluations of these fusion rules are carried out in Section 3.4. Section 3.5 addresses the problem of optimizing the sensing thresholds, the combining weights (for the case of energy-based fusion), and the sensing time to achieve the maximum secondary throughput. Simulation results are presented in Section 3.6. Section 3.7 concludes this chapter.

For convenience, the main mathematical symbols used in this chapter and their meanings are summarized in Table 3.1.

3.2 System Model

Fig. 3.1 illustrates the structure of cooperative spectrum sensing. As shown in the figure, there is one primary source, K CR nodes and one FC. For convenience, the source, CR nodes and fusion center are denoted and indexed by node 0, node i, $i = 1, \ldots, K$, and node $K + 1$, respectively.

All CR nodes operate in a half-duplex mode, i.e., a node cannot simultaneously transmit and receive. Each CR observes the primary user's signal, processes it using an energy detector, and makes a local decision on the binary hypotheses $\mathcal{H}_0$ and $\mathcal{H}_1$. These local decisions are then transmitted over independent Rayleigh fading channels to the FC.

Table 3.1 Mathematical symbols used in Chapter 3.

Symbol	Description
$x(t)$	Low-pass equivalent transmitted signal from the primary user
i	Index of the ith CR
$h_{0,i}$	Channel fading coefficient between node 0 (primary user) and CR node i
E_0	Average transmitted symbol energy of the source
$n_{0,i}(t)$	Filtered Gaussian noise process at CR node i
T_s, $f_s = 1/T_s$	Sampling period, and sampling rate
N	Number of samples collected for spectrum sensing
K	Number of CRs
W	Bandwidth of the BP filter at each CR
γ_i, ϵ_i	Received SNR, and decision threshold at CR node i
p_{f_i}, p_{d_i}	Probability of false alarm, and probability of detection at CR node i
$h_{i,K+1}$	Channel fading coefficient between the ith CR and the FC (in OOK)
$\dot{\boldsymbol{h}}_{i,K+1}$	Channel fading vector between the ith CR and the FC (in BFSK)
u_i, a, $\dot{a}$	Binary decision bit at CR, and transmission powers (OOK, BFSK)
v_i, $\dot{\boldsymbol{v}}_i$	OOK modulated signal, and BFSK modulated signal
ρ, $\dot{\rho}$	Average received SNR at the FC (OOK, BFSK)
z_i, $n_{i,\mathrm{FC}}$	Received signal, and noise component at the FC in OOK transmission
$\dot{\boldsymbol{z}}_i$, $\dot{\boldsymbol{n}}_{i,\mathrm{FC}}$	Received signal, and noise component at the FC in BFSK transmission
η	Sensing threshold at the FC
$\xi_i \triangleq (\sigma^2_{i,K+1}a^2)/\sigma^2_{\mathrm{FC}}$	Channel SNR corresponsing to CR node i at the FC
$\Gamma_i = \lvert z_i\rvert^2/\sigma^2_{\mathrm{FC}}$	Normalized signal energy received from the ith CR at the FC
w_i	The ith weight coefficient at the FC for energy detection
λ	Sensing threshold at the FC
$\hat{u}_i$	Decoded bit of CR i at FC
ϖ_i, ϑ_i	Correct and error probabilities for $\hat{u}_i = 1$ at FC (OOK)
$\wp_{d_i}$, $\wp_{f_i}$	Probabilities of detection, and false alarm of the ith CR at the FC
$\lambda^{(\mathrm{D})}$	Threshold for the decoding-based fusion rule
$\varphi_{0,i}$, $\varphi_{1,i}$	Weights for the decoding-based fusion rule
P_D, P_F	Probability of detection, and probability of false alarm at the FC

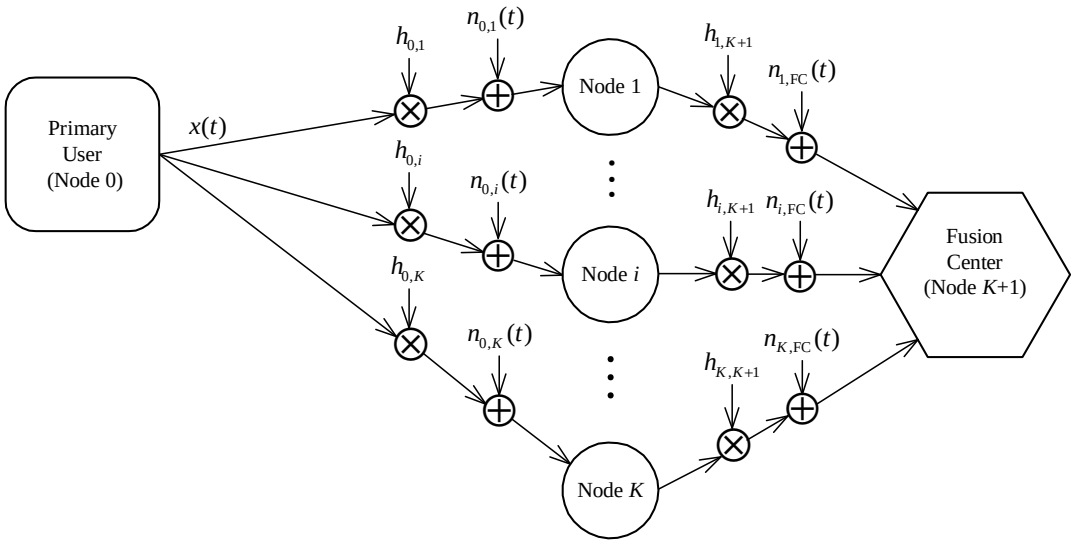

Figure 3.1 Structure of cooperative spectrum sensing under consideration.

Let $x(t)$ be the low-pass equivalent transmitted signal from the primary user. As described in [60], the received signal at each CR node is first passed to an ideal band-pass (BP) filter in order to limit the average noise power. The low-pass equivalent of the output of the BP filter at each node i, $i = 1, \ldots, K$, can be represented as:

$$x_{0,i}(t|\mathcal{H}_0) = n_{0,i}(t) \tag{3.1}$$

$$x_{0,i}(t|\mathcal{H}_1) = \sqrt{E_0} h_{0,i} x(t) + n_{0,i}(t) \tag{3.2}$$

where E_0 is the average transmitted symbol energy of the source, and $h_{0,i} \sim \mathcal{CN}(0, \sigma_{0,i}^2)$ denotes the channel fading coefficient between node 0 (primary user) and CR node i. In addition, $n_{0,i}(t)$ is the filtered additive white Gaussian noise process. The received signal $x_{0,i}(t)$ at each node is sampled with a rate of $f_s = \frac{1}{T_s}$ Hz over a time duration of $\tau = NT_s$ s, where T_s denotes the sampling period, and N denotes the number of samples collected for spectrum sensing. Let W be the bandwidth of the BP filter and assume that the sampling rate f_s is equal to the Nyquist rate of $1/W$ Hz.

Denote by $x_{0,i}[n]$ the received sample at time index n. Then, using (3.1) and (3.2), it

can be expressed as:

$$x_{0,i}[n|\mathcal{H}_0] = n_{0,i}(nT_s), \quad 1 \leq n \leq N; \tag{3.3}$$

$$x_{0,i}[n|\mathcal{H}_1] = \sqrt{E_0} h_{0,i} x(nT_s) + n_{0,i}(nT_s), \quad 1 \leq n \leq N, \tag{3.4}$$

where $n_{0,i}(nT_s)$ are the samples of $n_{0,i}(t)$, which can be shown to be independent and identically distributed (i.i.d.) complex Gaussian random variables with mean 0 and variance $\sigma^2_{\text{CR}} = WN_0$ [60–62]. Here N_0 is the one-sided power spectral density (PSD) of the white noise before the BP filter.

Without loss of generality, the noise variance at each CR node can be normalized to 1, i.e., $\sigma^2_{\text{CR}} = 1$. Then, the distribution of the received sample at each CR node is given as:

$$x_{0,i}[n|\mathcal{H}_0] \sim \mathcal{CN}(0, 1), \tag{3.5}$$

$$x_{0,i}[n|\mathcal{H}_1] \sim \mathcal{CN}(0, \gamma_i + 1), \tag{3.6}$$

where $\gamma_i \triangleq E_0 \sigma^2_{0,i} / \sigma^2_{\text{CR}}$ is the received SNR at each node. After collecting N signal samples, each of the CRs obtains its test statistics as follows:

$$y_i = \frac{1}{N} \sum_{n=1}^{N} |x_{0,i}[n]|^2, \ i = 1, \ldots, K. \tag{3.7}$$

In essence, the above test statistic is a measure of the average energy of the band-limited signal at each CR node over a duration of τ s. When the number of collected samples, N, is large, the central limit theorem can be applied to model y_i under both hypotheses with Gaussian distributions [5, 18, 19, 41]. Specifically [2],

$$f(y_i|\mathcal{H}_0) \sim \mathcal{N}\left(1, \frac{1}{N}\right), \tag{3.8}$$

$$f(y_i|\mathcal{H}_1) \sim \mathcal{N}\left(\gamma_i + 1, \frac{(\gamma_i + 1)^2}{N}\right). \tag{3.9}$$

The decision device at the ith CR node produces a binary decision (0 or 1, corresponding

[2]The notation $\mathcal{N}(\mathbf{m}, \mathbf{\Sigma})$ means a real Gaussian random vector (or variable) with mean vector $\mathbf{m}$ and covariance matrix $\mathbf{\Sigma}$.

to hypothesis $\mathcal{H}_0$ or $\mathcal{H}_1$, respectively) by comparing y_i to a decision threshold ϵ_i as follows:

$$u_i = \begin{cases} 0, \text{ if } y_i < \epsilon_i \\ \\ 1, \text{ if } y_i \geq \epsilon_i \end{cases}.$$

Let p_{f_i} and p_{d_i} denote the probability of false alarm and the probability of detection, respectively, at the ith CR node. They can be obtained as [18]:

$$p_{f_i} = \Pr(y_i \geq \epsilon_i | \mathcal{H}_0) = Q\left((\epsilon_i - 1)\sqrt{\tau f_s}\right), \tag{3.10}$$

$$p_{d_i} = \Pr(y_i \geq \epsilon_i | \mathcal{H}_1) = Q\left(\left(\frac{\epsilon_i}{\gamma_i + 1} - 1\right)\sqrt{\tau f_s}\right). \tag{3.11}$$

After making a local spectrum-sensing decision, every node modulates its binary decision and sends it to the FC. As aforementioned, to bypass the need of channel estimation, simple noncoherent communication schemes, namely OOK and BFSK shall be considered. In transmission with OOK, if a node decides $\mathcal{H}_0$, it remains silent and does not send a signal to the fusion center. In contrast, if the node decides $\mathcal{H}_1$, it sends a signal (specifically a sinusoidal carrier) to the fusion center. In the equivalent baseband representation, this modulation can simply be expressed in the following form:

$$v_i = a u_i. \tag{3.12}$$

On the other hand, for BFSK, the binary decision u_i is mapped to a pair of sinusoidal carriers and the corresponding frequency samples are:

$$\boldsymbol{v}_i = \begin{cases} [\dot{a}, 0]^T, \text{ if } u_i = 1 \\ \\ [0, \dot{a}]^T, \text{ if } u_i = 0 \end{cases} \tag{3.13}$$

Note that the parameters a and $\dot{a}$ in (3.12) and (3.13) set the average transmitted powers of OOK and BFSK schemes, respectively.

The CRs transmit their local sensing decisions to the FC through orthogonal channels. As far as OOK signaling is concerned, the received signal at the FC that corresponds to the ith CR node can be expressed as:

$$z_i = h_{i,K+1} v_i + n_{i,\text{FC}}. \tag{3.14}$$

where $h_{i,K+1} \sim \mathcal{CN}(0, \sigma^2_{i,K+1})$ represents the channel-fading coefficient between the ith CR and the FC, and $n_{i,\mathrm{FC}} \sim \mathcal{CN}(0, \sigma^2_{\mathrm{FC}})$ is the noise component of the received signal at the FC. Now, let ρ denote the average received SNR at the fusion center. For OOK modulation, ρ is given by

$$\rho = \frac{1}{K} \sum_{i=1}^{K} \frac{a^2 \sigma^2_{i,K+1}}{2\sigma^2_{\mathrm{FC}}} \left[\Pr(\mathcal{H}_0) p_{f_i} + \Pr(\mathcal{H}_1) p_{d_i} \right]. \tag{3.15}$$

On the other hand, for BFSK, the received signal at the fusion center from the ith CR node can be represented as a 2×1 vector in the following form:

$$\dot{\boldsymbol{z}}_i = \dot{\boldsymbol{h}}_{i,K+1} \odot \dot{\boldsymbol{v}}_i + \dot{\boldsymbol{n}}_{i,\mathrm{FC}}. \tag{3.16}$$

where the symbol $\odot$ defines element-wise multiplication of two vectors, $\dot{\boldsymbol{h}}_{i,K+1} \sim \mathcal{CN}(\mathbf{0}_{2\times1}, \sigma^2_{i,K+1}\mathbf{I}_{2\times2})$ is the channel vector, $\dot{\boldsymbol{n}}_{i,\mathrm{FC}} \sim \mathcal{CN}(\mathbf{0}_{2\times1}, \sigma^2_{\mathrm{FC}}\mathbf{I}_{2\times2})$ is the noise vector, and $\mathbf{0}_{2\times1}$ denotes the all-zero vector. The average received SNR for BFSK signalling is obtained as:

$$\begin{aligned} \dot{\rho} &= \frac{1}{K} \sum_{i=1}^{K} \left[\frac{\dot{a}^2 \sigma^2_{i,K+1}}{2\sigma^2_{\mathrm{FC}}} \left(\Pr(\mathcal{H}_0) p_{f_i} + \Pr(\mathcal{H}_1) p_{d_i} \right) \right. \\ &+ \left. \frac{\dot{a}^2 \sigma^2_{i,K+1}}{2\sigma^2_{\mathrm{FC}}} \left(\Pr(\mathcal{H}_0)(1 - p_{f_i}) + \Pr(\mathcal{H}_1)(1 - p_{d_i}) \right) \right] \\ &= \frac{\dot{a}^2 \sigma^2_{i,K+1}}{2\sigma^2_{\mathrm{FC}}}. \end{aligned} \tag{3.17}$$

The received signal samples at the FC are collectively represented as vectors $\mathbf{z} = [z_1, \ldots, z_K]^T$ and $\dot{\mathbf{z}} = [\dot{\boldsymbol{z}}_1^T, \ldots, \dot{\boldsymbol{z}}_K^T]^T$ for the OOK and BFSK schemes, respectively. Note that, during the sensing phase, the BFSK transmission of local decisions requires about twice as much the bandwidth as compared with OOK transmission. The relevant question is whether the extra bandwidth required for BFSK results in better sensing performance and higher achievable throughput for the secondary network. This issue will be examined in Sections 3.4 and 4.5 when the analysis and numerical results are presented.

The next section discusses fusion processing of the received signals in $\mathbf{z}$ and $\dot{\mathbf{z}}$ in order to achieve a desirable sensing performance. It starts with the likelihood ratio test (LRT) which

is the optimal fusion algorithm according to the Neyman-Pearson criterion [9]. Given the high complexity of the LRT, two sub-optimal fusion rules, the energy- and decoding-based fusion rules are then developed explicitly for OOK and BFSK schemes. The energy-based fusion rule with carefully designed weights is a simple, yet efficient fusion rule, while the decoding-based fusion rule normally achieves a better performance for high SNRs of the reporting links but at the expense of added complexity in the decoding step. These suboptimal fusion rules are analyzed in detail and the obtained analytical expressions are used in Section 3.5 to optimize the sensing parameters of both the fusion rules.

3.3 Fusion of Local Decisions Transmitted over Imperfect Reporting Channels

In general, the objective at the FC is to keep the probability of detection equal to or above a target value $\bar{P}_D$, while minimizing the probability of false alarm. As discussed in [63], such a sensing problem resembles the Neyman-Pearson hypothesis testing problem [9], and hence, the detection statistics can be obtained using the LRT. The following analysis mainly focuses on OOK signaling, whereas similar analysis can be performed for BFSK signaling.

Consider the vector $\mathbf{z} = [z_1, \ldots, z_K]^T$ of OOK received samples. Because z_i's are independent observations, the likelihood ratio under independent Rayleigh fading channels is [59]:

$$L(\mathbf{z}) = \frac{f(\mathbf{z}|\mathcal{H}_1)}{f(\mathbf{z}|\mathcal{H}_0)} = \prod_{i=1}^{K} \frac{f(z_i|\mathcal{H}_1)}{f(z_i|\mathcal{H}_0)}. \tag{3.18}$$

The quantities $f(z_i|\mathcal{H}_1)$ and $f(z_i|\mathcal{H}_0)$ can be computed as follows:

$$\begin{aligned} f(z_i|\mathcal{H}_1) =& f(z_i|\mathcal{H}_1, u_i = 1)\Pr(u_i = 1|\mathcal{H}_1) + f(z_i|\mathcal{H}_1, u_i = 0)\Pr(u_i = 0|\mathcal{H}_1) \\ =& \frac{1}{\pi}\left(\frac{1}{\sigma_{\mathrm{FC}}^2 + \sigma_{i,K+1}^2 a^2} \mathrm{e}^{-\frac{|z_i|^2}{\sigma_{\mathrm{FC}}^2 + \sigma_{i,K+1}^2 a^2}} p_{d_i} + \frac{1}{\sigma_{\mathrm{FC}}^2} \mathrm{e}^{-\frac{|z_i|^2}{\sigma_{\mathrm{FC}}^2}} (1 - p_{d_i})\right). \end{aligned} \tag{3.19}$$

$$\begin{aligned} f(z_i|\mathcal{H}_0) =& f(z_i|\mathcal{H}_0, u_i = 1)\Pr(u_i = 1|\mathcal{H}_0) + f(z_i|\mathcal{H}_0, u_i = 0)\Pr(u_i = 0|\mathcal{H}_0) \\ =& \frac{1}{\pi}\left(\frac{1}{\sigma_{\mathrm{FC}}^2 + \sigma_{i,K+1}^2 a^2} \mathrm{e}^{-\frac{|z_i|^2}{\sigma_{\mathrm{FC}}^2 + \sigma_{i,K+1}^2 a^2}} p_{f_i} + \frac{1}{\sigma_{\mathrm{FC}}^2} \mathrm{e}^{-\frac{|z_i|^2}{\sigma_{\mathrm{FC}}^2}} (1 - p_{f_i})\right). \end{aligned} \tag{3.20}$$

It then follows that:

$$L(\mathbf{z}) = \prod_{i=1}^{K} \frac{\frac{1}{\sigma_{\mathrm{FC}}^2+\sigma_{i,K+1}^2 a^2} \mathrm{e}^{-\frac{|z_i|^2}{\sigma_{\mathrm{FC}}^2+\sigma_{i,K+1}^2 a^2}} p_{d_i} + \frac{1}{\sigma_{\mathrm{FC}}^2} \mathrm{e}^{-\frac{|z_i|^2}{\sigma_{\mathrm{FC}}^2}} (1-p_{d_i})}{\frac{1}{\sigma_{\mathrm{FC}}^2+\sigma_{i,K+1}^2 a^2} \mathrm{e}^{-\frac{|z_i|^2}{\sigma_{\mathrm{FC}}^2+\sigma_{i,K+1}^2 a^2}} p_{f_i} + \frac{1}{\sigma_{\mathrm{FC}}^2} \mathrm{e}^{-\frac{|z_i|^2}{\sigma_{\mathrm{FC}}^2}} (1-p_{f_i})}. \tag{3.21}$$

The main disadvantage of using the aforementioned likelihood ratio as the decision statistic for the spectrum sensing problem considered in this paper is that it is mathematically intractable. As a consequence, to obtain a sensing threshold at the FC, extensive simulation has to be performed. Moreover it is very difficult, if not impossible, to optimize other sensing parameters to achieve an optimal sensing performance. In light of this difficulty, the following subsections develop two suboptimal fusion rules: 1) an energy-based fusion rule which is essentially a *soft* fusion of the received signals, and 2) a decoding-based fusion rule that combines the *hard* decisions of the signals received from individual CRs.

3.3.1 Energy-Based Fusion Rule

First, note that, under certain scenarios, the LRT can be approximated by an energy-based fusion rule. The first scenario is when the decisions made by individual sensors are reliable, i.e., $p_{f_i} \ll 1 - p_{f_i}$ and $p_{d_i} \gg 1 - p_{d_i}$. Then $L(\mathbf{z})$ is well approximated as:

$$L(\mathbf{z}) \simeq \prod_{i=1}^{K} \left(\frac{\sigma_{\mathrm{FC}}^2}{\sigma_{\mathrm{FC}}^2 + \sigma_{i,K+1}^2 a^2} \right) \frac{\mathrm{e}^{-\frac{|z_i|^2}{\sigma_{\mathrm{FC}}^2+\sigma_{i,K+1}^2 a^2}} p_{d_i}}{\mathrm{e}^{-\frac{|z_i|^2}{\sigma_{\mathrm{FC}}^2}} (1-p_{f_i})}. \tag{3.22}$$

By taking the logarithm of the above expression, the following test is obtained:

$$\sum_{i=1}^{K} \frac{\xi_i}{1+\xi_i} \frac{|z_i|^2}{\sigma_{\mathrm{FC}}^2} \underset{\mathcal{H}_0}{\overset{\mathcal{H}_1}{\lessgtr}} \eta \tag{3.23}$$

where η is a sensing threshold at the FC and ξ_i is the ith channel SNR at the FC, given by $\xi_i \triangleq (\sigma_{i,K+1}^2 a^2)/\sigma_{\mathrm{FC}}^2$. The above test describes a *weighted* energy detector, where the weights are determined by the SNRs of the reporting channels. Furthermore, for the case that $\xi_i \gg 1$, $\xi_i/(1+\xi_i) \simeq 1$ and (3.23) simplifies to the conventional energy detector, which is $\sum_{i=1}^{K} |z_i|^2 \underset{\mathcal{H}_0}{\overset{\mathcal{H}_1}{\gtrless}} \eta$.

The second scenario is when the reporting channels are in a very poor condition, or equivalently $\sigma^2_{\text{FC}} \to \infty$. As it is verified in [59], the LRT simplifies to

$$\sum_{i=1}^{K} (p_{di} - p_{fi}) \frac{\xi_i}{1+\xi_i} \frac{|z_i|^2}{\sigma^2_{\text{FC}}} \underset{\mathcal{H}_0}{\overset{\mathcal{H}_1}{\gtrless}} \eta, \tag{3.24}$$

which is also in the form of a weighted energy detector.

Based on the simplified energy-based tests in (3.23) and (3.24), a more general weighted energy detector at the fusion center is proposed as follows:

$$\Gamma = \sum_{i=1}^{K} w_i \Gamma_i \underset{\mathcal{H}_0}{\overset{\mathcal{H}_1}{\gtrless}} \lambda. \tag{3.25}$$

where $\Gamma_i = |z_i|^2/\sigma^2_{\text{FC}}$ is the normalized signal energy received from the ith CR, $w_i > 0$ is the weight coefficient assigned to the ith CR, and λ is the sensing threshold used at the FC. For the specific case in (3.23), the weights are given as functions of the channel SNRs at the FC, whereas for the case of very low "reporting" SNRs in (3.24), the weights mainly depend on the local performance of the CRs. For the general form in (3.25), the weights can be optimized for a given sensing performance according to both local sensing performance at CRs and the quality of the reporting links.

With BFSK signalling, a similar derivation gives the following general weighted energy detector:

$$\dot{\Gamma} = \sum_{i=1}^{K} \dot{w}_i \dot{\Gamma}_i \underset{\mathcal{H}_0}{\overset{\mathcal{H}_1}{\gtrless}} \dot{\lambda}. \tag{3.26}$$

where $\dot{\Gamma}_i = \frac{|\dot{z}_i[0]|^2 - |\dot{z}_i[1]|^2}{\sigma^2_{\text{FC}}}$ and $\dot{z}_i[0]$ and $\dot{z}_i[1]$ are the components of vector $\mathbf{z}_i = [\dot{z}_i[0], \dot{z}_i[1]]^T$ in (3.16). The above test makes a final sensing decision by determining the signal component (i.e., frequency) that has the dominant weighted energy.

3.3.2 Decoding-Based Fusion Rule

As shown, the weighted energy detectors in (3.25) and (3.26) involve simple linear combinations of signals received from CRs. One alternative and relevant strategy is to make a hard decision on the signal received from each individual CR and then combine the hard

decisions in some way. To see what would be the combining scheme of the hard decisions, proceed as follows.

Let $\boldsymbol{u} = [u_1, \ldots, u_K]$ denote the vector of bits sent by CRs, and $\hat{\boldsymbol{u}} = [\hat{u}_1, \ldots, \hat{u}_K]$ denote the vector of decoded bits at the FC. Whether $\hat{u}_i$ is the same as u_i, $i = 1, \ldots, K$ is determined by the correct/error probabilities of detection over the ith reporting channel. For OOK modulation, the detection rule for the ith reporting channel is:

$$\frac{|z_i|^2}{\sigma_{\mathrm{FC}}^2} \underset{\hat{u}_i=0}{\overset{\hat{u}_i=1}{\gtrless}} \frac{(1+\xi_i)\ln(1+\xi_i)}{\xi_i} \triangleq \varrho_i. \tag{3.27}$$

It follows that the correct and error probabilities for $\hat{u}_i = 1$ are as follows:

$$\begin{aligned} \varpi_i &= \Pr\left(\hat{u}_i = 1 | u_i = 1\right) = \Pr\left(\frac{|z_i|^2}{\sigma_{\mathrm{FC}}^2} > \varrho_i \Big| u_i = 1\right) = \mathrm{e}^{-\frac{\varrho_i}{1+\xi_i}}, \\ \vartheta_i &= \Pr\left(\hat{u}_i = 1 | u_i = 0\right) = \Pr\left(\frac{|z_i|^2}{\sigma_{\mathrm{FC}}^2} > \varrho_i \Big| u_i = 0\right) = \mathrm{e}^{-\varrho_i}. \end{aligned} \tag{3.28}$$

Similarly, for $\hat{u}_i = 0$, one has

$$\begin{aligned} \Pr\left(\hat{u}_i = 0 | u_i = 1\right) &= 1 - \varpi_i, \\ \Pr\left(\hat{u}_i = 0 | u_i = 0\right) &= 1 - \vartheta_i. \end{aligned} \tag{3.29}$$

For BFSK modulation, the detection rule is:

$$|\dot{\boldsymbol{z}}_i[1]|^2 - |\dot{\boldsymbol{z}}_i[2]|^2 \underset{\hat{u}_i=0}{\overset{\hat{u}_i=1}{\gtrless}} 0. \tag{3.30}$$

The correct and error probabilities can be easily shown to be:

$$\begin{aligned} \varpi_i &= \Pr\left(\hat{u}_i = 1 | u_i = 1\right) = \Pr\left(\hat{u}_i = 0 | u_i = 0\right) = \frac{1 + 2\dot{\xi}_i}{2(1+\dot{\xi}_i)}, \\ \vartheta_i &= \Pr\left(\hat{u}_i = 1 | u_i = 0\right) = \Pr\left(\hat{u}_i = 0 | u_i = 1\right) = \frac{1}{2(1+\dot{\xi}_i)} \\ &= 1 - \varpi_i. \end{aligned} \tag{3.31}$$

where $\dot{\xi}_i \triangleq \frac{\dot{a}^2 \sigma_{i,K+1}^2}{2\sigma_{\mathrm{FC}}^2}$ is the SNR of the ith reporting channel at the fusion center under BFSK transmission.

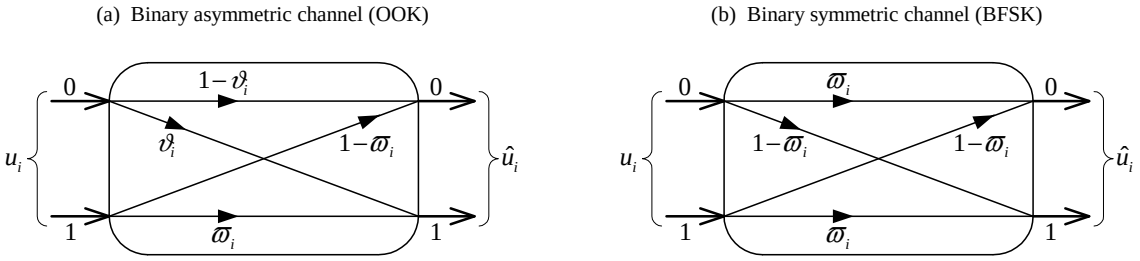

Figure 3.2 Equivalent binary channel models for OOK and BFSK transmissions.

Note that the transmission and detection of bit u_i from the ith CR can be represented succinctly by binary asymmetric channel (BAC) and binary symmetric channel (BSC) models corresponding to OOK and BFSK, respectively (see Fig. 3.2).

Now, at the fusion center, the following likelihood ratio can be formed for the decoded bits:

$$\hat{L}(\hat{\boldsymbol{u}}) = \frac{\Pr(\hat{\boldsymbol{u}}|\mathcal{H}_1)}{\Pr(\hat{\boldsymbol{u}}|\mathcal{H}_0)} = \frac{\prod_{i=1}^{K}(1-\wp_{d_i})^{(1-\hat{u}_i)}\wp_{d_i}^{\hat{u}_i}}{\prod_{i=1}^{K}(1-\wp_{f_i})^{(1-\hat{u}_i)}\wp_{f_i}^{\hat{u}_i}}. \tag{3.32}$$

where $\wp_{d_i} = \Pr(\hat{u}_i = 1|\mathcal{H}_1)$ and $\wp_{f_i} = \Pr(\hat{u}_i = 1|\mathcal{H}_0)$ are the probabilities of detection and probabilities of false alarm associated with the decoded bit $\hat{u}_i$. They are determined as follows:

$$\begin{aligned}\wp_{d_i} = \Pr(\hat{u}_i = 1|\mathcal{H}_1) =& \Pr(\hat{u}_i = 1|u_i = 1)\Pr(u_i = 1|\mathcal{H}_1) \\ &+ \Pr(\hat{u}_i = 1|u_i = 0)\Pr(u_i = 0|\mathcal{H}_1) \\ =& p_{d_i}\varpi_i + (1-p_{d_i})\vartheta_i. \end{aligned} \tag{3.33}$$

$$\begin{aligned}\wp_{f_i} = \Pr(\hat{u}_i = 1|\mathcal{H}_0) =& \Pr(\hat{u}_i = 1|u_i = 1)\Pr(u_i = 1|\mathcal{H}_0) \\ &+ \Pr(\hat{u}_i = 1|u_i = 0)\Pr(u_i = 0|\mathcal{H}_0) \\ =& p_{f_i}\varpi_i + (1-p_{f_i})\vartheta_i. \end{aligned} \tag{3.34}$$

Working with the logarithm of (3.32), the decoding-based fusion rule is given as:

$$L^{(\mathrm{D})}(\hat{\boldsymbol{u}}) = \sum_{i=1}^{K}\varphi_{0,i}(1-\hat{u}_i) + \varphi_{1,i}\hat{u}_i \underset{0}{\overset{1}{\gtrless}} \lambda^{(\mathrm{D})} \tag{3.35}$$

where $\lambda^{(\mathrm{D})}$ is the threshold, while the weights are $\varphi_{0,i} = \log\left((1-\wp_{d_i})\,/\,(1-\wp_{f_i})\right)$ and $\varphi_{1,i} = \log\left(\wp_{d_i}/\wp_{f_i}\right)$. Thus, according to (3.35), the combining of hard decisions is also a

linear combination, where the weights are inherently adjusted according to both the decision of the ith CR and the quality of its reporting link. In addition, note that the fusion rule in (3.35) resembles the one proposed in [38] for error-free reporting channels.

To optimize different sensing parameters and to compare the performance of the energy- and decoding-based fusion rules developed in this section, the next section obtains the expressions of the probability of detection, P_D, and the probability of false alarm, P_F, at the FC for both fusion rules.

3.4 Analysis of the Fusion Rules

Note that the focus of this chapter is to investigate how a large number of cheaply implemented sensors can help improving sensing performance. If the purpose is to find the exact distribution of the test statistics in (3.25), it can be done by using the distribution of quadratic forms in Gaussian random variables (for example, see [64]). However, by using the exact distribution, the individual roles of sensing parameters will not be easily reflected and interpreted in the analysis, and the optimization problem becomes intractable. On the other hand, finding the distribution of the detection statistics in (3.35) for the case of decoding-based fusion rule is a mathematically complex and intractable problem. By focusing on the case that the number of CRs K is large enough, the distributions of the test statistics in both fusion rules are approximated by Gaussian distributions according to the central limit theorem. Thus, to describe the statistical distributions of the test statistics, it suffices to find the mean and variance of the corresponding approximated Gaussian distribution for each fusion rule. The task is performed in the following two sections.

3.4.1 Energy-Based Fusion Rule

The mean and variance of the test statistics (3.25) can be obtained as:

$$\mu_j = \mathrm{E}[\Gamma|\mathcal{H}_j] = \sum_{i=1}^{K} w_i \mathrm{E}[\Gamma_i|\mathcal{H}_j] = \sum_{i=1}^{K} w_i \mu_{i,j},\ j = 0, 1, \tag{3.36}$$

$$\nu_j^2 = \mathrm{var}[\Gamma|\mathcal{H}_j] = \sum_{i=1}^{K} w_i^2 \mathrm{var}[\Gamma_i|\mathcal{H}_j] = \sum_{i=1}^{K} w_i^2 \nu_{i,j}^2,\ j = 0, 1. \tag{3.37}$$

where $\mu_{i,j} = \mathrm{E}[\Gamma_i|\mathcal{H}_j]$ and $\nu_{i,j}^2 = \mathrm{var}[\Gamma_i|\mathcal{H}_j]$. Using the total probability theorem yields:

$$\begin{aligned} f(\Gamma_i|\mathcal{H}_j) =& f(\Gamma_i|\mathcal{H}_j, u_i = 1)\Pr(u_i = 1|\mathcal{H}_j) \\ &+ f(\Gamma_i|\mathcal{H}_j, u_i = 0)\Pr(u_i = 0|\mathcal{H}_j),\ j = 0, 1. \end{aligned} \tag{3.38}$$

Therefore,

$$\begin{aligned} \mu_{i,0} = \mathrm{E}[\Gamma_i|\mathcal{H}_0] &= \mathrm{E}[\Gamma_i|\mathcal{H}_0, u_i = 1]\Pr(u_i = 1|\mathcal{H}_0) + \mathrm{E}[\Gamma_i|\mathcal{H}_0, u_i = 0]\Pr(u_i = 0|\mathcal{H}_0) \\ &= (\xi_i + 1)\, p_{f_i} + \left(1 - p_{f_i}\right) = p_{f_i}\xi_i + 1, \end{aligned} \tag{3.39}$$

$$\begin{aligned} \mu_{i,1} = \mathrm{E}[\Gamma_i|\mathcal{H}_1] &= \mathrm{E}[\Gamma_i|\mathcal{H}_1, u_i = 1]\Pr(u_i = 1|\mathcal{H}_1) + \mathrm{E}[\Gamma_i|\mathcal{H}_1, u_i = 0]\Pr(u_i = 0|\mathcal{H}_1) \\ &= (\xi_i + 1)\, p_{d_i} + (1 - p_{d_i}) = p_{d_i}\xi_i + 1. \end{aligned} \tag{3.40}$$

The variance of Γ_i is obtained as:

$$\nu_{i,j}^2 = \mathrm{var}[\Gamma_i|\mathcal{H}_j] = \mathrm{E}[\Gamma_i^2|\mathcal{H}_j] - \mathrm{E}^2[\Gamma_i|\mathcal{H}_j],\ j = 0, 1. \tag{3.41}$$

First

$$\begin{aligned} \mathrm{E}[\Gamma_i^2|\mathcal{H}_0] =& \mathrm{E}[\Gamma_i^2|\mathcal{H}_0, u_i = 0]\Pr(u_i = 0|\mathcal{H}_0) + \mathrm{E}[\Gamma_i^2|\mathcal{H}_0, u_i = 1]\Pr(u_i = 1|\mathcal{H}_0) \\ =& 2\left(\xi_i + 1\right)^2 p_{f_i} + 2(1 - p_{f_i}) = 2\left[(\xi_i + 1)^2 p_{f_i} + (1 - p_{f_i})\right]. \end{aligned} \tag{3.42}$$

Similarly,

$$\mathrm{E}[\Gamma_i^2|\mathcal{H}_1] = 2\left[(\xi_i + 1)^2 p_{d_i} + (1 - p_{d_i})\right]. \tag{3.43}$$

It follows from (3.39), (3.40), (3.42) and (3.43) that:

$$\nu_{i,0}^2 = 2\left[\xi_i^2 + \xi_i\right] p_{f_i} - \xi_i^2 {p_{f_i}}^2 + 1, \tag{3.44}$$

$$\nu_{i,1}^2 = 2\left[\xi_i^2 + \xi_i\right] p_{d_i} - \xi_i^2 {p_{d_i}}^2 + 1. \tag{3.45}$$

Based on the distribution $\mathcal{N}\left(\mu_j, \nu_j^2\right)$ of $\Gamma|\mathcal{H}_j$, the probability of false alarm and probability of detection at the fusion center are obtained as:

$$P_F(\boldsymbol{p_f}, \boldsymbol{w}, \lambda) = \Pr\left(\Gamma > \lambda | \mathcal{H}_0\right) = Q\left(\frac{\lambda - \mu_0}{\nu_0}\right), \tag{3.46}$$

$$P_D(\boldsymbol{p_d}, \boldsymbol{w}, \lambda) = \Pr\left(\Gamma > \lambda | \mathcal{H}_1\right) = Q\left(\frac{\lambda - \mu_1}{\nu_1}\right). \tag{3.47}$$

where $\boldsymbol{p_f} \triangleq \left\{p_{f_1}, \ldots, p_{f_K}\right\}$, $\boldsymbol{p_d} \triangleq \{p_{d1}, \ldots, p_{dK}\}$ and $\boldsymbol{w} \triangleq \{w_1, \ldots, w_K\}$. The quantities μ_0 and ν_0 are functions of $\boldsymbol{p_f}$, while $\boldsymbol{w}$, μ_1 and ν_1 are functions of $\boldsymbol{p_d}$ and $\boldsymbol{w}$. Therefore, P_F and P_D are expressed as functions of the sets $\boldsymbol{p_f}$, $\boldsymbol{p_d}$ and $\boldsymbol{w}$.

As far as BFSK is concerned, the mean and variance of the detection statistics $\dot{\Gamma}$ in (3.26) can be obtained in the same manner as that done for OOK signaling. The results are:

$$\begin{aligned}
\dot{\mu}_{i,0} =& \mathrm{E}(\dot{\Gamma}_i|\mathcal{H}_0) = 2\dot{\xi}_i\left[2p_{f_i} - 1\right], \\
\dot{\mu}_{i,1} =& \mathrm{E}(\dot{\Gamma}_i|\mathcal{H}_1) = 2\dot{\xi}_i\left[2p_{d_i} - 1\right].
\end{aligned} \tag{3.48}$$

$$\begin{aligned}
\dot{\nu}_{i,0}^2 =& 2\left[4\dot{\xi}_i^2 + 2\dot{\xi}_i + 1\right] - 4\dot{\xi}_i^2\left[2p_{f_i} - 1\right]^2, \\
\dot{\nu}_{i,1}^2 =& 2\left[4\dot{\xi}_i^2 + 2\dot{\xi}_i + 1\right] - 4\dot{\xi}_i^2\left[2p_{d_i} - 1\right]^2.
\end{aligned} \tag{3.49}$$

Consequently, the probabilities of false alarm and the probability of detection at the FC under BFSK are:

$$\dot{P}_F(\boldsymbol{p_f}, \boldsymbol{w}, \dot{\lambda}) = Q\left(\frac{\dot{\lambda} - \dot{\mu}_0}{\dot{\nu}_0}\right), \ \dot{P}_D(\boldsymbol{p_d}, \boldsymbol{w}, \dot{\lambda}) = Q\left(\frac{\dot{\lambda} - \dot{\mu}_1}{\dot{\nu}_1}\right). \tag{3.50}$$

where $\dot{\mu}_j = \sum_{i=1}^K \dot{w}_i\dot{\mu}_{i,j}$ and $\dot{\nu}_j^2 = \sum_{i=1}^K \dot{w}_i^2\dot{\nu}_{i,j}^2$, $j = 0, 1$.

3.4.2 Decoding-Based Fusion Rule

To perform the analysis, first from (3.33) and (3.34), one has:

$$\begin{aligned}
\mathrm{E}[\hat{u}_i|\mathcal{H}_0] =& \wp_{f_i} = \varpi_i p_{f_i} + \vartheta_i(1 - p_{f_i}), \\
\mathrm{E}[\hat{u}_i|\mathcal{H}_1] =& \wp_{d_i} = \varpi_i p_{d_i} + \vartheta_i(1 - p_{d_i}).
\end{aligned} \tag{3.51}$$

Using the above expression along with (3.35), one can obtain the means of the test statistic as:

$$\begin{aligned} m_0 =& \mathrm{E}[L^{(\mathrm{D})}(\hat{\boldsymbol{u}})|\mathcal{H}_0] = \sum_{i=1}^{K} m_{i,0}, \\ m_{i,0} =& \left[\varpi_i p_{f_i} + \vartheta_i(1-p_{f_i})\right]\left[\varphi_{1,i} - \varphi_{0,i}\right] + \varphi_{0,i}. \end{aligned} \tag{3.52}$$

$$\begin{aligned} m_1 =& \mathrm{E}[L^{(\mathrm{D})}(\hat{\boldsymbol{u}})|\mathcal{H}_1] = \sum_{i=1}^{K} m_{i,1}, \\ m_{i,1} =& \left[\varpi_i p_{d_i} + \vartheta_i(1-p_{d_i})\right]\left[\varphi_{1,i} - \varphi_{0,i}\right] + \varphi_{0,i}. \end{aligned} \tag{3.53}$$

The variances are:

$$\begin{aligned} \delta_0^2 =& \mathrm{Var}[L^{(\mathrm{D})}(\hat{\boldsymbol{u}})|\mathcal{H}_0] = \sum_{i=1}^{K} \delta_{i,0}^2, \\ \delta_{i,0}^2 =& \left[m_{i,0} - m_{i,0}^2\right]\left[\varphi_{1,i} - \varphi_{0,i}\right]^2. \end{aligned} \tag{3.54}$$

$$\begin{aligned} \delta_1^2 =& \mathrm{Var}[L^{(\mathrm{D})}(\hat{\boldsymbol{u}})|\mathcal{H}_1] = \sum_{i=1}^{K} \delta_{i,1}^2, \\ \delta_{i,1}^2 =& \left[m_{i,1} - m_{i,1}^2\right]\left[\varphi_{1,i} - \varphi_{0,i}\right]^2. \end{aligned} \tag{3.55}$$

Thus, the false alarm and detection probabilities of the decoding-based fusion rule are obtained as:

$$\begin{aligned} P_F^{(\mathrm{D})}(\boldsymbol{p_f}, \lambda^{(\mathrm{D})}) &= \Pr\left(L^{(\mathrm{D})}(\hat{\boldsymbol{u}}) > \lambda^{(\mathrm{D})} \middle| \mathcal{H}_0\right) \\ &= Q\left(\frac{\lambda^{(\mathrm{D})} - m_0}{\delta_0}\right), \end{aligned} \tag{3.56}$$

$$\begin{aligned} P_D^{(\mathrm{D})}(\boldsymbol{p_d}, \lambda^{(\mathrm{D})}) &= \Pr\left(L^{(\mathrm{D})}(\hat{\boldsymbol{u}}) > \lambda^{(\mathrm{D})} \middle| \mathcal{H}_1\right) \\ &= Q\left(\frac{\lambda^{(\mathrm{D})} - m_1}{\delta_1}\right). \end{aligned} \tag{3.57}$$

Note that the aforementioned analysis for the decoding-based fusion rule applies to both OOK and BFSK schemes. The difference between the two schemes is reflected in the equivalent channel models in Fig. 3.2: For BFSK one has $\vartheta_i = 1 - \varpi_i$.

After establishing the fusion rules at the fusion center and obtaining the expressions of P_F, P_D, $P_F^{(\mathrm{D})}$ and $P_D^{(\mathrm{D})}$, the next important step is to find the sensing parameters for each fusion rule. The next section considers the secondary throughput as the objective function to be maximized and shows how different sensing parameters can be efficiently determined to achieve this goal.

3.5 Joint Optimization of the Sensing Parameters

It is desired to obtain the maximum secondary throughput while ensuring that the primary user is sufficiently protected. To this end, sensing parameters at the CRs and the fusion center should be efficiently optimized. In the following sections, the optimization problems for both the energy-based and decoding-based fusion rules are addressed.

3.5.1 Optimizing Parameters for Energy-Based Fusion Rule

For the energy-based fusion rule, the sensing thresholds at the CR nodes and the fusion center, namely $\boldsymbol{\epsilon}$, λ, the sensing weights $\boldsymbol{w}$ and the sensing time τ can be jointly optimized to achieve the maximum secondary throughput. Similar to [5], the optimization problem is formulated as:

$$\begin{aligned} &\max_{\tau,\boldsymbol{\epsilon},\boldsymbol{w},\lambda} R_0(\tau,\boldsymbol{\epsilon},\boldsymbol{w},\lambda) \equiv \\ &\max_{\tau,\boldsymbol{\epsilon},\boldsymbol{w},\lambda} C_0 \Pr(\mathcal{H}_0)\left(1-\frac{\tau}{T}\right)\left[1-P_F(\boldsymbol{p_f},\boldsymbol{w},\lambda)\right] \\ &\text{s.t.} \quad P_D(\boldsymbol{p_d},\boldsymbol{w},\lambda) \geq \bar{P}_D. \end{aligned} \tag{3.58}$$

In the aforementioned optimization problem, C_0 represents the throughput of the secondary network in the absence of the primary user, $\bar{P}_D$ determines the required protection to the primary user and T is the total frame duration. The aforementioned equation explains that, when there is no false alarm, the CR network is able to transmit with a rate of $C_0\left(1-\frac{\tau}{T}\right)\left[1-P_F(\boldsymbol{p_f},\boldsymbol{w},\lambda)\right]$ b/s.

In (3.58), because P_D and P_F are functions of $p_{d_i}(\tau,\epsilon_i)$ and $p_{f_i}(\tau,\epsilon_i)$ at the CR nodes, they are functions of τ and $\boldsymbol{\epsilon}$ as well. Observe that, in (3.58), only $P_F(\boldsymbol{p_f},\boldsymbol{w},\lambda)$ and $P_D(\boldsymbol{p_d},\lambda,\boldsymbol{w})$

are functions of the sensing thresholds and weights. Therefore, (3.58) is equivalent to:

$$\begin{aligned} &\max_{\tau,\boldsymbol{\epsilon},\boldsymbol{w},\lambda} R_0(\tau,\boldsymbol{\epsilon},\boldsymbol{w},\lambda) \equiv \\ &\max_{\tau}\left[\left(1-\frac{\tau}{T}\right)\left(1-\min_{\boldsymbol{\epsilon},\boldsymbol{w},\lambda} P_F(\boldsymbol{p_f},\boldsymbol{w},\lambda)\right)\right] \\ &\text{s.t.} \quad P_D(\boldsymbol{p_d},\boldsymbol{w},\lambda) \geq \bar{P}_D \end{aligned} \tag{3.59}$$

The optimization problem in (3.59) is separated into two sub-problems.

Sub-Problem 1 (Obtaining the optimal sensing thresholds and combining weights):

$$\begin{aligned} \max_{\boldsymbol{\epsilon},\boldsymbol{w},\lambda} R_0(\boldsymbol{\epsilon},\boldsymbol{w},\lambda) \equiv \min_{\boldsymbol{\epsilon},\boldsymbol{w},\lambda} P_F(\boldsymbol{p_f},\boldsymbol{w},\lambda) \\ \text{s.t.} \quad P_D(\boldsymbol{p_d},\boldsymbol{w},\lambda) \geq \bar{P}_D \end{aligned} \tag{3.60}$$

The following proposition offers a solution to the preceding problem.

Proposition 1: The set of sensing thresholds which optimize the sub-problem in (3.60) are closely approximated as:

$$\epsilon_i^* = \left(1+\frac{1}{\gamma_i}\right)\log\left(\gamma_i+1\right), \tag{3.61}$$

and

$$\lambda^*(\tau) = \bar{\nu}_1(\tau)\, Q^{-1}\left(\bar{P}_D\right) + \bar{\mu}_1(\tau). \tag{3.62}$$

The combining weights are obtained as:

$$w_i^*(\tau) = \xi_i \frac{\overline{p}_{di}(\tau) - \overline{p}_{f_i}(\tau)}{\bar{\nu}_{i,0}(\tau)}. \tag{3.63}$$

In (3.62), $\bar{\mu}_1(\tau)$ and $\bar{\nu}_1(\tau)$ are obtained by replacing $p_d = \overline{p}_{di}(\tau)$ and $w_i = w_i^*(\tau)$ in (3.36), (3.37), (3.40), and (3.45). That is,

$$\bar{\mu}_1(\tau) \triangleq \sum_{i=1}^{K} w_i^*(\tau)\left[\overline{p}_{di}(\tau)\xi_i + 1\right]. \tag{3.64}$$

and

$$\bar{\nu}_1^2(\tau) \triangleq \sum_{i=1}^{K} w_i^{*2}(\tau)\left(2\left[\xi_i^2+\xi_i\right]\overline{p}_{di}(\tau) - \xi_i^2 \overline{p}_{di}^{\,2}(\tau) + 1\right). \tag{3.65}$$

Furthermore, using (3.10), (3.11), one has:

$$\begin{aligned}\overline{p}_{f_i}(\tau) &= p_{f_i}(\tau,\epsilon_i)\Big|_{\epsilon_i=\epsilon_i^*} \\ &= Q\left(\left(\left(1+\frac{1}{\gamma_i}\right)\log\left(1+\gamma_i\right)-1\right)\sqrt{\tau f_s}\right). \end{aligned} \tag{3.66}$$

and

$$\begin{aligned}\overline{p}_{d_i}(\tau) &= p_{d_i}(\tau,\epsilon_i)\Big|_{\epsilon_i=\epsilon_i^*} \\ &= Q\left(\left(\frac{1}{\gamma_i}\log\left(1+\gamma_i\right)-1\right)\sqrt{\tau f_s}\right). \end{aligned} \tag{3.67}$$

Also in (3.63), $\bar{\nu}_{i,0}(\tau)$ is defined using (3.44) as:

$$\bar{\nu}_{i,0}^2(\tau) \triangleq 2\left[\xi_i^2+\xi_i\right]\overline{p}_{f_i}(\tau) - \xi_i^2\overline{p}_{f_i}^{\,2}(\tau)+1. \tag{3.68}$$

Proof: Refer to Appendix B.1.

Remark: When the received SNR at each CR node is very small, i.e., $\gamma_i \ll 1$, one can use the tight approximation $\log(\gamma_i+1) \simeq \gamma_i - \frac{\gamma_i^2}{2}$, which is obtained by truncating the Taylor series. As a result, ϵ_i^* can be closely approximated as $\epsilon_i^* = (1+\frac{1}{\gamma_i})\log(\gamma_i+1) \simeq (\gamma_i+1)(1-\frac{\gamma_i}{2})$. Consequently, p_{f_i} and p_{d_i} at each CR node are obtained as:

$$\begin{aligned} p_{f_i}\Big|_{\epsilon_i=\epsilon_i^*} =& Q\left(\left((1+\frac{1}{\gamma_i})\log(\gamma_i+1)\right)\sqrt{\tau f_s}\right) \\ \simeq& Q\left(\frac{1}{2}\gamma_i\left(1-\gamma_i\right)\sqrt{\tau f_s}\right)Q\left(\frac{\gamma_i}{2}\sqrt{\tau f_s}\right), \\ p_{d_i}\Big|_{\epsilon_i=\epsilon_i^*} \simeq& Q\left(-\frac{\gamma_i}{2}\sqrt{\tau f_s}\right). \end{aligned} \tag{3.69}$$

It then follows that, $p_{d_i}+p_{f_i} \simeq 1$. This approximation is also helpful to make a comparison between the average received SNRs at the fusion center for BFSK and OOK. By comparing (3.15) and (3.17) and using $p_{f_i}+p_{d_i} \simeq 1$, it is seen that $\dot{\rho} \simeq 2(\frac{\dot{a}}{a})^2\rho$.

Sub-Problem 2 (Optimizing the sensing time): To obtain the optimal sensing time, the problem in (3.58) is simplified by replacing the optimal sensing parameters from solving *Sub-Problem 1* into (3.58). This gives the following problem:

$$\max_{\tau}\ \bar{R}_0(\tau) = C_0\Pr(\mathcal{H}_0)\left(1-\frac{\tau}{T}\right)\left(1-\bar{P}_F(\tau)\right), \tag{3.70}$$

where it follows from (3.46) that:

$$\bar{P}_F(\tau) = Q\left(\frac{\lambda^*(\tau) - \bar{\mu}_0(\tau)}{\bar{\nu}_0(\tau)}\right). \tag{3.71}$$

The parameters $\bar{\mu}_0(\tau)$ and $\bar{\nu}_0(\tau)$ are obtained by substituting $p_d = \overline{p}_{di}(\tau)$ and $w_i = w_i^*(\tau)$ in (3.44), (3.36) and (3.37). This yields:

$$\bar{\mu}_0(\tau) \triangleq \sum_{i=1}^{K} w_i^*(\tau)\left[\overline{p}_{f_i}(\tau)\xi_i + 1\right], \tag{3.72}$$

and

$$\bar{\nu}_0^2(\tau) \triangleq \sum_{i=1}^{K} (w_i^*(\tau))^2 \left(2\left[\xi_i^2 + \xi_i\right]\overline{p}_{f_i}(\tau) - \xi_i^2 \overline{p}_{f_i}^{\,2}(\tau) + 1\right). \tag{3.73}$$

To solve (3.70), the following proposition is employed.

Proposition 2: $\bar{R}_0(\tau)$ is a concave function for $\bar{P}_F(\tau) \leq 0.5$ and has a unique maximum point.

Proof: See Appendix B.2.

Because $\bar{R}_0(\tau)$ is a uniomodal function, (3.70) can be easily solved by standard algorithms such as the bisection method, Golden section method, Newton's method, etc. [63]. Table 3.2 summarizes the algorithm to find the sensing parameters for the energy-based fusion rule.

3.5.2 Optimizing Parameters for the Decoding-Based Fusion Rule

The throughput optimization problem for decoding-based fusion rule can be described in the same fashion as it was done for the energy-based fusion rule in (3.58). The major difference is that there is no need to optimize for the combining weights as they are already incorporated in the fusion rule itself (see (3.35)). Similar sub-problems to that of (3.60) and (3.70) are discussed as follows.

Sub-Problem 3 (Obtaining the optimal sensing thresholds):

$$\begin{aligned} &\min_{\boldsymbol{\epsilon}, \lambda^{(\mathrm{D})}} \; P_F^{(\mathrm{D})}(\boldsymbol{p_f}, \lambda^{(\mathrm{D})}) \\ &\text{s.t.} \quad P_D^{(\mathrm{D})}(\boldsymbol{p_d}, \lambda^{(\mathrm{D})}) \geq \bar{P}_D \end{aligned} \tag{3.74}$$

Table 3.2 Procedure to find the sensing parameters for energy-based fusion rule.

1	Set $P_D = \bar{P}_D$.
2	Find the sensing threshold at each CR node ϵ_i^* from (4.12): $\epsilon_i^* = \left(1 + \frac{1}{\gamma_i}\right) \log\left(\gamma_i + 1\right).$
3	Obtain $\bar{P}_F(\tau)$ from (3.71) as: $\bar{P}_F(\tau) = Q\left(\frac{\lambda^*(\tau) - \bar{\mu}_0(\tau)}{\bar{\nu}_0(\tau)}\right).$
4	Find the sensing duration τ^* by solving (3.70). $\tau^* = \arg\max\left\{\left(1 - \frac{\tau}{T}\right)\left(1 - \bar{P}_F(\tau)\right)\right\}$
5	Find the sensing threshold at the fusion center, λ^*, from (3.62): $\lambda^* = \bar{\nu}_1\left(\tau^*\right) Q^{-1}\left(\bar{P}_D\right) + \bar{\mu}_1\left(\tau^*\right)$
6	Find the weight coefficients at the fusion center, w_i^*, from (3.63): $w_i^* = \xi_i \left(\frac{\overline{p}_{d_i}(\tau^*) - \overline{p}_{f_i}(\tau^*)}{\bar{\nu}_{i,0}(\tau^*)}\right)$

As it is verified in Appendix B.3, the set of sensing thresholds that optimize the aforementioned subproblem are closely approximated as:

$$\epsilon_i^{(\mathrm{D})*} = \left(1 + \frac{1}{\gamma_i}\right) \log\left(\gamma_i + 1\right) \tag{3.75}$$

$$\lambda^{(\mathrm{D})*}(\tau) = \bar{\delta}_1(\tau) Q^{-1}\left(\bar{P}_D\right) + \bar{m}_1(\tau) \tag{3.76}$$

where $\bar{\delta}_1(\tau)$ and $\bar{m}_1(\tau)$ are obtained from (3.53) and (3.55) by replacing p_{d_i} with $\overline{p}_{d_i}(\tau)$ and p_{f_i} with $\overline{p}_{f_i}(\tau)$.

Similar to Proposition 2, it can be verified that using the above sensing thresholds leads to a concave throughput function in terms of the sensing time. A such, the algorithm to optimize the sensing parameters for the decoding-based fusion rule is basically the same as that given in Table 3.2.

3.6 Simulation Results

This section presents numerical and simulation results on the performance of the proposed fusion rules with noncoherent transmission of local decisions over i.i.d Rayleigh fading channels. Each point in the simulation curves is obtained with 10^6 random realizations for

the primary transmitted signal, fading channels and noise. For each realization, the CR decision is transmitted over the Rayleigh fading channel to the FC. The sensing and fusion results are then obtained by averaging over all the realizations. For convenience, in all simulations, it is simply assumed that $\Pr(\mathcal{H}_0) = \Pr(\mathcal{H}_1) = 0.5$. Unless stated otherwise, the *average* received SNR is set to be 7 dB (i.e., $\rho = \dot{\rho} = 7$ dB) at the FC, whereas $K = 50$ and $f_s = 1$ MHz. When $\gamma_i = \gamma$ and $\rho_i = \rho$, i.e., all the SNRs at the CRs and FC are respectively, equal, equal combining is used in the energy-based fusion rule. All the simulation and analytical results are obtained by applying the optimized sensing threshold at the CR nodes given as $\epsilon_i^* = (1 + \frac{1}{\gamma_i})\log(\gamma_i + 1)$.

First, Fig. 3.3 depicts the probability of a missed detection versus the average SNR at the CRs when the energy-based fusion rule is used. The figure considers the case when all CR nodes have the same average SNR, i.e., $\gamma_i = \gamma$ for $i = 1, \ldots, K$. The missed detection probabilities are determined at each CR ($p_m = 1 - p_d$) and at the fusion center with OOK ($P_M = 1 - P_D$) and BFSK ($\dot{P}_M = 1 - \dot{P}_D$). For this figure $N = 0.2\text{ms} \times 1\text{MHz} = 200$ samples. Similarly, Fig. 3.4 illustrates the false alarm probability at the nodes (p_f) and the fusion center (P_F and $\dot{P}_F$). From these two figures, it is clearly seen that cooperation among CRs significantly decreases the missed detection probability and the false alarm probability at the fusion center. It can also be observed that the analytical and simulation results match very well. Furthermore, one can see that the BFSK scheme performs better than OOK for the same set of parameters.

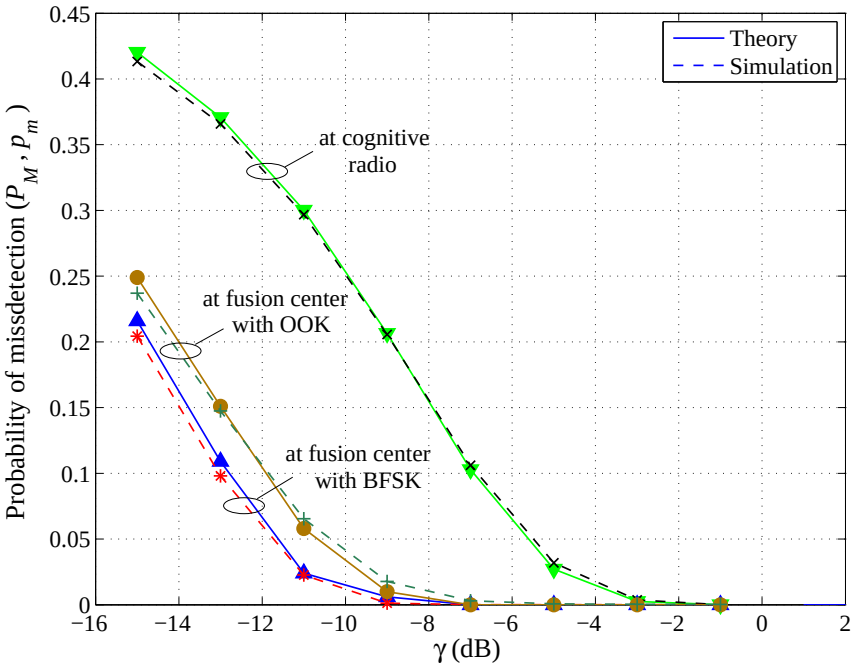

Figure 3.3 Theoretical and simulation results for the missed detection probabilities at the nodes and fusion center versus the SNR at each node. The energy-based fusion rule is applied.

Figs. 3.5 and 3.6 compare the false alarm probabilities achieved with the energy- and decoding-based fusion rules when $\bar{P}_D = 0.9$, $K = 30$, $N = 100$ and the SNRs of all reporting links are equal (i.e., $\xi_i = \xi$) and vary from -5 to 15 dB. For both figures, the received SNRs at the CRs are set at $\gamma = -10$dB. The two figures clearly show that for both OOK and BFSK schemes, the decoding-based fusion rule performs better than energy-based fusion rule at high "reporting" channel SNR. This result can be explained by the fact that performing hard decisions on individual reporting channels at high "reporting" SNRs can completely remove the noise on each channel (i.e., most of the decision bits can be perfectly retrieved at the FC), whereas the noise is always accumulated in the energy-based fusion rule. At low "reporting" channel SNR values, both decoding-based and energy-based fusion rules have the same performance for OOK scheme, whereas for BFSK, the energy-based fusion rule outperforms the decoding-based fusion rule. From the results in Figs. 3.5 and 3.6, it can be concluded that for low channel SNRs, the energy-based fusion rule is preferred over the decoding-based fusion rule as it has a lower complexity while delivering equal or better

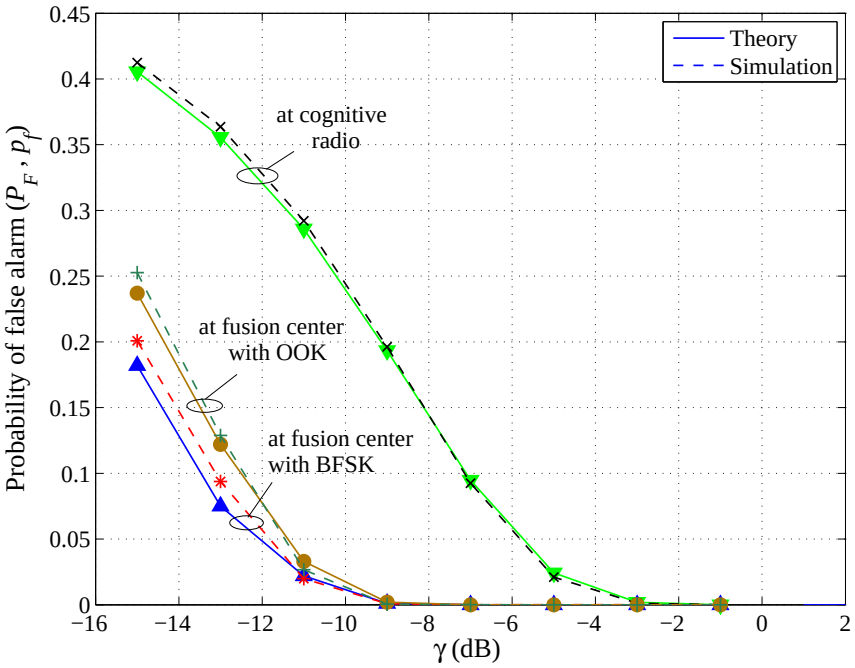

Figure 3.4 Theoretical and simulation results for the false alarm probabilities at the nodes and fusion center versus the SNR at each node. The energy-based fusion rule is applied.

performance.

In Fig. 3.7, the normalized throughput, defined as $(1-\tau/T)\left(1-\bar{P}_F(\tau)\right)$ versus an entire time frame of 1ms, which is equivalent to $1,000$ samples, is illustrated when λ is selected to fix the probability of a missed detection at $1-\bar{P}_D = 0.1$ while $\gamma_i = \gamma = -15$ dB. It is shown that, for the same set of parameters (p_f, p_d, $\bar{P}_D$ and average SNR), BFSK signalling achieves a higher secondary throughput than OOK signalling. As mentioned, the superior performance of BFSK over OOK in terms of achievable secondary throughput in the transmission phase comes at the expense of a larger transmission bandwidth used in the sensing phase. It is also shown that the throughput functions are concave and BFSK attains a maximum point which is higher than that of the OOK scheme by about 0.1. This case means that, by employing BFSK for sensing, the CR network is capable of transmitting about 10% more data than the rate achieved with OOK. By comparing the analytical and simulation results, it is observed that the central limit theorem which has been employed for analytical evaluations leads to

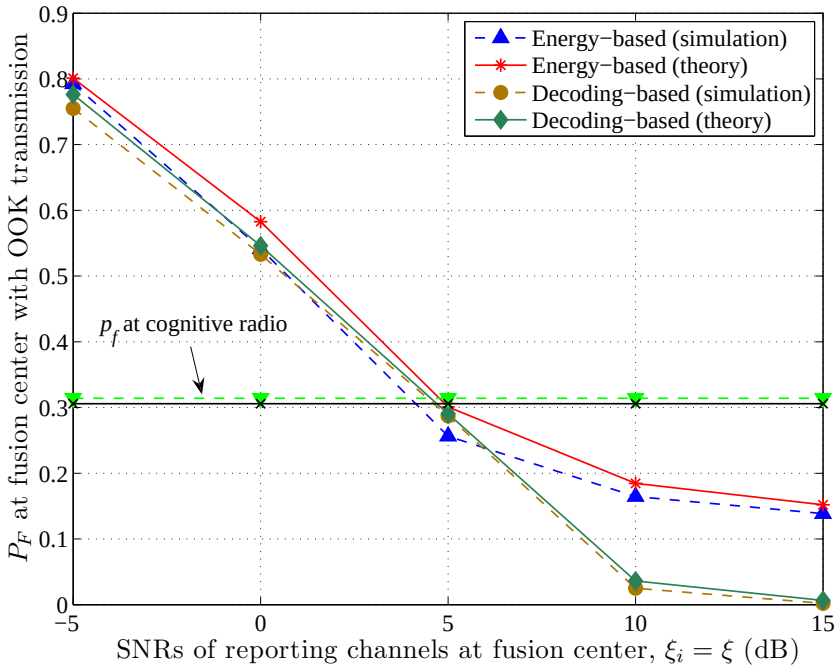

Figure 3.5 Comparison of the false alarm probability achieved with energy-based and decoding-based fusion rules. The SNRs of individual reporting channels at the FC are the same ($\xi_i = \xi$) and vary. OOK transmission is considered.

a very good approximation even when the number of CRs is limited to $K = 50$.

Fig. 3.8 compares the analytical evaluations for throughput of BFSK and OOK when $\gamma_i = \gamma = -15$ dB and two sensing thresholds are employed at CR nodes. The first one, ϵ^* minimizes the probability of error, p_e and the second one, denoted as *optimal* ϵ, is obtained by exhaustive search to minimize $\bar{P}_F(\tau, \epsilon) = Q(\phi(\tau, \epsilon))$ (OOK scheme) and $\dot{\bar{P}}_F(\tau, \epsilon) = Q(\dot{\phi}(\tau, \epsilon))$ (BFSK scheme) by maximizing the arguments of the Q functions (see Appendix B.3). It is seen that for OOK signaling, there is only a slight difference between the achievable secondary throughputs obtained with the two different threshold values. On the other hand, for BFSK signalling, the throughputs resulting from both thresholds overlap. As discussed in Appendix B.3, the reason is that ϵ^* is a very good approximation to the optimal ϵ for BFSK. In order to justify the above discussion using analytical evaluations, the arguments of Q functions, i.e., $\phi(\tau, \epsilon)$ and $\dot{\phi}(\tau, \epsilon)$, are evaluated and plotted as functions of sensing time for

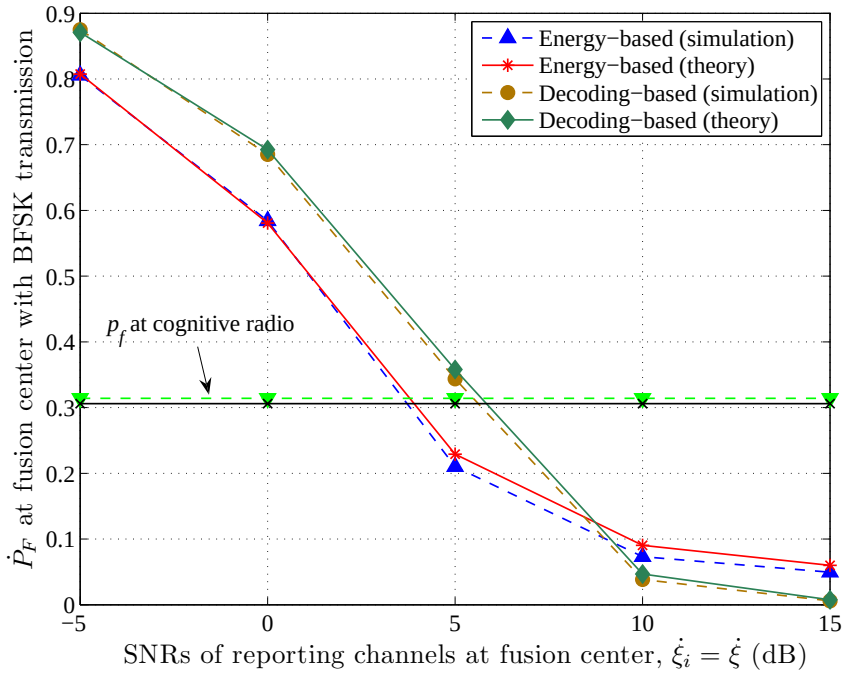

Figure 3.6 Comparison of the false alarm probability achieved with energy-based and decoding-based fusion rules. The SNRs of individual reporting channels at FC are the same ($\dot{\xi}_i = \dot{\xi}$) and vary. BFSK transmission is considered.

two different sensing thresholds in Fig 3.9. As can be seen, for BFSK, both thresholds give the same result, while for OOK, approximations cause a slight difference between the arguments. This difference increases with sensing time since the approximations work well around $p_f = p_d = 0.5$ (see Appendix B.1). As the sensing time increases, p_f and p_d diverge from 0.5 causing the discarded terms in the approximation of $\phi(\tau, \epsilon)$ to become more significant.

Finally, simulation results in Figs. 3.10 and 3.11 demonstrate the effect of choosing the weighting coefficients in the energy-based fusion rule ($\boldsymbol{w}$ in (3.25) and (3.26)) for the situation when the SNRs are different at the CR nodes as well as at the FC. For comparison purposes, the CRs are divided into 10 groups of 5 CRs each and two different scenarios are examined. In the first scenario, all CRs transmit their sensing results to the fusion center with equal SNR of $\xi = \dot{\xi} = 5$ dB, but each group of CRs experiences a different "sensing" SNR from the primary user. The "sensing" SNRs spread over a large range of values given as

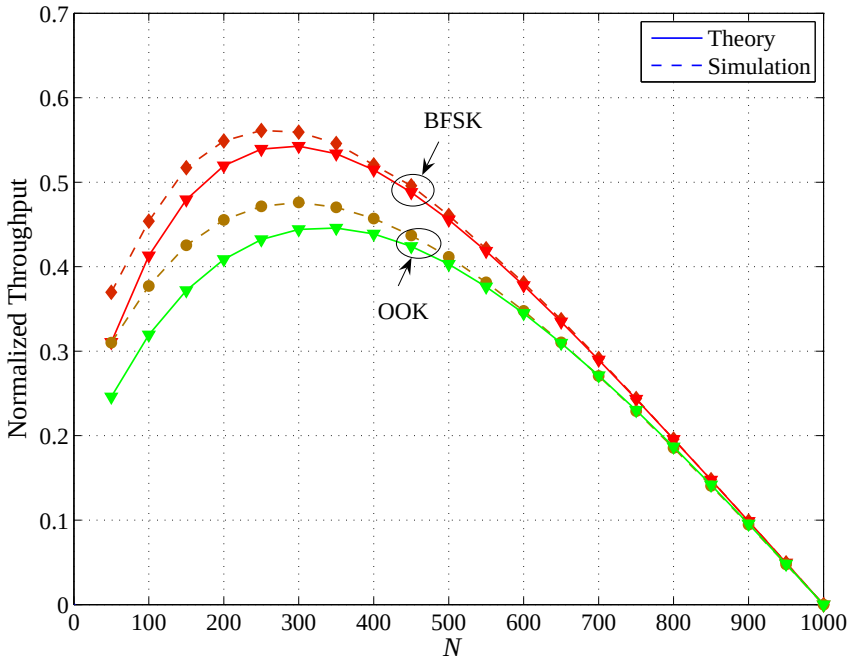

Figure 3.7 Comparison of analytical and simulation results for throughput with $\epsilon = \epsilon^*$ and energy-based fusion rule.

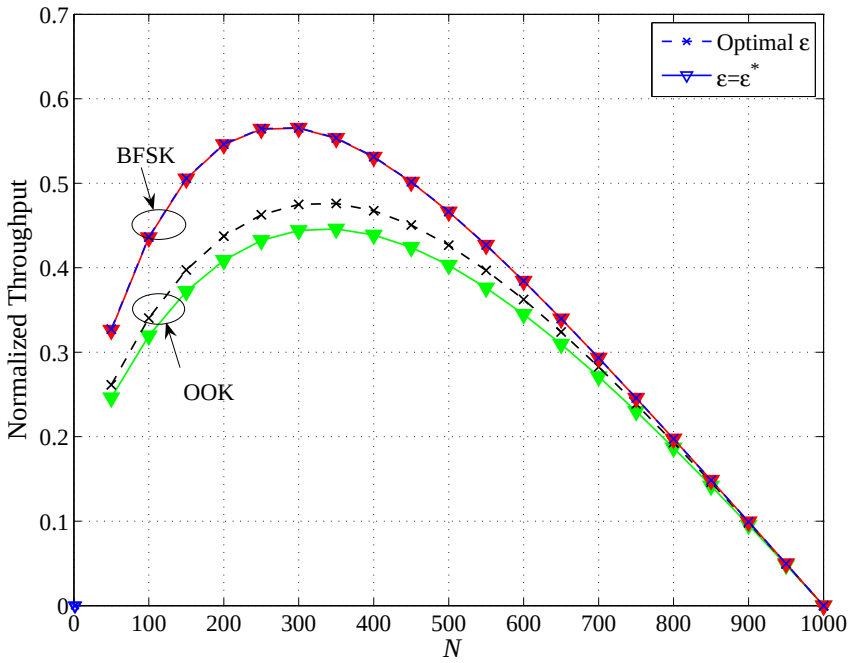

Figure 3.8 Comparison of analytical throughput for different sensing thresholds used at CR nodes when the energy-based fusion rule is employed.

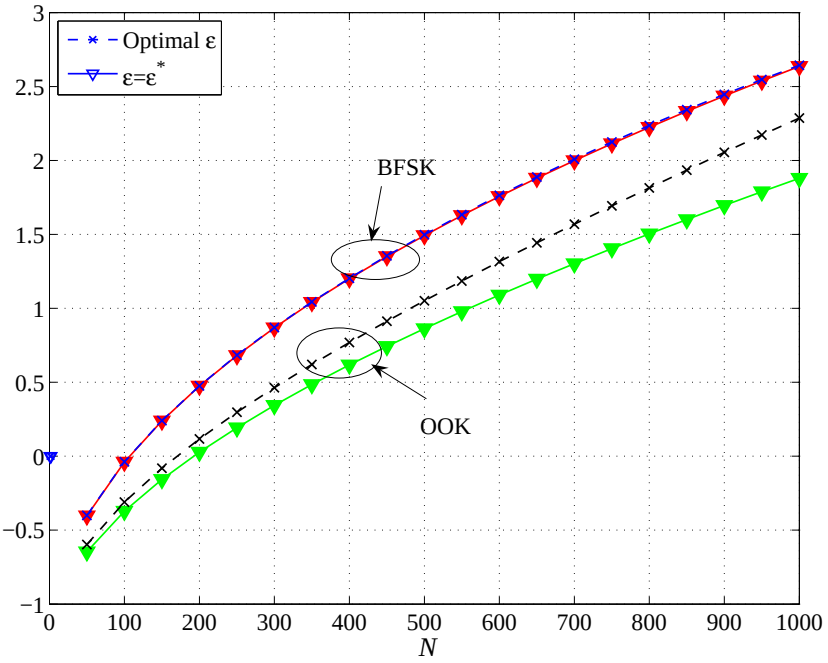

Figure 3.9 Comparing the arguments of Q functions for $\bar{P}_F(\tau)$ and $\dot{\bar{P}}_F(\tau)$ for different sensing thresholds under the energy-based fusion rule.

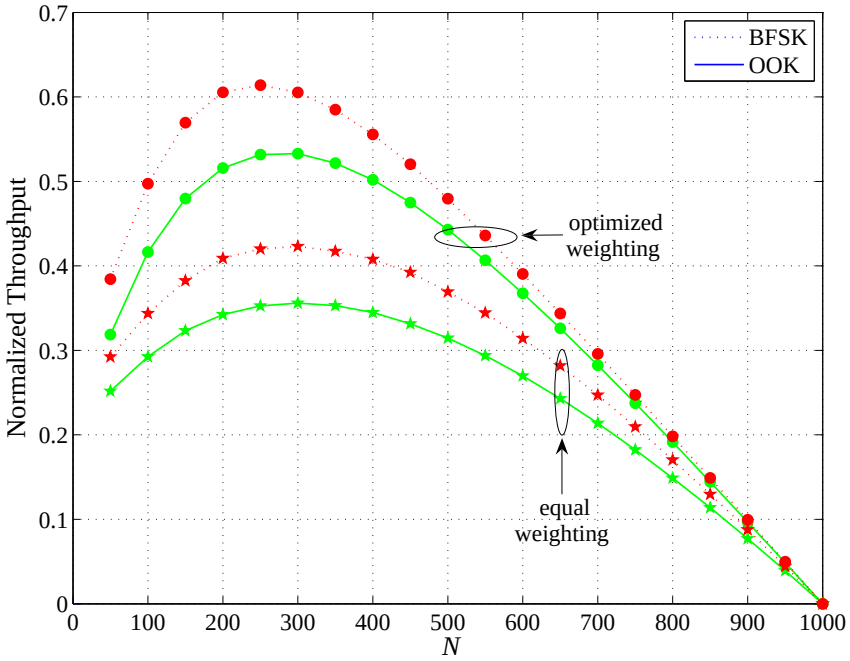

Figure 3.10 Comparison of using equal and optimized weights in the energy-based fusion rule for scenario 1.

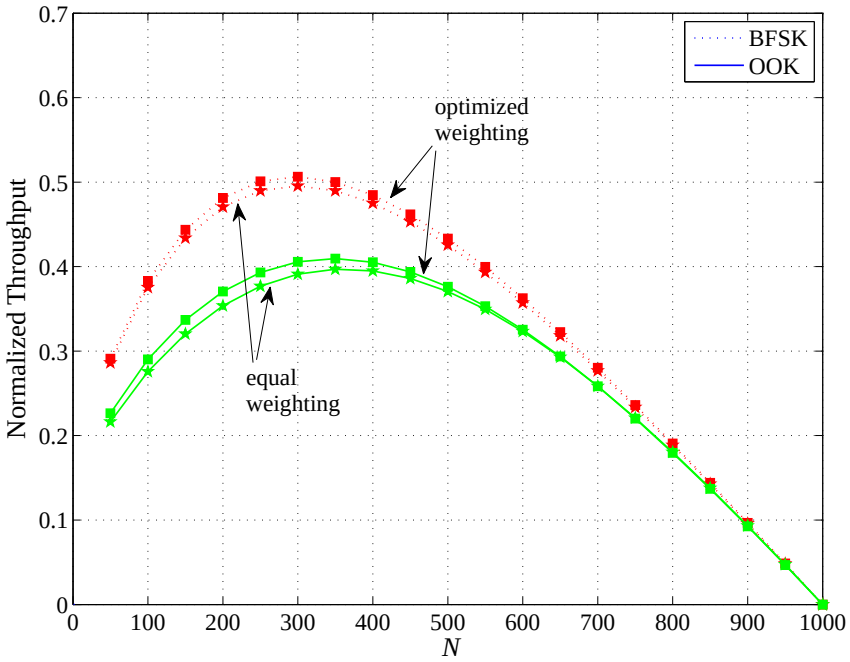

Figure 3.11 Comparison of using equal and optimized weights in the energy-based fusion rule for scenario 2.

$\{-10, -15, -12, -18, -19, -20, -21, -22, -23, -24\}$ dB. In the second scenario, the "sensing" SNRs are considered to be $\{-11, -12, -13, -14, -15, -15, -14, -13, -12, -11\}$ dB, which in comparison to the first scenario are higher in average and have a smaller variation. Moreover, for the second scenario, the received signals at the FC experience different SNRs of $\{-10, -5, 0, 5, 10, -10, -5, 0, 5, 10\}$ dB. As can be seen, both figures show that the throughput is improved with the proposed optimal combining weights as compared to the simple equal combining in both cases of OOK and BFSK signalling. The improvement is much larger in the first scenario than in the second scenario. This is because in the second scenario the sensing results at CRs are almost the same, and even with the optimal combining weights, the reporting links with high SNRs are mainly involved in the combining (with weights close to 1), which is essentially equal combining.

3.7 Conclusions

In this chapter, cooperative spectrum sensing schemes for cognitive radio networks where the channel impairments prevent the CR signals to be perfectly received at the FC were proposed and analyzed. To overcome the problem of channel estimation, the noncoherent OOK and BFSK signalling schemes were employed to transmit binary decisions to the fusion center. Since the likelihood-ratio fusion rule is not practically attractive nor analytically tractable, energy- and decoding-based fusion rules were developed. For each of these fusion rules, the optimum sensing parameters are obtained to achieve the maximum secondary throughput. For both fusion rules, it was shown that the secondary throughput with the optimum sensing parameters is a concave function of sensing time and hence there exists an optimum solution for the sensing time. The excellent match between simulation and analytical results verify the accuracy of the analysis.

4. A Decoding-Based Fusion Rule for Cooperative Spectrum Sensing with Nonorthogonal Transmission of Local Decisions

4.1 Introduction

As outlined in the previous chapters, cognitive radio (CR) is an attractive technology to deal with the spectrum scarcity issue and to provide wireless access to potential users by opportunistically detecting the unused licensed bands. The technique of distributed spectrum sensing has also been studied as an attractive technology for enabling a reliable spectrum sensing technique, in which the observations of CR nodes are collected and transmitted to a fusion center (FC) for a final sensing decision. The fusion center aggregates the information pieces transmitted from the CRs and combines them according to some fusion rule in order to make a final decision about the absence (denoted by $\mathcal{H}_0$) or presence (denoted by $\mathcal{H}_1$) of the primary user in the band of the interest. The research in the preceding chapter proposes a collaborative weighted energy-based fusion rule with noncoherent transmission of one-bit decisions where the sensing results are reported to the FC over *orthogonal* channels. The main focus is to optimize the sensing thresholds at the local CRs, the combining gains at the fusion center and the sensing time to maximize the secondary throughput of a CR network[1]. However, for large-scale CR networks, assigning orthogonal channels to all CRs might lead to an unaffordable bandwidth expenditure.

Since the transmission of the local sensing data to the FC can be costly in terms of

[1]The contribution in this chapter is published in [65].

bandwidth requirement, particularly for large-scale distributed CR networks, some form of local data compression is preferred in which each CR sends to the FC only one or a few bits of data, representing its local sensing result. To further reduce bandwidth consumption while maintaining simple fusion processing, *nonorthogonal* transmission of local decisions can be employed by means of on-off keying (OOK) [37]. In such a transmission technique, the CRs are allocated with nonorthogonal (correlated) signature vectors (SVs). If the length of the signature vectors is substantially less than the number of CRs, the bandwidth efficiency can be significantly improved [37, 66].

This chapter adopts the nonorthogonal transmission framework of [37] for the reporting phase. Different from [37], the main contribution here is to develop a low-complexity decoding-based fusion rule as an alternative to the energy-based fusion rule in order to efficiently suppress the noise in the received signal at the fusion center and achieve a better sensing performance when the reporting channels are strong. The performance of the proposed fusion rule is analyzed and compared with the performance of the energy-based fusion rule under different scenarios. It has to be noted that the most of the development in this chapter mimics that of Chapter 3 but is included for completeness so that Chapter 4 can be read independently of Chapter 3 with the essential difference that there is nonorthogonal transmission of the decisions.

The chapter is organized as follows. Section 4.2 introduces the model of cooperative spectrum sensing with nonorthogonal transmission of local decisions. Section 4.3 summarizes the energy-based fusion rule, whereas the decoding-based fusion rule is developed and analyzed in Section 4.4. Simulation results are presented and discussed in Section 4.5. Finally, Section 4.6 draws conclusions. It is also noted that most of the mathematical symbols used in this chapter are the same as those of Chapter 3 (see Table 3.1).

4.2 System Model

The structure of cooperative spectrum sensing under consideration is illustrated in Fig. 4.1. There is one primary source, K CR nodes, and one fusion center. For simplicity, the

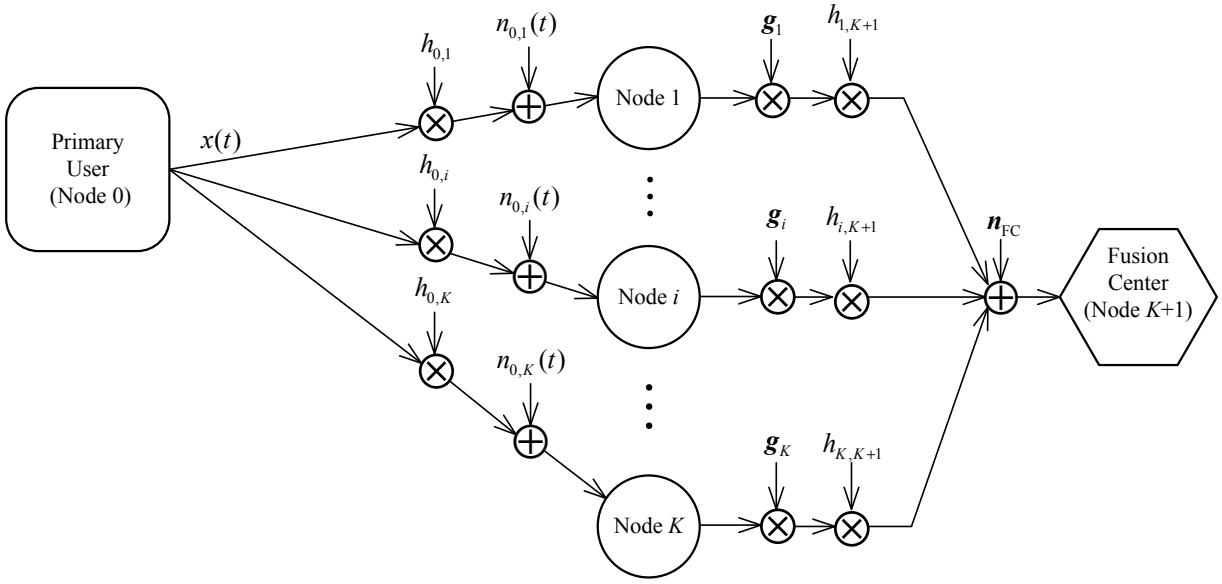

Figure 4.1 Structure of cooperative spectrum sensing with nonorthogonal transmission in the reporting phase.

primary source is indexed by node 0, CR nodes are denoted by nodes i, $i = 1, \ldots, K$, and the fusion center is identified as node $K + 1$.

During the *sensing* period, each CR collects its observations from the primary user's signal in order to make a local decision on the binary hypothesis $\mathcal{H}_0$ or $\mathcal{H}_1$. Due to the presence of Rayleigh fading channels between the primary user and CRs, the local observations at CRs can be treated as independent and identically distributed (i.i.d) random variables. For processing the observations at each CR, an energy detector is implemented. In particular, local binary decisions are obtained by comparing the energy of the collected signals to a sensing threshold.

In the *reporting* phase, the local decisions are transmitted to the fusion center over Rayleigh fading channels. For such transmission, the same framework presented in [37] is adopted. The local decision at the kth CR is multiplied (i.e., modulated) with a unique signature vector $\boldsymbol{g}_k$ whose length is $M < K$. All the K 'modulated' signature vectors are then transmitted simultaneously in M chip intervals to the fusion center. As mentioned before, the main reason for having $M < K$ is to reduce the transmission bandwidth when

compared to the case of $M = K$, i.e., orthogonal transmission. The latter has been studied in Chapter 3.

The following description of signal processing at CRs in the sensing phase is basically the same as that in Chapter 3 and it is briefly described so that Chapter 4 can be read independently from Chapter 3. The low-pass equivalent of the output of the BP filter at CR node i, $i = 1, \ldots, K$, is denoted by $x_{0,i}(t)$ and it is represented in (3.1) and (3.2) under $\mathcal{H}_0$ and $\mathcal{H}_1$ respectively. At the ith CR node, $x_{0,i}(t)$ is sampled with a rate of $f_s = \frac{1}{T_s}$ Hz over a time duration of $\tau = NT_s$ seconds, where T_s denotes the sampling period and N denotes the number of samples collected for spectrum sensing. As given in (3.7), y_i represents the average energy of the sampled band-limited signal at each CR node over a duration of τ seconds, where $f(y_i|\mathcal{H}_0) \sim \mathcal{N}\left(1, \frac{1}{N}\right)$, and $f(y_i|\mathcal{H}_1) \sim \mathcal{N}\left(\gamma_i + 1, \frac{(\gamma_i+1)^2}{N}\right)$. The decision device at the ith CR node produces a binary decision (0 or 1, corresponding to hypothesis $\mathcal{H}_0$ or $\mathcal{H}_1$, respectively) by comparing y_i to a decision threshold ϵ_i (see page 60). The probability of false alarm and the probability of detection at the ith CR node are denoted, respectively, as p_{f_i} and p_{d_i}, and they are given in (3.10) and (3.11).

After making a local binary decision, if the CR decides $\mathcal{H}_1$ (i.e., $u_i = 1$), the signal vector to be transmitted to the fusion center is obtained as the product of a_i and the $M \times 1$ signature vector $\boldsymbol{g}_i$. All the signature vectors have unit energy, i.e., $\|\boldsymbol{g}_i\|^2 = 1$, $i = 1, \ldots, K$. On the other hand, if a node decides $\mathcal{H}_0$ ($u_i = 0$), it remains silent and does not send a signal to the fusion center. Equivalently, the transmission scheme can also be viewed as a censoring scheme, where only the CRs with non-zero decisions transmit [37]. The transmitted signal from the ith CR can simply be expressed as $v_i\boldsymbol{g}_i = (a_iu_i)\boldsymbol{g}_i$, where $v_i = a_iu_i$. It should be noted that the parameter a_i sets the average transmitted power of the ith CR. Here, we assume that all CRs are similar and without loss of generality they can transmit with an average gain of $a_i = 1$. For the case of $M = K$, one can choose $\boldsymbol{g}_i = \boldsymbol{e}_i$, where $\boldsymbol{e}_i$ is a column vector of length K with the ith element equal to 1 and all other elements equal to 0. Obviously, the choice leads to orthogonal transmission of OOK modulated signals, which has been treated in Chapter 3. In contrast, the main focus of this chapter is the case when $M < K$ and the SVs cannot be made orthogonal. The key benefit of using shorter SVs is

that the transmission in the reporting phase can be conducted with a smaller bandwidth.

After all the K signal vectors are transmitted in M chip intervals to the FC over independent Rayleigh fading channels, the $M \times 1$ received signal vector $\boldsymbol{z} = [z_1, \ldots, z_M]^\top$ at the FC is given as:

$$\boldsymbol{z} = \sum_{i=1}^{K} h_{i,K+1} v_i \boldsymbol{g}_i + \boldsymbol{n}_{\mathrm{FC}}, \tag{4.1}$$

where $h_{i,K+1} \sim \mathcal{CN}(0, \sigma^2_{i,K+1})$ represents the channel fading coefficient between the ith CR and the FC, and $\boldsymbol{n}_{\mathrm{FC}} = [n_{1,\mathrm{FC}}, \ldots, n_{M,\mathrm{FC}}]^\top \sim \mathcal{CN}(\mathbf{0}, \sigma^2_{\mathrm{FC}}\mathbf{I})$ is the $M \times 1$ noise vector at the FC. Let $\boldsymbol{G} = [\boldsymbol{g}_1, \boldsymbol{g}_2, \ldots, \boldsymbol{g}_K]$ be a $M \times K$ matrix whose columns are the SVs of the CRs, $\boldsymbol{H}$ be a $K \times K$ diagonal matrix whose diagonal entries are $\{h_{1,K+1}, h_{2,K+1}, \ldots, h_{K,K+1}\}$ and define $\boldsymbol{v} = [v_1, v_2, \ldots, v_K]^\top$. Then (4.1) can also be written as:

$$\boldsymbol{z} = \boldsymbol{G}\boldsymbol{H}\boldsymbol{v} + \boldsymbol{n}_{\mathrm{FC}}. \tag{4.2}$$

The next sections examine two fusion rules, namely, the energy-based fusion rule and the decoding-based fusion rule. In fact, the simple energy-based fusion rule was also discussed in [37]. However its analysis does not explicitly take into account the signal processing at the CRs and cannot be used for parameter optimizations. On the other hand, the decoding-based fusion rule presented in this chapter is novel and offers an attractive performance-complexity tradeoff when compared to the simple energy-based fusion rule or the optimum fusion rule in [37]. It should also be pointed out that the optimum fusion rule in [37] not only has the complexity that is exponential in the number of CRs, but is also difficult to analyze for the purpose of parameter optimizations. Similar to Chapter 3 and [5], the objective of optimizing parameters for a fusion rule is to maximize the secondary throughput while maintaining the probability of detection equal or above a target value $\bar{P}_D$. For a given sensing time, maximizing the throughput function for a target $\bar{P}_D$ is equivalent to minimizing the probability of false alarm.

4.3 Energy-Based Fusion Rule

Let $\Upsilon = \boldsymbol{z}^H \boldsymbol{z}/\sigma_{\mathrm{FC}}^2$ denote the normalized output of the energy detector. The energy-based fusion rule is simply:

$$\Upsilon \underset{\mathcal{H}_0}{\overset{\mathcal{H}_1}{\gtrless}} \lambda^{(\mathrm{E})}, \tag{4.3}$$

where $\lambda^{(\mathrm{E})}$ is the decision threshold at the FC.

Although Υ has a quadratic form of zero-mean Gaussian random variables, we shall approximate it by a Gaussian distribution. The mean and variance of random variable Υ under each hypothesis are obtained as follows. First, it follows from (4.2) that:

$$\mu_0 \triangleq \mathcal{E}\left[\Upsilon|\mathcal{H}_0\right] = \sum_{i=1}^{K} \xi_i p_{f_i} \|\boldsymbol{g}_i\|_2^2 + M = \sum_{i=1}^{K} \xi_i p_{f_i} + M, \tag{4.4}$$

$$\mu_1 \triangleq \mathcal{E}\left[\Upsilon|\mathcal{H}_1\right] = \sum_{i=1}^{K} \xi_i p_{d_i} \|\boldsymbol{g}_i\|_2^2 + M = \sum_{i=1}^{K} \xi_i p_{d_i} + M, \tag{4.5}$$

where $\xi_i \triangleq \sigma_{i,K+1}^2/\sigma_{\mathrm{FC}}^2$.

Next, the variance is calculated as $\mathrm{var}\left[\Upsilon\right] = \mathcal{E}\left[\Upsilon^2\right] - \left(\mathcal{E}\left[\Upsilon\right]\right)^2$. Using (4.2) one has:

$$\mathcal{E}\left[\Upsilon^2\right] = \mathcal{E}\left[\sum_{i,j=1,i\neq j}^{K} u_i^2 u_j^2 \xi_i \xi_j \left(\boldsymbol{g}_i^H \boldsymbol{g}_j\right)^2 + 2\sum_{i=1}^{K} u_i^4 \xi_i^2 + \sum_{i,j=1,i\neq j}^{K} u_i^2 u_j^2 \xi_i \xi_j + M + M^2 + (2+2M)\sum_{i=1}^{K} u_i^2 \xi_i\right]. \tag{4.6}$$

Then, the variance conditioned on each hypothesis is:

$$\nu_0^2 \triangleq \mathrm{var}\left[\Upsilon|\mathcal{H}_0\right] = \sum_{i,j=1,i\neq j}^{K} p_{f_i} p_{f_j} \xi_i \xi_j \left(\boldsymbol{g}_i^H \boldsymbol{g}_j\right)^2 + 2\sum_{i=1}^{K} p_{f_i} \xi_i^2 + \sum_{i,j=1,i\neq j}^{K} p_{f_i} p_{f_j} \xi_i \xi_j + M + M^2 + (2+2M)\left(\sum_{i=1}^{K} p_{f_i} \xi_i\right) - \mu_0^2. \tag{4.7}$$

$$\nu_1^2 \triangleq \mathrm{var}\left[\Upsilon|\mathcal{H}_1\right] = \sum_{i,j=1,i\neq j}^{K} p_{d_i} p_{d_j} \xi_i \xi_j \left(\boldsymbol{g}_i^H \boldsymbol{g}_j\right)^2 + 2\sum_{i=1}^{K} p_{d_i} \xi_i^2 + \sum_{i,j=1,i\neq j}^{K} p_{d_i} p_{d_j} \xi_i \xi_j + M + M^2 + (2+2M)\left(\sum_{i=1}^{K} p_{d_i} \xi_i\right) - \mu_1^2. \tag{4.8}$$

It is noted that only the conditional variances depend on the set of SVs. Furthermore, for the special case of orthogonal transmission, one can easily verify that the means and variances reduce to the expressions given in Chapter 3 (see page 68).

The probability of false alarm and probability of detection are then obtained as:

$$P_F^{(\mathrm{E})}(\boldsymbol{p_f}, \lambda^{(\mathrm{E})}) = \Pr\left(\Upsilon > \lambda^{(\mathrm{E})} \middle| \mathcal{H}_0\right) = Q\left(\frac{\lambda^{(\mathrm{E})} - \mu_0}{\nu_0}\right), \tag{4.9}$$

and

$$P_D^{(\mathrm{E})}(\boldsymbol{p_d}, \lambda^{(\mathrm{E})}) = \Pr\left(\Upsilon > \lambda^{(\mathrm{E})} \middle| \mathcal{H}_1\right) = Q\left(\frac{\lambda^{(\mathrm{E})} - \mu_1}{\nu_1}\right). \tag{4.10}$$

From (4.9) and (4.10), for a target $\bar{P}_D$ we obtain:

$$P_F^{(\mathrm{E})}(\boldsymbol{p_f}, \bar{P}_D) = Q\left(\frac{Q^{-1}\left(\bar{P}_D\right)\nu_1 + \mu_1 - \mu_0}{\nu_0}\right). \tag{4.11}$$

For a given set of SVs, it is of interest to find the optimal sensing thresholds at the cognitive radios in order to minimize $P_F^{(\mathrm{E})}(\boldsymbol{p_f}, \bar{P}_D)$ in (4.11). The solution for the case of low sensing SNR, i.e., $\gamma_i \ll 1$ can be derived in a similar way as in Chapter 3. The result is:

$$\epsilon_i^* = \left(1 + \frac{1}{\gamma_i}\right)\log\left(\gamma_i + 1\right). \tag{4.12}$$

Furthermore, one can also try to find the set of signature vectors to further minimize $P_F^{(\mathrm{E})}(\boldsymbol{p_f}, \bar{P}_D)$. Unfortunately, such an optimization problem in its general form appears to be very complex, and finding a closed-form solution for optimal $\boldsymbol{G}$ seems intractable. Nevertheless, a good set of signature vectors can be found by generating a large set of random signature vectors and picking the one that maximizes the expression in (4.11).

For the simple case when the sensing channels as well as the reporting channels have the same average SNRs, i.e., $\gamma_i = \gamma$ and $\xi_i = \xi$, it can be shown that the so-called Welch-bound equality (WBE) sequences [2] [67] yield the optimal signature vectors. The proof is as

[2]Welch's bound for a set of M complex equi-energy sequences is a lower bound on the sum of the squares of the magnitudes of the inner products between all pairs of these sequences. If the sequences meet the Welch bound with equality, they are referred to as WBE sequences.

follows: Observe from (4.7) and (4.8) that both ν_0 and ν_1 are functions of the total squared correlation (TSC), namely $\sum_{i,j=1,i\neq j}^{K}\left(\boldsymbol{g}_i^H\boldsymbol{g}_j\right)^2$. Then, in order to maximize $\frac{Q^{-1}\left(\bar{P}_D\right)\nu_1+\mu_1-\mu_0}{\nu_0}$, it is clear that $\sum_{i,j=1,i\neq j}^{K}\left(\boldsymbol{g}_i^H\boldsymbol{g}_j\right)^2$ has to be minimized. It is well-known that the WBE sequences minimize the TSC [66].

4.4 Decoding-Based Fusion Rule

Though being very simple, the energy-based fusion rule might not work well in certain channel conditions. This is because noise is also included in the energy calculation. To see how one can improve the performance of the energy-based fusion rule, define $\boldsymbol{D}=\text{diag}\left(a_1^2|h|_{1,K+1}^2,\ldots,a_K^2|h|_{K,K+1}^2\right)$. Then the energy computed at the FC can be written as:

$$\boldsymbol{z}^H\boldsymbol{z}=\boldsymbol{u}^T\boldsymbol{D}\boldsymbol{G}^T\boldsymbol{G}\boldsymbol{D}\boldsymbol{u}+\boldsymbol{n}_{\text{FC}}^H\boldsymbol{n}_{\text{FC}}+2\boldsymbol{u}^T\boldsymbol{D}\boldsymbol{G}^T\boldsymbol{n}_{\text{FC}}. \tag{4.13}$$

As can be seen, $\boldsymbol{z}^H\boldsymbol{z}$ is actually a weighted sum of the local decisions and noise terms. This suggests that one might decode the received signal first and then combine the hard decisions in the hope of achieving a better performance due to better noise reduction under certain channel conditions.

To develop a decoding-based fusion rule, it is proposed to perform the minimum mean-square error (MMSE) estimation of the transmitted vector $\boldsymbol{v}_{\boldsymbol{h}}\triangleq\boldsymbol{H}\boldsymbol{v}$ first, followed by a detection of the transmitted bits from the estimated vector $\hat{\boldsymbol{v}}_{\boldsymbol{h}}$. The MMSE estimation yields [68]:

$$\hat{\boldsymbol{v}}_{\boldsymbol{h}}=\boldsymbol{C}\boldsymbol{z}, \tag{4.14}$$

where $\boldsymbol{C}\triangleq\bar{\boldsymbol{D}}\boldsymbol{G}^T\left[\boldsymbol{G}\bar{\boldsymbol{D}}\boldsymbol{G}^T+\sigma_{\text{FC}}^2\boldsymbol{I}\right]^{-1}$, $\bar{\boldsymbol{D}}=\text{diag}\left(\bar{d}_1,\ldots,\bar{d}_K\right)$ with $\bar{d}_i=a_i^2\sigma_{i,K+1}^2\kappa_i$ and $\kappa_i\triangleq\left[p_{f_i}\Pr(\mathcal{H}_0)+p_{d_i}\Pr(\mathcal{H}_1)\right]$. It is not hard to show the following relationship between $\hat{\boldsymbol{v}}_{\boldsymbol{h}}$ and $\boldsymbol{v}_{\boldsymbol{h}}$:

$$\hat{\boldsymbol{v}}_{\boldsymbol{h}}=\boldsymbol{v}_{\boldsymbol{h}}+\boldsymbol{\chi}, \tag{4.15}$$

where $\hat{\boldsymbol{v}}_{\boldsymbol{h}}=[\hat{\boldsymbol{v}}_{\boldsymbol{h},1},\ldots,\hat{\boldsymbol{v}}_{\boldsymbol{h},K}]^T$ and $\boldsymbol{\chi}=[\chi_1,\ldots,\chi_K]$ is a zero-mean Gaussian vector. More

importantly, the normalized MMSE for each decoded bit can be shown to be:

$$\frac{\mathcal{E}\left[\left(\hat{v}_{\boldsymbol{h},i}-v_{\boldsymbol{h},i}\right)^2\right]}{\bar{d}_i}=1-\boldsymbol{g}_i^T\left(\boldsymbol{G}\bar{\boldsymbol{D}}\boldsymbol{G}^T+\sigma_{\mathrm{FC}}^2\boldsymbol{I}\right)^{-1}\boldsymbol{g}_i\bar{d}_i. \tag{4.16}$$

In general, the MMSE is a useful performance measure for parameter estimation. In many research papers concerning the detection performance over overloaded code-division multiple access (CDMA) systems, signature vectors are obtained by minimizing MMSE-related metrics and WBE sequences (or weighted WBE sequences) turn out to be the optimum signature vectors [66, 68]. However, in the spectrum sensing problem the main performance measures are mainly related to the probability of false alarm and probability of detection, and the WBE sequences are not necessarily the ones that optimize the performance.

The influence of the choice of the SVs on the performance of the proposed decoding-based fusion rule can be analyzed as follows. First, the likelihood ratio test (LRT) for decoding the bits sent by the ith CR is:

$$\frac{f(\hat{v}_{\boldsymbol{h},i}|u_i=1)}{f(\hat{v}_{\boldsymbol{h},i}|u_i=0)}\underset{\hat{u}_i=0}{\overset{\hat{u}_i=1}{\gtrless}}\frac{\Pr(u_i=0)}{\Pr(u_i=1)}=\frac{1-p_{f_i}\Pr(\mathcal{H}_0)-p_{d_i}\Pr(\mathcal{H}_1)}{p_{f_i}\Pr(\mathcal{H}_0)+p_{d_i}\Pr(\mathcal{H}_1)}. \tag{4.17}$$

where the above threshold is obtained by calculating $\Pr(u_i=0)=\Pr(y_i<\epsilon_i|\mathcal{H}_0)\Pr(\mathcal{H}_0)+\Pr(y_i<\epsilon_i|\mathcal{H}_1)\Pr(\mathcal{H}_1)=(1-p_{f_i})\Pr(\mathcal{H}_0)+(1-p_{d_i})\Pr(\mathcal{H}_1)=1-p_{f_i}\Pr(\mathcal{H}_0)-p_{d_i}\Pr(\mathcal{H}_1)$. Similarly, $\Pr(u_i=1)=p_{f_i}\Pr(\mathcal{H}_0)+p_{d_i}\Pr(\mathcal{H}_1)$. It is noted that for the case of $\Pr(\mathcal{H}_0)=\Pr(\mathcal{H}_1)$ and having $p_{f_i}+p_{d_i}\cong 1$ when the signal-to-noise ratios of the sensing links are low [39], the threshold in (4.17) is approximately 1. Note also that each density function in the above LRT is the density of a zero-mean complex Gaussian variable. As such, the LRT is determined by $\mathcal{E}(|\hat{v}_{\boldsymbol{h},i}|^2|u_i=1)$ and $\mathcal{E}(|\hat{v}_{\boldsymbol{h},i}|^2|u_i=0)$. These two expectations are computed as follows. First, according to (4.14), one has:

$$\mathcal{E}(|\hat{v}_{\boldsymbol{h},i}|^2|u_i=1)=\left[\boldsymbol{C}\boldsymbol{\mathcal{K}}_{i,1}\boldsymbol{C}\right]_{i,i}\triangleq\zeta_{i,1}. \tag{4.18}$$

where

$$\boldsymbol{\mathcal{K}}_{i,1}=\mathcal{E}(\boldsymbol{z}\boldsymbol{z}^H|u_i=1)=\boldsymbol{G}\bar{\boldsymbol{D}}_{i,1}\boldsymbol{G}^T+\sigma_{\mathrm{FC}}^2\boldsymbol{I}, \tag{4.19}$$

and $[\bar{\boldsymbol{D}}_{i,1}]_{k,k}=\bar{d}_k$, $k\neq i$, and $[\bar{\boldsymbol{D}}_{i,1}]_{i,i}=\frac{\bar{d}_i}{\kappa_i}$. Similarly,

$$\mathcal{E}(|\hat{v}_{\boldsymbol{h},i}|^2|u_i=0)=\left[\boldsymbol{C}\boldsymbol{\mathcal{K}}_{i,0}\boldsymbol{C}\right]_{i,i}\triangleq\zeta_{i,0}, \tag{4.20}$$

with

$$\boldsymbol{\mathcal{K}}_{i,0} = \mathcal{E}(\boldsymbol{z}\boldsymbol{z}^H | u_i = 0) = \boldsymbol{G}\bar{\boldsymbol{D}}_{i,0}\boldsymbol{G}^T + \sigma_{\mathrm{FC}}^2 \boldsymbol{I}. \tag{4.21}$$

and $[\bar{\boldsymbol{D}}_{i,0}]_{k,k} = \bar{d}_k$, $k \neq i$, and $[\bar{\boldsymbol{D}}_{i,0}]_{i,i} = 0$. Simplifying (4.17) gives:

$$|\hat{v}_{\boldsymbol{h},i}|^2 \underset{\hat{u}_i=0}{\overset{\hat{u}_i=1}{\gtrless}} \frac{\ln\left(\frac{1-p_{f_i}\Pr(\mathcal{H}_0)-p_{di}\Pr(\mathcal{H}_1)}{p_{f_i}\Pr(\mathcal{H}_0)+p_{di}\Pr(\mathcal{H}_1)} \cdot \frac{\zeta_{i,1}}{\zeta_{i,0}}\right)}{\frac{\zeta_{i,1}-\zeta_{i,0}}{\zeta_{i,1}\zeta_{i,0}}} \triangleq \varrho_i. \tag{4.22}$$

The reliability of the hard decision rule in (4.22) concerning the bit sent by the ith CR can be evaluated by the following set of correct/error probabilities:

$$\varpi_i = \Pr(\hat{u}_i = 1 | u_i = 1) = \Pr\left(|\hat{v}_{\boldsymbol{h},i}|^2 > \varrho_i \middle| u_i = 1\right) = \mathrm{e}^{-\frac{\varrho_i}{\zeta_{i,1}}}, \tag{4.23}$$

$$\vartheta_i = \Pr(\hat{u}_i = 1 | u_i = 0) = \Pr\left(|\hat{v}_{\boldsymbol{h},i}|^2 > \varrho_i \middle| u_i = 0\right) = \mathrm{e}^{-\frac{\varrho_i}{\zeta_{i,0}}}. \tag{4.24}$$

Note that $\Pr(\hat{u}_i = 0 | u_i = 1) = 1 - \varpi_i$ and $\Pr(\hat{u}_i = 0 | u_i = 0) = 1 - \vartheta_i$.

The next processing step in the fusion center is to combine the hard decisions $\hat{u}_i$, $i = 1, \ldots, K$, to make a final sensing decision. This can be done in the same manner as in Chapter 3 by forming the following likelihood ratio for the decoded bits:

$$L^{(\mathrm{D})}(\hat{\boldsymbol{u}}) = \frac{\Pr(\hat{\boldsymbol{u}}|\mathcal{H}_1)}{\Pr(\hat{\boldsymbol{u}}|\mathcal{H}_0)} = \frac{\prod_{i=1}^{K}(1-\wp_{di})^{(1-\hat{u}_i)}\wp_{di}^{\hat{u}_i}}{\prod_{i=1}^{K}(1-\wp_{f_i})^{(1-\hat{u}_i)}\wp_{fi}^{\hat{u}_i}}, \tag{4.25}$$

where $\wp_{di} = \Pr(\hat{u}_i = 1|\mathcal{H}_1)$ and $\wp_{f_i} = \Pr(\hat{u}_i = 1|\mathcal{H}_0)$ are the probabilities of detection and probabilities of false alarm associated with the decoded bits $\hat{u}_i$. They are shown in Chapter 3 to be given as $\wp_{di} = p_{di}\varpi_i + (1 - p_{di})\vartheta_i$ and $\wp_{f_i} = p_{f_i}\varpi_i + (1 - p_{f_i})\vartheta_i$.

Working with the logarithm of (4.25), the decoding-based fusion rule is given as:

$$L^{(\mathrm{D})}(\hat{\boldsymbol{u}}) = \sum_{i=1}^{K} \left[\varphi_{0,i}(1 - \hat{u}_i) + \varphi_{1,i}\hat{u}_i\right] \underset{\mathcal{H}_0}{\overset{\mathcal{H}_1}{\gtrless}} \lambda^{(\mathrm{D})}, \tag{4.26}$$

where $\lambda^{(\mathrm{D})}$ is the threshold, while the weights are $\varphi_{0,i} = \log\frac{1-\wp_{di}}{1-\wp_{f_i}}$ and $\varphi_{1,i} = \log\frac{\wp_{di}}{\wp_{f_i}}$. Note that the above fusion rule is simply a weighted linear combinations of the hard-decision bits. Moreover, the weights are inherently adjusted according to both the decision of the ith CR and the quality of the reporting channel.

By approximating $L^{(\mathrm{D})}(\hat{\boldsymbol{u}})$ as a Gaussian random variable under each hypothesis, the expressions of the probability of false alarm and the probability of detection at the fusion center are as follows:

$$P_F^{(\mathrm{D})}(\boldsymbol{p_f}, \lambda^{(\mathrm{D})}) = \Pr\left(L^{(\mathrm{D})}(\hat{\boldsymbol{u}}) > \lambda^{(\mathrm{D})} \middle| \mathcal{H}_0\right) = Q\left(\frac{\lambda^{(\mathrm{D})} - m_0}{\delta_0}\right), \tag{4.27}$$

and

$$P_D^{(\mathrm{D})}(\boldsymbol{p_d}, \lambda^{(\mathrm{D})}) = \Pr\left(L^{(\mathrm{D})}(\hat{\boldsymbol{u}}) > \lambda^{(\mathrm{D})} \middle| \mathcal{H}_1\right) = Q\left(\frac{\lambda^{(\mathrm{D})} - m_1}{\delta_1}\right). \tag{4.28}$$

The mean values, m_0 and m_1, and the variances, δ_0^2 and δ_1^2, can be determined in a similar fashion as in Chapter 3. The means are given as:

$$\begin{aligned} m_0 =& \mathcal{E}[L^{(\mathrm{D})}(\hat{\boldsymbol{u}})|\mathcal{H}_0] = \sum_{i=1}^{K} m_{i,0}, \\ m_{i,0} =& \left[\varpi_i p_{f_i} + \vartheta_i(1 - p_{f_i})\right][\varphi_{1,i} - \varphi_{0,i}] + \varphi_{0,i}, \end{aligned} \tag{4.29}$$

and

$$\begin{aligned} m_1 =& \mathcal{E}[L^{(\mathrm{D})}(\hat{\boldsymbol{u}})|\mathcal{H}_1] = \sum_{i=1}^{K} m_{i,1}, \\ m_{i,1} =& [\varpi_i p_{di} + \vartheta_i(1 - p_{di})][\varphi_{1,i} - \varphi_{0,i}] + \varphi_{0,i}. \end{aligned} \tag{4.30}$$

Using the fact that $\mathcal{E}[\hat{u}_i|\mathcal{H}_0] = \wp_{f_i}$ and $\mathcal{E}[\hat{u}_i|\mathcal{H}_1] = \wp_{di}$, the variances are:

$$\begin{aligned} \delta_0^2 =& \mathrm{Var}[L^{(\mathrm{D})}(\hat{\boldsymbol{u}})|\mathcal{H}_0] = \sum_{i=1}^{K} \mathcal{E}\left[\hat{u}_i^2|\mathcal{H}_0\right][\varphi_{1,i} - \varphi_{0,i}]^2 \\ &+ \sum_{i,j=1,i\neq j}^{K} [\varphi_{1,i} - \varphi_{0,i}][\varphi_{1,j} - \varphi_{0,j}]\,\mathcal{E}\left[\hat{u}_i\hat{u}_j|\mathcal{H}_0\right] - m_0^2 \\ =& \sum_{i=1}^{K} \wp_{f_i}[\varphi_{1,i} - \varphi_{0,i}]^2 + \sum_{i,j=1,i\neq j}^{K} [\varphi_{1,i} - \varphi_{0,i}][\varphi_{1,j} - \varphi_{0,j}]\,\mathcal{C}_0(i,j) - m_0^2, \end{aligned} \tag{4.31}$$

and

$$\delta_1^2 = \mathrm{Var}[L^{(\mathrm{D})}(\hat{\boldsymbol{u}})|\mathcal{H}_1] = \sum_{i=1}^{K} \mathcal{E}\left[\hat{u}_i^2|\mathcal{H}_1\right]\left[\varphi_{1,i}-\varphi_{0,i}\right]^2$$
$$+ \sum_{i,j=1,i\neq j}^{K} \left[\varphi_{1,i}-\varphi_{0,i}\right]\left[\varphi_{1,j}-\varphi_{0,j}\right]\mathcal{E}\left[\hat{u}_i\hat{u}_j|\mathcal{H}_1\right] - m_1^2$$
$$= \sum_{i=1}^{K} \wp_{di}\left[\varphi_{1,i}-\varphi_{0,i}\right]^2 + \sum_{i,j=1,i\neq j}^{K} \left[\varphi_{1,i}-\varphi_{0,i}\right]\left[\varphi_{1,j}-\varphi_{0,j}\right]\mathcal{C}_1(i,j) - m_1^2. \tag{4.32}$$

Observe that, different from the case of orthogonal transmission considered in Chapter 3, the above variances depend on the correlations of the decoded bits, $\hat{u}_i$ and $\hat{u}_j$, under the two hypotheses. These correlations are determined as follows:

$$\mathcal{C}_0(i,j) \triangleq \mathcal{E}\left[\hat{u}_i\hat{u}_j|\mathcal{H}_0\right] = \Pr\left(|\hat{v}_{\boldsymbol{h},i}|^2 > \varrho_i, |\hat{v}_{\boldsymbol{h},j}|^2 > \varrho_j|\mathcal{H}_0\right) = \mathrm{e}^{-\boldsymbol{\varrho}_{ij}^{\mathrm{T}}([\boldsymbol{\zeta}_0(i,j)])^{-1}\boldsymbol{\varrho}_{ij}}, \tag{4.33}$$

$$\mathcal{C}_1(i,j) \triangleq \mathcal{E}\left[\hat{u}_i\hat{u}_j|\mathcal{H}_1\right] = \Pr\left(|\hat{v}_{\boldsymbol{h},i}|^2 > \varrho_i, |\hat{v}_{\boldsymbol{h},j}|^2 > \varrho_j|\mathcal{H}_1\right) = \mathrm{e}^{-\boldsymbol{\varrho}_{ij}^{\mathrm{T}}([\boldsymbol{\zeta}_1(i,j)])^{-1}\boldsymbol{\varrho}_{ij}}. \tag{4.34}$$

where $\boldsymbol{\varrho}_{ij} \triangleq [\varrho_i, \varrho_j]^T$, $\boldsymbol{\zeta}_0 \triangleq \boldsymbol{G}\boldsymbol{D}_0\boldsymbol{G}^T + \sigma_{\mathrm{FC}}^2\boldsymbol{I}$, and $\boldsymbol{\zeta}_1 \triangleq \boldsymbol{G}\boldsymbol{D}_1\boldsymbol{G}^T + \sigma_{\mathrm{FC}}^2\boldsymbol{I}$.

Recall that an approximation of the optimal sensing thresholds used at the cognitive radios for the energy-based fusion rule is given in (4.12). The same result applies to the decoding-based fusion rule presented in this section. The proof of this follows the same steps in Appendix B.3.

The next section compares the performance of the energy-based and decoding-based fusion rules and also verifies the accuracy of our analysis. It is pointed out that the simple expressions of the probability of false alarm and the probability of detection ((Eqns. (4.9), (4.10) for energy-based fusion rule or Eqns. (4.27), (4.28) for energy-based fusion rule) are very convenient not only in determining the threshold at the fusion center ($\lambda^{(\mathrm{E})}$ or $\lambda^{(\mathrm{D})}$) for a given target probability of false-alarm (or probability of detection), but also in evaluating the performance of different sets of signature vectors used in nonorthogonal transmission of local decisions.

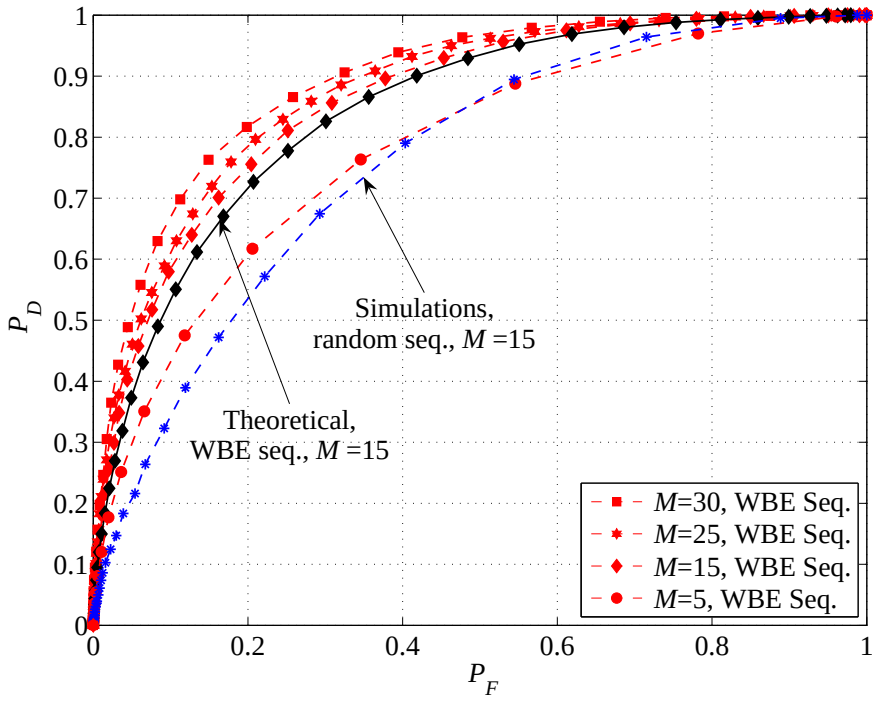

Figure 4.2 Probability of detection versus probability of false alarm for the energy-based fusion rule.

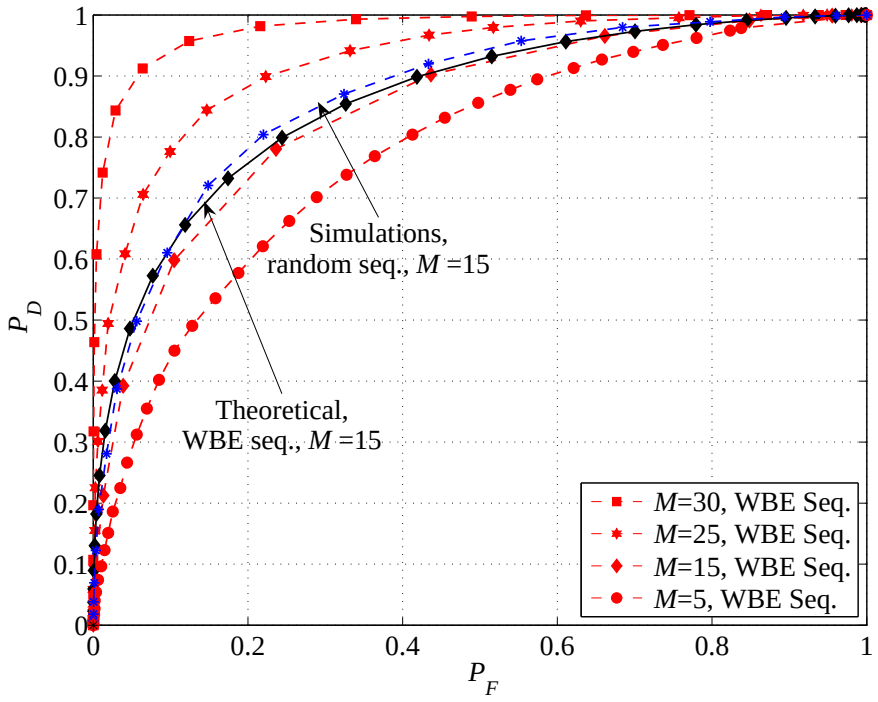

Figure 4.3 Probability of detection versus probability of false alarm for the decoding-based fusion rule.

4.5 Simulation Results

Each point in the simulations results is obtained by averaging over 10^4 random realizations for primary transmitted signal, fading channels and noise. For the sake of simplify, it is assumed that $\Pr(\mathcal{H}_0) = \Pr(\mathcal{H}_1) = 0.5$. Unless otherwise stated, the number of the CRs is set to $K = 30$, the number of samples taken is $N = 500$ and the set of WBE signature sequences are assigned to CR users.

Fig. 4.2 and Fig. 4.3 depict the probabilities of detection versus the probabilities of false alarm when the energy-based and decoding-based fusion rules are used, respectively. For both figures, all the sensing channels have the same average SNR of $\gamma_i = \gamma = -15$dB, and also all the reporting channels have the same SNR of $\xi_i = \xi = 20$ dB. The sensing threshold is chosen as $\epsilon_i = \epsilon^* = \left(1 + \frac{1}{\gamma}\right) \log(\gamma + 1)$ at each CR node. For the energy-based fusion rule, it is clearly seen from Fig. 4.2 that by increasing the length of signature vectors from $M = 5$ to $M = 15$ the probability of detection versus the probability of false alarm increases significantly, whereas increasing M beyond 15 only improves the sensing performance slightly. This suggests that, compared to the case of orthogonal transmission, the transmission bandwidth for the reporting phase can be reduced by half by using WBE sequences with $M = 15$ while not loosing too much the sensing performance. It can also be observed that the analytical and simulation results match very well.[3] For comparison purpose, the performance with random signature vectors was also obtained and plotted in Fig. 4.2 for $M = 15$. Specifically, the result is obtained by averaging over 10^4 random realizations of the signature vectors. As expected, the performance of using WBE sequences significantly outperforms the performance with random sequences.

On the other hand, for the proposed decoding-based fusion rule, Fig. 4.3 shows that the sensing performance is significantly improved not only when increasing M from 5 to 15, but also by further increasing M to 30. Such an improvement can be explained by the fact that detection of the transmitted bits from CRs strongly depends on the interference

[3]To avoid having too many curves on the same figure, only the analytical result for the case of $M = 15$ is shown.

caused by nonorthogonal transmission. As the interference reduces with longer signature vectors (larger M), the detection performance is greatly enhanced when all the reporting channels are fairly strong. The figure also shows that the theoretical result (with $M = 15$) follows the simulation result closely. Another observation from Fig. 4.3 is that with random signature vectors, the sensing performance is slightly better than the performance with WBE sequences. As pointed out before, it is difficult to obtain the optimal set of signature vectors for the proposed decoding-based fusion rule. The results in Fig. 4.3 suggest that either randomly-generated or WBE sequences can be used for the proposed decoding-based fusion rule.

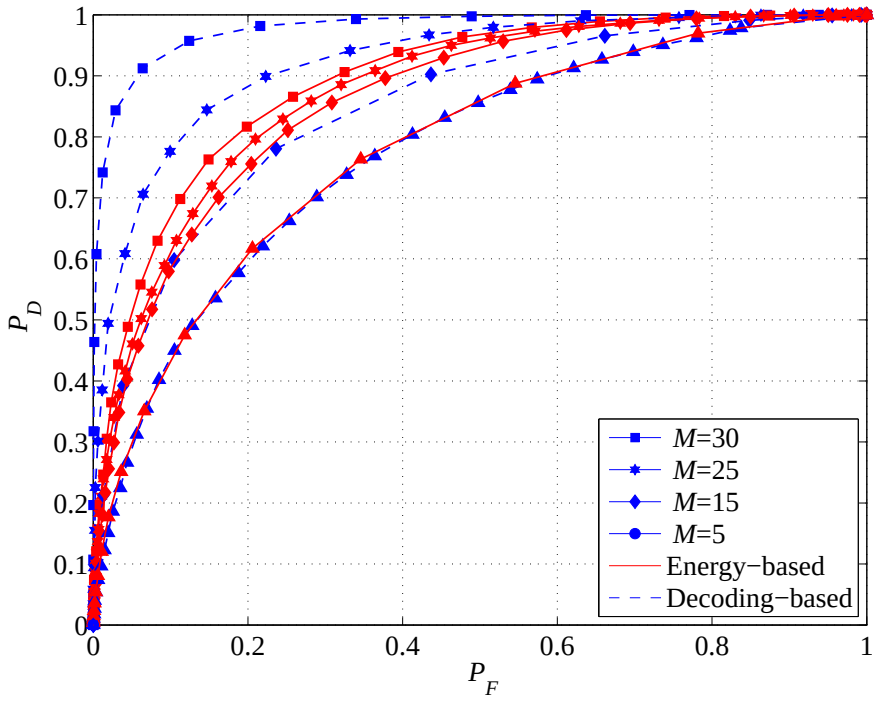

Figure 4.4 Probability of detection versus probability of false alarm: Comparison between decoding-based and energy-based fusion rules.

Fig. 4.4 compares the probabilities of detection obtained by simulation with the energy-based and decoding-based fusion rules for different values of M and when the WBE sequences are used. As can be seen, even in the presence of strong reporting channels, the energy-based fusion rule performs equally or better than the decoding-based fusion rule when $M \leq 15$. On the contrary, for $M > 15$, the decoding-based fusion rule outperforms the energy-based

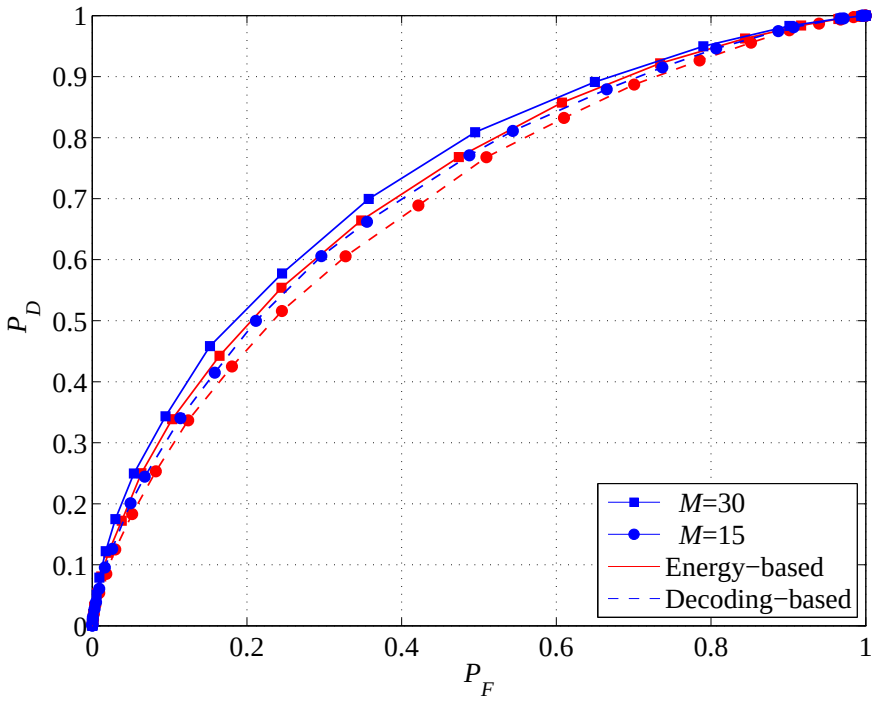

Figure 4.5 Probability of detection versus probability of false alarm for scenario 1.

fusion rule. The obtained results suggest that the energy-based fusion rule can be employed as an efficient fusion rule in cognitive radio applications under very limited transmission bandwidth (i.e., $M \leq 15$).

Figs. 4.5 and 4.6 present performance comparison between the two sensing algorithms for the situations when the SNRs are different at the CRs and/or the FC. In the first scenario all the CRs experience the same "sensing" SNR of $\gamma = \gamma_i = -15$ dB from the primary user but each group of CRs transmit their sensing results to the fusion center with the "reporting" SNRs of -5 dB (6 CRs), -1 dB (6 CRs), 0 dB (12 CRs) and 5 dB (6 CRs). In the second scenario, the CRs are divided into 6 groups of 5 CRs each. The "sensing" SNRs are given as $\{-15, -24, -5, -10, -20\}$ dB, whereas the reporting SNRs are considered to be $\{5, 10, 1, 1, 5\}$ dB. In comparison to the first scenario, the second scenario has stronger reporting channels.

As can be seen in Figs. 4.5 and 4.6, both figures show performance improvement when M increases from 15 to 30. However for the first scenario with the weak reporting links the

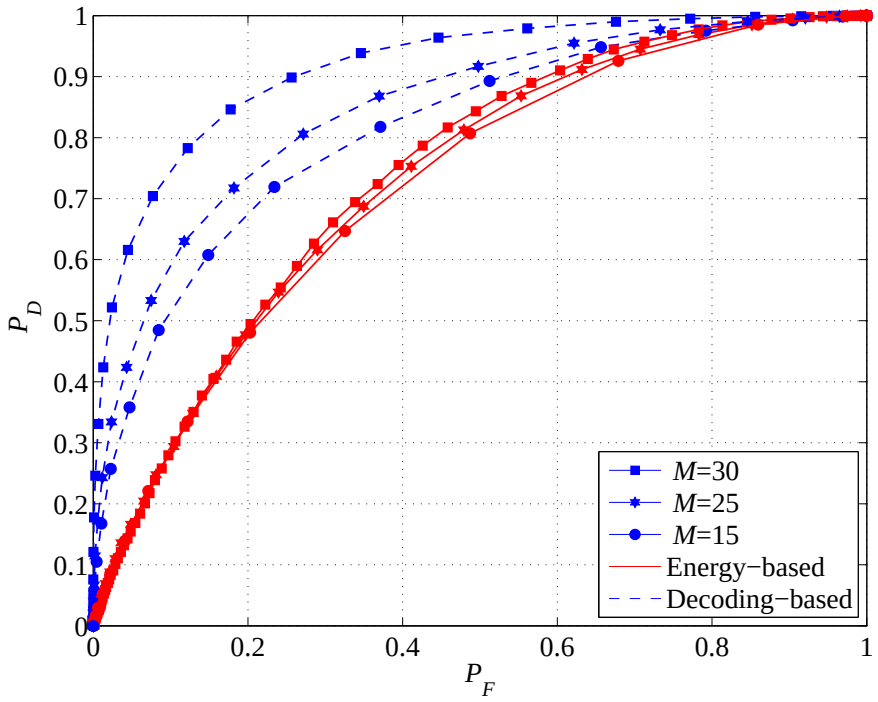

Figure 4.6 Probability of detection versus probability of false alarm for scenario 2.

improvement is marginal. This is because the sensing performance in this scenario is mostly affected by the noise at the FC rather than the interference caused by shorter signature vectors. Another important observation is that the energy-based fusion rule outperforms the decoding-based rule. Thus it can be concluded that for low channel SNRs, the energy-based fusion rule is preferred over the decoding-based fusion rule due to its lower complexity while at the same time delivering equal or better performance.

For the second scenario, when the channels are fairly strong, the decoding-based detection significantly outperforms the energy-based detection. Also as M increases, the performance of the decoding-based fusion rule quickly improves due to the reduction of interference. However for the energy-based fusion rule, interference reduction does not play a significant role in improving the sensing performance.

Fig. 4.7 presents a comparison between the probabilities of detection of the two sensing algorithms for the situation when $N = 500$ and P_F is fixed at 0.05 at the fusion center. The sensing SNRs are -12 and -9 dB at the CRs and the reporting SNRs are 20 dB.

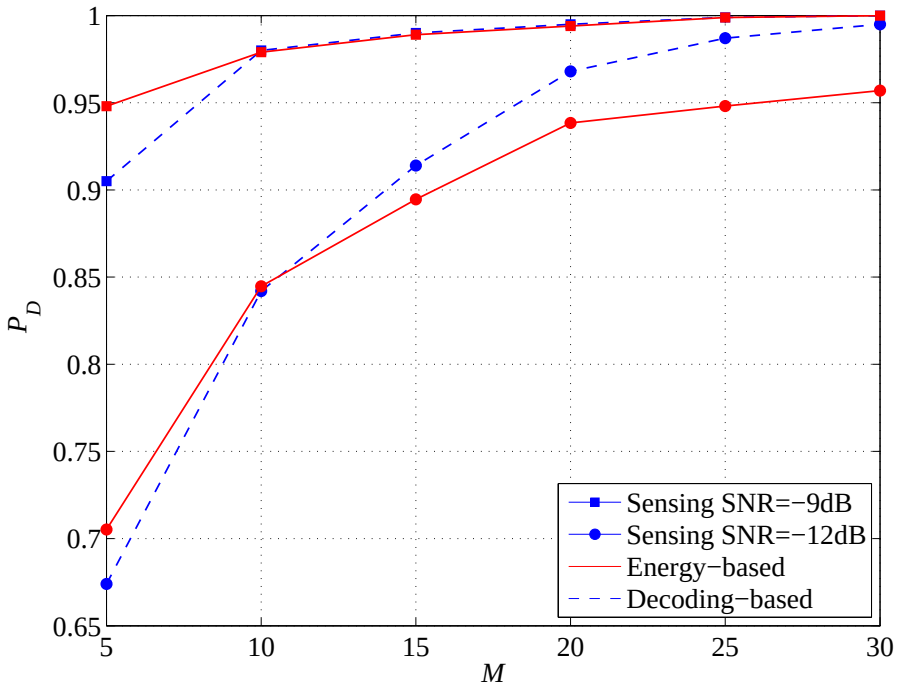

Figure 4.7 Probability of detection versus M for $P_F = 0.05$.

As can be seen, for a lower sensing SNR, the performance of both algorithms improves significantly with increasing M. Such an improvement can be explained by the fact that as M increases, the interference caused by nonorthogonal transmission is reduced, which helps to enhance the sensing quality. On the other hand, when the sensing SNR increases, the individual CR sensing performance quickly improves, which makes the overall desirable sensing performance be achieved by using shorter-length signature vectors. For example, given the target $P_F = 0.05$ and the sensing time of 500 samples, in order to achieve a target $P_D = 0.9$ when the sensing SNRs are -12 dB, it is seen that setting $M = 15$ is sufficient. The use of such shorter signature vectors translates to half of the bandwidth as required by orthogonal signature vectors.

Finally, in Fig. 4.8, the normalized throughput, defined as $\left(1 - \frac{N}{T}\right)(1 - P_F)$, is plotted versus the entire time frame of 1 ms (which is equivalent to $T = 1,000$ samples). Here the threshold $\lambda^{(D)}$ is selected to fix the probability of detection at $P_D = 0.8$. Two sets of signature vectors, whose lengths are $M = 25$ and $M = 10$, are considered. For the given target P_D and for the case $M = 25$, it can be seen that the decoding-based fusion rule achieves a higher

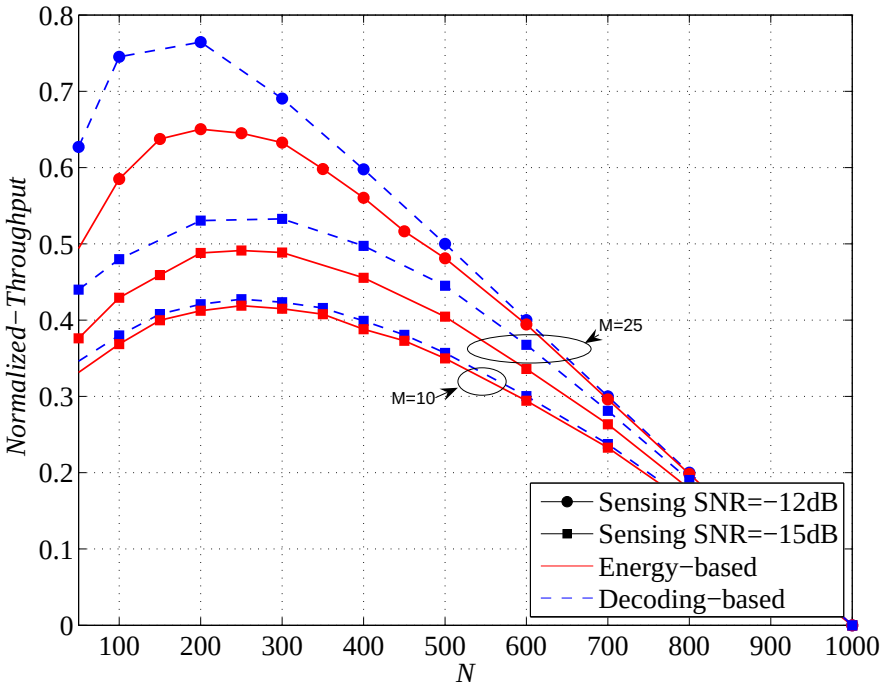

Figure 4.8 Normalized throughput versus time samples N for $P_D = 0.8$.

secondary throughput than the energy-based fusion rule. However, for the case $M = 10$, both the decoding-based and energy-based fusion rules achieve almost the same secondary throughput. These results are in agreement with our previous discussion concerning Fig. 4.4. Another important observation of Fig. 4.8 is that the throughput functions are concave and attain a maximum point at a certain sensing time. This means that for a given a target P_D, an optimal sensing time can be found to maximize the secondary throughput. Alternatively, for a given target P_D, the minimum length of the signature vectors can be determined to achieve a target secondary throughput within the allowable sensing time.

4.6 Conclusions

In this chapter, a low-complexity decoding-based fusion rule for cognitive radio networks is proposed with nonorthogonal transmission of local decisions in the presence of channel impairments and noise. The proposed fusion rule first performs the MMSE estimation of the transmitted information, makes decisions on the individual bits sent by the cognitive radios and then combines these hard-decision bits in a linearly-weighted manner. Performance com-

parison with the energy-based fusion rule shows the superiority of the proposed fusion rule when the reporting channels are reasonably strong. The excellent match between simulation and analytical results verify the accuracy of the performance analysis of the proposed fusion rule.

5. Summary and Suggestions for Further Studies

5.1 Summary

This thesis focused mainly on developing spectrum sensing schemes for wireless cognitive radio networks with different network topologies and channel state information assumptions. Specifically, the main contributions of this thesis are summarized as follows:

- Regarding wideband spectrum sensing, a spectrum sensing method for OFDM-based cognitive radio systems has been developed based on the GLRT framework. In order to enhance the ML estimations of unknown parameters, the structure (constraint) of the covariance matrix of the underlying OFDM signals has been taken into account (Chapter 2). Simulation results with different channel scenarios revealed the robustness and efficiency of the proposed method. In particular, the developed algorithms greatly outperform energy detection in an environment with noise uncertainty.

- As a further step in improving the reliability of spectrum sensing, the thesis also developed a collaborative spectrum sensing scheme for cognitive radio networks with orthogonal CR transmissions (Chapter 3). To overcome the problem of channel estimation, the noncoherent OOK and BFSK signalling schemes were employed to transmit binary decisions to the fusion center. A detailed comparison between the noncoherent OOK and BFSK signalling schemes has been carried out to illustrate the trade-offs involved in implementing these two transmission schemes. Due to their practical feasibility for a large CR network, energy- and decoding-based fusion rules were implemented at the FC. For both fusion rules, it was shown that the secondary throughput with the optimum sensing parameters is a concave function of sensing time and hence there exists

an optimum solution for the sensing time. The accuracy of the analysis was verified by the excellent match between simulation and analytical results.

- Finally, Chapter 4 developed and analyzed spectrum sensing algorithms under a non-orthogonal transmission of local decisions. Such a transmission scheme is particularly suitable for large-scale distributed CR networks in which the bandwidth consumption can be reduced while maintaining simple fusion processing. In particular, a decoding-based fusion rule was investigated in which the MMSE estimation of the transmitted bits from the CRs are obtained at the fusion center and then they are combined in a linearly-weighted manner. The proposed decoding-based fusion rule was shown to be superior to the energy-based fusion rule when the reporting channels are reasonably strong. The simulation and analytical results also showed the accuracy of the performance analysis for different scenarios.

5.2 Suggestions for Further Studies

Currently, research efforts on different aspects of spectrum sensing techniques are still needed in order to incorporate the cooperative/wideband spectrum sensing schemes into real-world applications. While conducting this research, several issues arose that should be interesting for further studies. These issues are elaborated next.

- The first issue that exists in any cognitive radio network is the rate of primary user activity. In this thesis, it is implicitly assumed that the primary user has a low activity rate so that the CR network can take advantage of the licensed bandwidth most of the time. In such an overlay scheme, if the primary user becomes active, the cognitive radio users have to stop their transmission. However, in a more desirable situation, the cognitive radios can switch to the underlay paradigm when the licensed bandwidth is concurrently shared with the CR network. In that case, the transmission power distribution has to be carefully designed among the CRs according to the interference issues. The mutual dependence between spectrum sensing and power allocation for cognitive radios manifests itself in the average secondary throughput. Since the main

goal for a cognitive radio network is to maximize the opportunistic throughput, it is important to obtain the best sensing time and power allocations to achieve the target opportunistic throughput while satisfying the interference constraints.

- Regarding the wideband spectrum sensing, there is a need to investigate OFDM standard signals. One of the main standards for OFDM-based cognitive radio applications is the mobile worldwide interoperability for microwave access (WiMAX) and third-Generation Partnership Project Long Term Evolution (3GPP LTE). The particular structure of these signals allows for developing robust spectrum sensing algorithms which take into account preambles, pilots, and reference signals (RS). Conforming to the OFDM structure, both mobile WiMAX and LTE OFDM signals exhibit CP-induced cyclostationarity. In particular, it is promising to incoporate the distinctive preamble-induced correlation of the mobile WiMAX OFDM-based signals and the distinctive RS-induced correlation of the LTE OFDM-based signals in a GLRT-based test statistics to improve the detection performance.

- OFDM can be used as a multiple access scheme allowing simultaneous frequency-separated transmissions to/from multiple mobile terminals using OFDMA (Orthogonal Frequency Division Multiple Access) technology. Among the mobile broadband wireless access standards, IEEE 802.20 is an efficient OFDMA-based air interface that is optimized for the transport of IP-based services to enable worldwide deployment of affordable multi-provider networks for full mobility up to vehicular speeds of 250 km/h [69]. In the scenario when the primary user employs OFDMA as the air interface, the cognitive radio network has to be able to carefully detect the idle portions of the licensed spectrum. The timing misalignment due to the mobility and multipath channels may deteriorate the synchronization and decoding of the received signals due to introduced inter-carrier interference (ICI) [70]. In order to implement a CR network with OFDMA-based primary signal the following issues need to be considered:

  (i) There is a need to develop and compare efficient spectrum sensing methods which are robust to the timing misalignment. The aim is to minimize the false and

missed detections probabilities.

(ii) A cooperative sensing mode is worthwhile to be developed for detecting OFDMA-based primary signals. In computing the test statistics at each CR, different subcarriers have to be allocated different weights to minimize the ICI effect in sensing. Since the CRs's sensing data is transmitted over fading channels, the performance reliability of each CR has to be taken into account in the final decision at the fusion center. The design of the weights at the CRs and fusion center can be carried out so that the total transmission rate of the CR network is maximized while the interference introduced to the primary users is maintained within an acceptable limit.

A. Appendices for Chapter 2

A.1 Proof of Equation (2.46)

For a fixed SNR and an i.i.d channel with $\mathrm{E}\{|h_i|^2\} = \sigma_h^2$, one has

$$\mathrm{SNR} = \mathrm{E}\left\{\frac{\sigma_S^2}{\sigma_v^2}\sum_{i=1}^{L_c}|h_i|^2\right\} = \frac{L_c\sigma_S^2\sigma_h^2}{\sigma_v^2} \tag{A.1}$$

First rewrite $\mathcal{N}_{\mathbf{h}}$ as

$$\mathcal{N}_{\mathbf{h}} = 2\sigma_S^2\left[\sum_{j=1}^{L_c-1}\sum_{i=1}^{j}|h_i|^2 + \sum_{j=L_c}^{L_p}\sum_{i=1}^{j}|h_i|^2\right]. \tag{A.2}$$

It can be easily seen that

$$\mathrm{E}\{\mathcal{N}_{\mathbf{h}}\} = 2\sigma_S^2\sigma_h^2\left[\frac{L_c(L_c-1)}{2} + (L_p - L_c)L_c\right] = 2\sigma_v^2\mathrm{SNR}\left[\frac{2L_p - L_c + 1}{2}\right], \tag{A.3}$$

and

$$\mathrm{E}\{\mathcal{D}_{\mathbf{h}}\} = \mathcal{D}_{\mathbf{h}} = 2L_p\sigma_v^2\left[\mathrm{SNR} + 1\right]. \tag{A.4}$$

Therefore

$$\mathcal{H}_1 : \tilde{\rho} = \mathrm{E}\{\tilde{\rho}_{\mathbf{h}}\} = \frac{\mathrm{E}\{\mathcal{N}_{\mathbf{h}}\}}{\mathcal{D}_{\mathbf{h}}} = \frac{\mathrm{SNR}}{1+\mathrm{SNR}}\left[\frac{2L_p - L_c + 1}{2L_p}\right]. \tag{A.5}$$

A.2 Developing the MPCC Test

First observe from (2.66) that

$$\left(\det(\widehat{\mathbf{R}}_{\ddot{\mathbf{x}}})\right)^{\frac{1}{L}} = \mathrm{e}^{\ln\left(\det(\widehat{\mathbf{R}}_{\ddot{\mathbf{x}}})^{\frac{1}{L}}\right)} \tag{A.6}$$

and

$$\ln\left(\det(\widehat{\mathbf{R}}_{\ddot{\mathbf{x}}})\right)^{\frac{1}{L}} = \frac{1}{L}\ln\left(\det(\widehat{\mathbf{R}}_{\ddot{\mathbf{x}}})\right) = \frac{1}{L}\sum_{k=1}^{L}\ln(\tilde{\lambda}_k), \tag{A.7}$$

where $\tilde{\lambda}_k$'s are the eigenvalues of $\widehat{\mathbf{R}}_{\ddot{\mathbf{x}}}$. From (2.51), one has

$$\tilde{\lambda}_k = \widehat{\gamma}_0 + \sum_{m=1}^{L_p-1}\mathrm{Re}\left(\widehat{\gamma}_m \mathrm{e}^{-\frac{j2\pi km}{L}}\right). \tag{A.8}$$

Hence,

$$\begin{aligned}\ln(\tilde{\lambda}_k) =& \ln\left(\widehat{\gamma}_0 + \sum_{m=1}^{L_p-1}\mathrm{Re}\left(\widehat{\gamma}_m \mathrm{e}^{\frac{j2\pi km}{L}}\right)\right) = \ln\left(\widehat{\gamma}_0\left(1 + \frac{\sum_{m=1}^{L_p-1}\mathrm{Re}\left(\widehat{\gamma}_m \mathrm{e}^{\frac{j2\pi km}{L}}\right)}{\widehat{\gamma}_0}\right)\right) \\ =& \ln(\widehat{\gamma}_0) + \ln\left(1 + \frac{\sum_{m=1}^{L_p-1}\mathrm{Re}\left(\widehat{\gamma}_m \mathrm{e}^{\frac{j2\pi km}{L}}\right)}{\widehat{\gamma}_0}\right).\end{aligned} \tag{A.9}$$

Since $\frac{\sum_{m=1}^{L_p-1}\mathrm{Re}\left(\widehat{\gamma}_m \mathrm{e}^{\frac{j2\pi km}{L}}\right)}{\widehat{\gamma}_0} \ll 1$ for low SNR values, the second term of (A.9) can be expanded by keeping the first two terms of the Taylor series. That is

$$\begin{aligned}&\ln\left(1 + \frac{\sum_{m=1}^{L_p-1}\mathrm{Re}\left(\widehat{\gamma}_m \mathrm{e}^{\frac{j2\pi km}{L}}\right)}{\widehat{\gamma}_0}\right) \\ &\approx \frac{\sum_{m=1}^{L_p-1}\mathrm{Re}\left(\widehat{\gamma}_m \mathrm{e}^{\frac{j2\pi km}{L}}\right)}{\widehat{\gamma}_0} - \frac{1}{2}\left(\frac{\sum_{m=1}^{L_p-1}\mathrm{Re}\left(\widehat{\gamma}_m \mathrm{e}^{\frac{j2\pi km}{L}}\right)}{\widehat{\gamma}_0}\right)^2.\end{aligned} \tag{A.10}$$

Therefore

$$\begin{aligned}&\frac{1}{L}\sum_{k=1}^{L}\ln(\tilde{\lambda}_k) \\ &\cong \ln\widehat{\gamma}_0 + \frac{1}{L}\sum_{k=1}^{L}\left[\frac{\sum_{m=1}^{L_p-1}\mathrm{Re}\left(\widehat{\gamma}_m \mathrm{e}^{-\frac{j2\pi km}{L}}\right)}{\widehat{\gamma}_0} - \frac{1}{2}\left(\frac{\sum_{m=1}^{L_p-1}\mathrm{Re}\left(\widehat{\gamma}_m \mathrm{e}^{-\frac{j2\pi km}{L}}\right)}{\widehat{\gamma}_0}\right)^2\right].\end{aligned} \tag{A.11}$$

The first term inside the square brackets of (A.11) can be simplified as follows:

$$\frac{\sum_{m=1}^{L_p-1}\sum_{k=1}^{L}\mathrm{Re}\left(\widehat{\gamma}_m \mathrm{e}^{-\frac{j2\pi km}{L}}\right)}{\widehat{\gamma}_0} = \frac{\sum_{m=1}^{L_p-1}\mathrm{Re}\left(\widehat{\gamma}_m \sum_{k=1}^{L}\mathrm{e}^{-\frac{j2\pi km}{L}}\right)}{\widehat{\gamma}_0} = 0. \tag{A.12}$$

And the second term can be rewritten as

$$
\begin{aligned}
&\sum_{k=1}^{L}\left(\frac{\sum_{m=1}^{L_p-1}\mathrm{Re}\left(\widehat{\gamma}_m \mathrm{e}^{-\frac{j2\pi km}{L}}\right)}{\widehat{\gamma}_0}\right)^2 \\
=&\sum_{k=1}^{L}\left(\frac{\sum_{m=1}^{L_p-1}\frac{1}{2}\left(\widehat{\gamma}_m \mathrm{e}^{-\frac{j2\pi km}{L}}+\widehat{\gamma}_m^* \mathrm{e}^{\frac{j2\pi km}{L}}\right)}{\widehat{\gamma}_0}\right)^2 \\
=&\sum_{k=1}^{L}\frac{\sum_{m=1}^{L_p-1}\sum_{q=1}^{L_p-1}\frac{1}{4}\left(\widehat{\gamma}_m\widehat{\gamma}_q \mathrm{e}^{-\frac{j2\pi (k+q)m}{L}}+\widehat{\gamma}_m^*\widehat{\gamma}_q^* \mathrm{e}^{\frac{j2\pi (k+q)m}{L}})\right)}{\widehat{\gamma}_0^2} \\
+&\sum_{k=1}^{L}\frac{\sum_{m=1}^{L_p-1}\sum_{q=1}^{L_p-1}\frac{1}{2}\mathrm{Re}(\widehat{\gamma}_m\widehat{\gamma}_q^* \mathrm{e}^{-\frac{j2\pi (k-q)m}{L}})}{\widehat{\gamma}_0^2} \\
=&\frac{\sum_{m=1}^{L_p-1}\sum_{q=1}^{L_p-1}\frac{1}{4}\sum_{k=1}^{L}\left(\widehat{\gamma}_m\widehat{\gamma}_q \mathrm{e}^{-\frac{j2\pi (k+q)m}{L}}+\widehat{\gamma}_m^*\widehat{\gamma}_q^* \mathrm{e}^{\frac{j2\pi (k+q)m}{L}}\right)}{\widehat{\gamma}_0^2} \\
+&\frac{\sum_{m=1}^{L_p-1}\sum_{q=1}^{L_p-1}\frac{1}{2}\mathrm{Re}(\widehat{\gamma}_m\widehat{\gamma}_q^*\sum_{k=1}^{L} \mathrm{e}^{-\frac{j2\pi (k-q)m}{L}})}{\widehat{\gamma}_0^2} \\
=&0+\frac{1}{4}\frac{\sum_{m=1}^{L_p-1}\|\widehat{\gamma}_m\|^2}{\widehat{\gamma}_0^2}=\frac{1}{4}\frac{\sum_{m=1}^{L_p-1}\|\widehat{\gamma}_m\|^2}{\widehat{\gamma}_0^2}.
\end{aligned}
\tag{A.13}
$$

Therefore, (A.11) can be approximated by

$$
\frac{1}{L}\sum_{k=1}^{L}\ln(\tilde{\lambda_k})\cong \ln\widehat{\gamma}_0-\frac{1}{4}\sum_{m=1}^{L_p-1}\frac{|\widehat{\gamma}_m|^2}{\widehat{\gamma}_0^2}. \tag{A.14}
$$

Consequently,

$$
\left(\det(\widehat{\mathbf{R}}_{\ddot{\mathbf{x}}})\right)^{\frac{1}{L}}\cong \widehat{\gamma}_0 \mathrm{e}^{-\frac{1}{4}\sum_{m=1}^{L_p-1}\frac{\|\widehat{\gamma}_m\|^2}{\widehat{\gamma}_0^2}}. \tag{A.15}
$$

By noting that $\frac{1}{L}\left(\mathrm{tr}(\widehat{\mathbf{R}}_{\ddot{\mathbf{x}}})\right)=\widehat{\gamma}_0$, the test statistics given in (2.66) can be closely approximated as

$$
\mathcal{T}_{\mathrm{G}}(\ddot{\mathbf{x}})=\frac{\frac{1}{L}\mathrm{tr}(\widehat{\mathbf{R}}_{\mathbf{x}})}{\det(\widehat{\mathbf{R}}_{\mathbf{x}})^{\frac{1}{L}}}\cong\frac{\widehat{\gamma}_0}{\widehat{\gamma}_0 \mathrm{e}^{-\frac{1}{4}\sum_{m=1}^{L_p-1}\frac{|\widehat{\gamma}_m|^2}{\widehat{\gamma}_0{}^2}}}=\mathrm{e}^{\frac{1}{4}\sum_{m=1}^{L_p-1}\frac{\|\widehat{\gamma}_m\|^2}{\widehat{\gamma}_0}}. \tag{A.16}
$$

Taking the logarithm of the above test yields the following equivalent test:

$$
\widetilde{\mathcal{T}}(\ddot{\mathbf{x}})=\frac{\sum_{m=1}^{L_p-1}\|\widehat{\gamma}_m\|^2}{\widehat{\gamma}_0^2}. \tag{A.17}
$$

The ratio $\widehat{\varrho}_m = \frac{\widehat{\gamma}_m}{\widehat{\gamma}_0}$ can be easily obtained from (2.56) and is given by

$$\widehat{\varrho}_m = \frac{\sum_{n=1}^{N} \sum_{i=0}^{L-1} x_n(i) x_n^* \left((i-m) \bmod L\right)}{\sum_{n=1}^{N} \sum_{i=0}^{L-1} |x_n(i)|^2}. \tag{A.18}$$

Recall that $\varrho_m = \frac{\mathrm{E}\{x_n(k)x_n^*(k-m)\}}{\mathrm{E}\{x_n(k)x_n^*(k)\}}$, $m = 0, \ldots, L_p - 1$, is the correlation coefficients between the ISI-free portions of OFDM block. On the other hand, $\widehat{\varrho}_m$ represents the sample correlation coefficient corresponding to a delay of m samples.

B. Appendices for Chapter 3

B.1 Proof of Proposition 1

First, from (3.47), λ is obtained to satisfy the target probability of detection $\bar{P}_D$ as:

$$\bar{\lambda} = \nu_1 Q^{-1}\left(\bar{P}_D\right) + \mu_1 \tag{B.1}$$

The choice of the above threshold toward maximizing the secondary throughput is justified by a similar argument as in [5]: When all other parameters are fixed, choosing $\lambda_1 < \bar{\lambda}$ gives $P_D(\boldsymbol{p_d}, \boldsymbol{w}, \lambda_1) > \bar{P}_D$ and also $P_F(\boldsymbol{p_d}, \boldsymbol{w}, \lambda_1) > P_F(\boldsymbol{p_d}, \boldsymbol{w}, \lambda)$, which results into a lower secondary throughput.

Replacing $\bar{\lambda}$ into problem (3.60) yields the following optimization problem:

$$\min_{\boldsymbol{\epsilon}, \boldsymbol{w}} \ \bar{P}_F(\tau, \boldsymbol{\epsilon}, \boldsymbol{w}). \tag{B.2}$$

From (3.46) and (B.1), one has:

$$\begin{aligned}
\bar{P}_F(\tau, \boldsymbol{\epsilon}, \boldsymbol{w}) =& Q\left(\frac{\nu_1 Q^{-1}(\bar{P}_D) + (\mu_1 - \mu_0)}{\nu_0}\right) \\
=& Q\left(\frac{\nu_1 Q^{-1}(\bar{P}_D) + \sum_{i=1}^{K} w_i \xi_i \left(p_{d_i} - p_{f_i}\right)}{\nu_0}\right) \\
=& Q\left(\phi(\tau, \boldsymbol{\epsilon}, \boldsymbol{w})\right).
\end{aligned} \tag{B.3}$$

where

$$\phi(\tau, \boldsymbol{\epsilon}, \boldsymbol{w}) = \frac{\nu_1 Q^{-1}(\bar{P}_D) + \sum_{i=1}^{K} w_i \xi_i \left(1 - (p_{m_i} + p_{f_i})\right)}{\nu_0}. \tag{B.4}$$

and $p_{m_i} = 1 - p_{d_i}$ represents the misdetection probability at the ith CR. Note also that $\vartheta_i = \frac{p_{m_i} + p_{f_i}}{2}$ is the overall probability of error for each CR. From (B.3), it is seen that $\bar{P}_F(\tau, \boldsymbol{\epsilon}, \boldsymbol{w})$ is minimized when the argument of the Q function, namely $\phi(\tau, \boldsymbol{\epsilon}, \boldsymbol{w})$ is maximized.

Since finding an exact solution for $\boldsymbol{\epsilon}$ in terms of other parameters to maximize $\phi(\tau, \boldsymbol{\epsilon}, \boldsymbol{w})$ appears intractable, in what follows, approximations are applied to obtain a closed-form solution for $\boldsymbol{\epsilon}$ that does not depend on the fading channels between CR nodes and FC. First, by taking the first derivative of $\phi(\tau, \boldsymbol{\epsilon}, \boldsymbol{w})$ with respect to ϵ_i, it is seen that the following expression has to set to zero to find ϵ_i:

$$\theta(\epsilon_i) = \left[-Q^{-1}(\bar{P}_D)\frac{\partial \nu_1}{\partial p_{d_i}}\frac{\partial p_{mi}}{\partial \epsilon_i} - 2w_i\xi_i\frac{\partial \vartheta_i}{\partial \epsilon_i}\right] - \phi(\tau, \boldsymbol{\epsilon}, \boldsymbol{w})\frac{\partial \nu_0}{\partial p_{f_i}}\frac{\partial p_{f_i}}{\partial \epsilon_i}. \tag{B.5}$$

where $\frac{\partial \nu_1}{\partial p_{d_i}} = \frac{w_i^2\left(\xi_i^2[1-p_{d_i}]+\xi_i\right)}{\nu_1} \ll w_i\xi_i$ for $K \gg 1$. Also from (B.3), it is seen that for a typical value of $\bar{P}_D \simeq 0.9$, $Q^{-1}(\bar{P}_D) \simeq -1.2$. Consequently the first term in the square brackets of (B.5) is negligible compared to the second term. As such (B.5) can be approximated as:

$$\theta(\epsilon_i) \simeq -2w_i\xi_i\frac{\partial \vartheta_i}{\partial \epsilon_i} - \phi(\tau, \boldsymbol{\epsilon}, \boldsymbol{w})\frac{\partial \nu_0}{\partial p_{f_i}}\frac{\partial p_{f_i}}{\partial \epsilon_i}. \tag{B.6}$$

Furthermore, the second term in (B.6) is also negligible when compared to the first term. This is because $-1 < \phi(\tau, \boldsymbol{\epsilon}, \boldsymbol{w}) < 1.5$ for $0.06 < \bar{P}_F < 0.8$ and $\frac{\partial \nu_0}{\partial p_{f_i}} = \frac{w_i^2\left(\xi_i^2[1-p_{f_i}]+\xi_i\right)}{\nu_0} \ll w_i\xi_i$ for $K \gg 1$. As such the first term is the significant part of (B.6) and ϵ_i is found by solving $\frac{\partial \vartheta_i}{\partial \epsilon_i} = 0$.

As it is verified in [50], the sensing threshold which minimizes ϑ_i at each CR node is given as:

$$\epsilon_i^* = \left(1 + \frac{1}{\gamma_i}\right)\log\left(\gamma_i + 1\right) \tag{B.7}$$

which is fixed and depends solely on the signal to noise ratio of the primary received signal at each CR node.

Remark 1: For BFSK, in a similar manner carried out for OOK, one has:

$$\dot{\bar{P}}_F(\tau, \boldsymbol{\epsilon}, \boldsymbol{w}) = Q\left(\frac{\dot{\nu}_1 Q^{-1}(\bar{P}_D) + (\dot{\mu}_1 - \dot{\mu}_0)}{\dot{\nu}_0}\right) = Q\left(\dot{\phi}(\tau, \boldsymbol{\epsilon}, \boldsymbol{w})\right) \tag{B.8}$$

where $\dot{\phi}(\tau, \boldsymbol{\epsilon}, \boldsymbol{w}) = \frac{\dot{\nu}_1 Q^{-1}(\bar{P}_D) + (\dot{\mu}_1 - \dot{\mu}_0)}{\dot{\nu}_0}$.

From (3.49) it is seen that $\dot{\nu}_0$ and $\dot{\nu}_1$ vary slightly with the changes in $\boldsymbol{p_f}$ and $\boldsymbol{p_d}$. In fact $\frac{\partial \dot{\nu}_1}{\partial p_{d_i}}\Big|_{p_{di}=0.5} = \frac{\partial \dot{\nu}_0}{\partial p_{f_i}}\Big|_{p_{f_i}=0.5} = 0$. On the other hand, for OOK, $\frac{\partial \nu_1}{\partial p_{d_i}}\Big|_{p_{di}=0.5} = \frac{\partial \nu_0}{\partial p_{f_i}}\Big|_{p_{f_i}=0.5} \approx \frac{1}{2}\frac{w_i^2\xi_i^2}{\nu_1}$. Also from (3.48) it is seen that for BFSK, $\dot{\mu}_1 - \dot{\mu}_0 = 2\sum_{i=1}^{K} \dot{w}_i\dot{\xi}_i\left(p_{d_i} - p_{f_i}\right)$, while

for OOK $\mu_1 - \mu_0 = \sum_{i=1}^{K} w_i \xi_i \left(p_{di} - p_{f_i}\right)$. Hence for the same received SNR at FC, one has $\dot{\mu}_1 - \dot{\mu}_0 = \mu_1 - \mu_0$. These observations suggest that the variation in $\dot{\phi}(\tau, \boldsymbol{\epsilon}, \boldsymbol{w})$ is mostly due to the variation in the term $\dot{\mu}_1 - \dot{\mu}_0 = 4\sum_{i=1}^{K} \dot{w}_i \dot{\xi}_i \left(p_{di} - p_{f_i}\right)$. As such the value ϵ_i^* obtained by maximizing ϑ_i will be a closer to the optimal ϵ_i for BFSK than for OOK.

From the previous discussion it is seen that ν_1 and ν_0 in (B.3) demonstrate only small variations in terms of p_{di} and p_{f_i} when compared to the term $\sum_{i=1}^{K} w_i \xi_i \left(p_{di} - p_{f_i}\right)$. Therefore, to optimize $\boldsymbol{w}$, the following problem can be solved:

$$\max_{\boldsymbol{w}} \frac{\boldsymbol{w}^T \boldsymbol{q}}{\nu_0} \equiv \max_{\boldsymbol{w}} \frac{\left(\boldsymbol{w}^T \boldsymbol{q}\right)^2}{\boldsymbol{w} \boldsymbol{\Phi} \boldsymbol{w}^T} \tag{B.9}$$

where $\boldsymbol{w} = [w_1, \ldots, w_K]^T$, $\boldsymbol{q} = \left[\xi_1 \left(p_{d1} - p_{f_1}\right), \ldots, \xi_K \left(p_{dK} - p_{f_K}\right)\right]^T$, $\boldsymbol{\Phi} = \text{diag}\left(\nu_{1,0}^2, \ldots, \nu_{K,0}^2\right)$. Using the Rayleigh-Ritz theorem [71], the solution to (B.9) is given as:

$$\boldsymbol{w} = c\boldsymbol{\Phi}^{-1/2}\boldsymbol{q}. \tag{B.10}$$

where c is a scalar constant. Without loss of generality c can be set to 1 and w_i's are obtained as:

$$w_i(\tau, \boldsymbol{\epsilon}) = \frac{\xi_i \left(p_{di} - p_{f_i}\right)}{\nu_{i,0}}. \tag{B.11}$$

Substituting $\overline{p}_{f_i}(\tau) = p_{f_i}(\tau, \epsilon^*)$ and $\overline{p}_{di}(\tau) = p_{di}(\tau, \epsilon^*)$ in the above yields $w_i^*(\tau) = w_i(\tau, \boldsymbol{\epsilon}^*)$ and the proof is completed. □

B.2 Proof of Proposition 2

We need to show that $\frac{\partial^2 \bar{R}_0(\tau)}{\partial \tau^2} < 0$. First, one has:

$$\frac{\partial \bar{R}_0(\tau)}{\partial \tau} = -C_0 \left(1 - \bar{P}_F(\tau) + (T - \tau)\frac{\partial \bar{P}_F(\tau)}{\partial \tau}\right), \tag{B.12}$$

$$\frac{\partial^2 \bar{R}_0(\tau)}{\partial \tau^2} = C_0 \left(2\frac{\partial \bar{P}_F(\tau)}{\partial \tau} - T\frac{\partial^2 \bar{P}_F(\tau)}{\partial \tau^2}\right). \tag{B.13}$$

It follows from (3.62), (3.63) and (3.71) that

$$\bar{P}_F(\tau) = Q\left(\underbrace{\frac{Q^{-1}(\bar{P}_D)\bar{\nu}_1(\tau) + \sum_{i=1}^{K} \frac{\xi_i}{\bar{\nu}_0(\tau)} \left(\overline{p}_{di}(\tau) - \overline{p}_{f_i}(\tau)\right)^2}{\bar{\nu}_0(\tau)}}_{\bar{\phi}(\tau)}\right). \tag{B.14}$$

Next, one obtains $\frac{\partial \bar{P}_F(\tau)}{\partial \tau}$ as follows:

$$\frac{\partial \bar{P}_F(\tau)}{\partial \tau} = -\frac{1}{\sqrt{2\pi}\exp\left(-\bar{\phi}(\tau)^2/2\right)\frac{\partial \bar{\phi}(\tau)}{\partial \tau}}$$

$$= -\frac{1}{\sqrt{2\pi}\bar{\nu}_0(\tau)}\exp\left(-\bar{\phi}(\tau)^2/2\right) \times \Bigg[\underbrace{-Q^{-1}(\bar{P}_D)\sum_{i=1}^{K}\left(\frac{\partial \bar{\nu}_1(\tau)}{\partial \overline{p}_{d_i}(\tau)}\frac{\partial \overline{p}_{d_i}(\tau)}{\partial \tau}\right)}_{t(\tau)}$$

$$\underbrace{-\sum_{i=1}^{K}\xi_i\left(\frac{2}{\bar{\nu}_{i,0}(\tau)}\left(\overline{p}_{d_i}(\tau)-\overline{p}_{f_i}(\tau)\right)\left(\frac{\partial \overline{p}_{d_i}(\tau)}{\partial \tau}-\frac{\partial \overline{p}_{f_i}(\tau)}{\partial \tau}\right)-\frac{\left(\overline{p}_{d_i}(\tau)-\overline{p}_{f_i}(\tau)\right)^2}{\bar{\nu}_{i,0}(\tau)^2}\frac{\partial \bar{\nu}_{i,0}(\tau)}{\partial \overline{p}_{f_i}(\tau)}\frac{\partial \overline{p}_{f_i}(\tau)}{\partial \tau}\right)}_{u(\tau)}$$

$$\underbrace{-\bar{\phi}(\tau)\sum_{i=1}^{K}\frac{\partial \bar{\nu}_0(\tau)}{\partial \overline{p}_{f_i}(\tau)}\frac{\partial \overline{p}_{f_i}(\tau)}{\partial \tau}}_{v(\tau)}\Bigg]. \tag{B.15}$$

From (3.10) and (3.11), one has:

$$\frac{\partial \overline{p}_{f_i}(\tau)}{\partial \tau} = -\frac{\alpha_i\sqrt{f_s}}{2\sqrt{2\tau\pi}}\exp\left(-\alpha_i^2\tau f_s/2\right) \tag{B.16}$$

and

$$\frac{\partial \overline{p}_{d_i}(\tau)}{\partial \tau} = -\frac{\beta_i\sqrt{f_s}}{2\sqrt{2\tau\pi}}\exp\left(-\beta_i^2\tau f_s/2\right) \tag{B.17}$$

where $\alpha_i = (1+\frac{1}{\gamma_i})\log(1+\gamma_i)-1 > 0$ and $\beta_i = \frac{1}{\gamma_i}\log(1+\gamma_i)-1 < 0$. Therefore, $\frac{\partial \overline{p}_{f_i}(\tau)}{\partial \tau} < 0$, $\frac{\partial \overline{p}_{d_i}(\tau)}{\partial \tau} > 0$. Moreover, $\frac{\partial \bar{\nu}_0(\tau)}{\partial \overline{p}_{f_i}(\tau)} > 0$, $\frac{\partial \bar{\nu}_1(\tau)}{\partial \overline{p}_{d_i}(\tau)} > 0$ and $\frac{\partial \bar{\nu}_{i,0}(\tau)}{\partial \overline{p}_{f_i}(\tau)} > 0$. Also, for $\bar{P}_F(\tau) \leq 0.5$, $\bar{\phi}(\tau) > 0$. Thus it can be seen from (B.15) that $\frac{\partial \bar{\phi}(\tau)}{\partial \tau} > 0$ which proves that that $\frac{\partial \bar{P}_F(\tau)}{\partial \tau} < 0$.

Next, consider:

$$\frac{\partial^2 \bar{P}_F(\tau)}{\partial \tau^2} = -\frac{1}{\sqrt{2\pi}}\exp\left(-\bar{\phi}(\tau)^2/2\right)\left(-\bar{\phi}(\tau)\left(\frac{\partial \bar{\phi}(\tau)}{\partial \tau}\right)^2+\frac{\partial^2 \bar{\phi}(\tau)}{\partial \tau^2}\right) \tag{B.18}$$

It follows from (B.16) and (B.17) that:

$$\frac{\partial^2 \overline{p}_{f_i}(\tau)}{\partial \tau^2} = \frac{\beta_i^3 f_s\sqrt{f_s}}{4\sqrt{2\tau\pi}}\exp\left(-\beta_i^2\tau f_s/2\right)+\frac{\beta_i\sqrt{f_s}}{4\tau\sqrt{2\tau\pi}}\exp\left(-\beta_i^2\tau f_s/2\right) < 0 \tag{B.19}$$

$$\frac{\partial^2 \overline{p}_{d_i}(\tau)}{\partial \tau^2} = -\frac{\alpha_i^3 f_s\sqrt{f_s}}{4\sqrt{2\tau\pi}}\exp\left(-\alpha_i^2\tau f_s/2\right)-\frac{\alpha_i\sqrt{f_s}}{4\tau\sqrt{2\tau\pi}}\exp\left(-\alpha_i^2\tau f_s/2\right) > 0 \tag{B.20}$$

Using the above along with (B.16) and (B.17), it can be easily seen from (B.15) that $\frac{\partial^2\bar{\phi}(\tau)}{\partial\tau^2} = \frac{\partial(t(\tau)+v(\tau)+u(\tau))}{\partial\tau} < 0$. Clearly for $\bar{P}_F(\tau) \leq 0.5$, $\bar{\phi}(\tau) > 0$, so in (B.18) the term $\left(-\bar{\phi}(\tau)\left(\frac{\partial\bar{\phi}(\tau)}{\partial\tau}\right)^2 + \frac{\partial^2\bar{\phi}(\tau)}{\partial\tau^2}\right) < 0$ and $\frac{\partial^2\bar{P}_F(\tau)}{\partial\tau^2} > 0$. Combining the results of $\frac{\partial\bar{P}_F(\tau)}{\partial\tau} < 0$ and $\frac{\partial^2\bar{P}_F(\tau)}{\partial\tau^2} > 0$ in (B.13) leads to $\frac{\partial^2\bar{R}_0(\tau)}{\partial\tau^2} < 0$ and the proof is concluded. □

B.3 Obtaining Sensing Thresholds

First, $\lambda^{(\mathrm{D})}$ is obtained from (4.28) to satisfy the target probability of detection $\bar{P}_D$ as:

$$\bar{\lambda}^{(\mathrm{D})} = \delta_1 Q^{-1}\left(\bar{P}_D\right) + m_1. \tag{B.21}$$

Then from (4.28) and (B.21), one has:

$$\bar{P}_F(\tau,\boldsymbol{\epsilon}) = Q\left(\frac{\delta_1 Q^{-1}(\bar{P}_D) + (m_1 - m_0)}{\delta_0}\right) = Q\left(\phi^{(\mathrm{D})}(\tau,\boldsymbol{\epsilon})\right), \tag{B.22}$$

where

$$\phi^{(\mathrm{D})}(\tau,\boldsymbol{\epsilon}) = \frac{\delta_1 Q^{-1}(\bar{P}_D) + \sum_{i=1}^{K}\left[\left(p_{d_i} - p_{f_i}\right)\left(\varpi_i - \vartheta_i\right)\left(\varphi_{1,i} - \varphi_{0,i}\right)\right]}{\delta_0}. \tag{B.23}$$

By taking the first derivative of $\phi^{(\mathrm{D})}(\tau,\boldsymbol{\epsilon})$ with respect to ϵ_i, it is seen that the following expression has to set to zero to find ϵ_i:

$$\begin{aligned}\theta^{(\mathrm{D})}(\epsilon_i) = \Bigg[& Q^{-1}(\bar{P}_D)\frac{\partial\delta_1}{\epsilon_i} + \frac{\partial\left(p_{d_i} - p_{f_i}\right)}{\partial\epsilon_i}\left(\varpi_i - \vartheta_i\right)\left(\varphi_{1,i} - \varphi_{0,i}\right) \\ & + \left(p_{d_i} - p_{f_i}\right)\left(\varpi_i - \vartheta_i\right)\frac{\partial\left(\varphi_{1,i} - \varphi_{0,i}\right)}{\partial\epsilon_i}\Bigg] - \phi^{(\mathrm{D})}(\tau,\boldsymbol{\epsilon})\frac{\partial\delta_0}{\partial\epsilon_i}.\end{aligned} \tag{B.24}$$

Since $\frac{\partial\delta_1}{\partial\epsilon_i} = \frac{\delta_{i,1}}{\delta_1}\frac{\partial\delta_{i,1}}{\partial\epsilon_i} \ll 1$, $\theta^{(\mathrm{D})}(\epsilon_i)$ can be well approximated as:

$$\theta^{(\mathrm{D})}(\epsilon_i) \simeq \frac{\partial\left(p_{d_i} - p_{f_i}\right)}{\partial\epsilon_i}\left(\varpi_i - \vartheta_i\right)\left(\varphi_{1,i} - \varphi_{0,i}\right) + \left(p_{d_i} - p_{f_i}\right)\left(\varpi_i - \vartheta_i\right)\frac{\partial\left(\varphi_{1,i} - \varphi_{0,i}\right)}{\partial\epsilon_i}. \tag{B.25}$$

where

$$\frac{\partial\left(\varphi_{1,i} - \varphi_{0,i}\right)}{\partial\epsilon_i} = \left(\varpi_i - \vartheta_i\right) \times \left[\frac{1}{\wp_{d_i}(1-\wp_{d_i})}\frac{\partial p_{d_i}}{\partial\epsilon_i} - \frac{1}{\wp_{f_i}(1-\wp_{f_i})}\frac{\partial p_{f_i}}{\partial\epsilon_i}\right]. \tag{B.26}$$

On the other hand, from (4.27) and (4.28), one has:

$$\wp_{d_i} - \wp_{f_i} = (\varpi_i - \vartheta_i)\left(p_{d_i} - p_{f_i}\right). \tag{B.27}$$

If the reporting link to FC is good enough, i.e., $\varpi_i \to 1$ and $\vartheta_i \to 0$, (e.g., $\varpi_i = 0.9$, $\vartheta_i = 0.1$) then $\wp_{d_i} \simeq p_{d_i}$ and $\wp_{f_i} \simeq p_{f_i}$. Now assume that $\epsilon_i = \epsilon_i^*$ which is a solution to $\frac{\partial\left(p_{d_i} - p_{f_i}\right)}{\partial \epsilon_i} = 0$. Since $p_{d_i} + p_{f_i} \simeq 1$ for $\epsilon_i = \epsilon_i^*$, it is then concluded that $\wp_{f_i}(1 - \wp_{f_i}) \simeq \wp_{d_i}(1 - \wp_{d_i})$. So $\epsilon_i = \epsilon_i^*$ is also the solution to $\frac{\partial(\varphi_{1,i} - \varphi_{0,i})}{\partial \epsilon_i} = 0$ and $\theta^{(\mathrm{D})}(\epsilon_i^*) = 0$.

If on the other hand, ϖ_i and ϑ_i are far from 1 and 0 respectively, $(\varpi_i - \vartheta_i) < 1$. Also $\left(p_{d_i} - p_{f_i}\right) < 1$, therefore $\wp_{f_i}(1 - \wp_{f_i}) - \wp_{d_i}(1 - \wp_{d_i}) = (\varpi_i - \vartheta_i)(p_{d_i} - p_{f_i})(2\wp_{d_i} - 1) \simeq 0$ and again ϵ_i^* will be a close solution to $\frac{\partial(\varphi_{1,i} - \varphi_{0,i})}{\partial \epsilon_i} = 0$ and consequently $\theta^{(\mathrm{D})}(\epsilon_i^*) = 0$.

The above analysis implies that

$$\epsilon_i^{(\mathrm{D})*} = \epsilon_i^* \simeq \arg\max \phi^{(\mathrm{D})}(\tau, \boldsymbol{\epsilon}), \tag{B.28}$$

which completes the proof. □

References

[1] J. Ma, G. Y. Li, and B. H. Juang, "Signal processing in cognitive radio," *Proc. IEEE*, vol. 97, pp. 805–823, May 2009.

[2] Federal Communications Commision, "Spectrum policy task force report," ET Docket No. 02-135, Nov. 2002.

[3] H. Kim and K. G. Shin, "In-band spectrum sensing in cognitive radio networks: Energy detection or feature detection," in *MobiCom08*, pp. 14–25, Sep. 2008.

[4] H. Mu and J. Tugnait, "Joint soft-decision cooperative spectrum sensing and power control in multiband cognitive radios," *IEEE Trans. Signal Process.*, vol. 60, no. 10, pp. 5334–5346, 2012.

[5] Y. C. Liang, Y. Zeng, E. C. Peh, and A. T. Hoang, "Sensing-throughput tradeoff for cognitive radio networks," *IEEE Trans. Wireless Commun.*, vol. 7, pp. 1326–1337, April 2008.

[6] S. Almalfouh and G. Stuber, "Joint spectrum-sensing design and power control in cognitive radio networks: A stochastic approach," *IEEE Trans. Wireless Commun.*, vol. 11, no. 12, pp. 4372–4380, 2012.

[7] L. Luo and S. Roy, "Efficient spectrum sensing for cognitive radio networks via joint optimization of sensing threshold and duration," *IEEE Trans. Commun.*, vol. 60, no. 10, pp. 2851–2860, 2012.

[8] S. M. Kay, *Fundamentals of Statistical Signal Processing: Detection Theory.* Prentice Hall, 1998.

[9] H. V. Poor, *An introduction to signal detection and estimation.* New York: Springer, 1994.

[10] S. Stotas and A. Nallanathan, "On the throughput and spectrum sensing enhancement of opportunistic spectrum access cognitive radio networks," *IEEE Trans. Wireless Commun.*, vol. 11, no. 1, pp. 97–107, 2012.

[11] W. Han, J. Li, Z. Li, J. Si, and Y. Zhang, "Efficient soft decision fusion rule in cooperative spectrum sensing," *sig*, vol. 61, no. 8, pp. 1931–1943, 2013.

[12] W. Yin, P. Ren, Q. Du, and Y. Wang, "Delay and throughput oriented continuous spectrum sensing schemes in cognitive radio networks," *IEEE Trans. Wireless Commun.*, vol. 11, no. 6, pp. 2148–2159, 2012.

[13] R. Tandra and A. Sahai, "SNR walls for signal detection," *IEEE J. Select. Topics in Signal Process.*, vol. 2, pp. 4–17, Feb. 2008.

[14] Y. Zeng, C. L. Koh, and Y. C. Liang, "Maximum eigenvalue detection: Theory and application," in *Proc. IEEE Int. Conf. Commun.*, pp. 4160–4164, May 2008.

[15] Y. Zeng and Y. C. Liang, "Eigenvalue-based spectrum sensing algorithms for cognitive radio," *IEEE Trans. Commun.*, vol. 57, pp. 1784–1793, June 2009.

[16] F. Penna, R. Garello, and M. A. Spirito, "Cooperative spectrum sensing based on the limiting eigenvalue ratio distribution in Wishart matrices," *IEEE Commun. Letters*, vol. 13, pp. 507–509, July 2009.

[17] Y. Zeng and Y. C. Liang, "Spectrum-sensing algorithms for cognitive radio based on statistical covariances," *IEEE Trans. Veh. Technol.*, vol. 58, pp. 1804–1815, May 2009.

[18] Z. Quan, S. Cui, A. H. Sayed, and H. V. Poor, "Optimal multiband joint detection for spectrum sensing in cognitive radio networks," *IEEE Trans. Signal Process.*, vol. 57, pp. 1128–1140, May 2009.

[19] Z. Quan, S. Cui, and A. H. Sayed, "Optimal linear cooperation for spectrum sensing in cognitive radio networks," *IEEE J. Select. Topics in Signal Process.*, vol. 2, pp. 28–40, Feb. 2008.

[20] Y. Pei, Y. C. Liang, K. C. Teh, and K. H. Li, "How much time is needed for wideband spectrum sensing," *IEEE Trans. Wireless Commun.*, vol. 8, pp. 5466–5471, Nov. 2009.

[21] F. Digham, M. S. Alouini, and M. K. Simon, "On the energy detection of unknown signals over fading channels," *IEEE Trans. Commun.*, vol. 55, pp. 21–24, Jan. 2007.

[22] S. Zhang, T. Wu, and V. K. N. Lau, "A low-overhead energy detection based cooperative sensing protocol for cognitive radio systems," *IEEE Trans. Wireless Commun.*, vol. 8, pp. 5575 – 5581, Nov. 2009.

[23] S. S. Jeong, W. S. Jeon, and D. G. Jeong, "Collaborative spectrum sensing for multiuser cognitive radio systems," *IEEE Trans. Veh. Technol.*, vol. 58, pp. 2564 – 2569, June 2009.

[24] M. Barkat, *Signal Detection and Estimation.* Artech House, 1991.

[25] T. J. Lim, R. Zhang, Y. C. Liang, and Y. Zeng, "GLRT-based spectrum sensing for cognitive radio," in *Proc. IEEE Global Telecommun. Conf.*, pp. 1–5, Nov. 2008.

[26] S. Chaudhari, V. Koivunen, and H. V. Poor, "Autocorrelation-based decentralized sequential detection of OFDM signals in cognitive radios," *IEEE Trans. Signal Process.*, vol. 57, pp. 2690–2700, July 2009.

[27] H. A. Mahmoud, T. Yucek, and H. Arslan, "OFDM for cognitive radio: Merits and challenges," *IEEE Wireless Communications Magazine*, vol. 16, pp. 6–15, April 2009.

[28] H. G. Myung, J. Lim, and D. J. Goodman, "Single carrier FDMA for uplink wireless transmission," *IEEE Vehicular Technology Magazine*, vol. 1, pp. 30–38, Sep. 2006.

[29] T. Hwang, C. Yang, G. Wu, S. Li, and G. Y. Li, "OFDM and its wireless applications: A survey," *IEEE Trans. Veh. Technol.*, vol. 58, pp. 1673 –1694, May 2009.

[30] A. Taherpour, S. Gazor, and M. Nasiri-Kenari, "Invariant wideband spectrum sensing under unknown variances," *IEEE Trans. Wireless Commun.*, vol. 8, pp. 2182–2186, May 2009.

[31] S. Bokharaiee, H. Nguyen, and E. Shwedyk, "Blind spectrum sensing for ofdm-based cognitive radio systems," *Vehicular Technology, IEEE Transactions on*, vol. 60, pp. 858 –871, march 2011.

[32] R. Zhang, T. J. Lim, Y. C. Liang, and Y. Zeng, "Multi-antenna based spectrum sensing for cognitive radios: A GLRT approach," *IEEE Trans. Commun.*, vol. 58, pp. 84–88, Jan. 2010.

[33] A. Taherpour, M. Nasiri-Kenari, and S. Gazor, "Multiple antenna spectrum sensing in cognitive radios," *IEEE Trans. Wireless Commun.*, vol. 9, pp. 814–823, Feb. 2010.

[34] K. Umebayashi, J. Lehtomaki, T. Yazawa, and Y. Suzuki, "Efficient decision fusion for cooperative spectrum sensing based on or-rule," *IEEE Trans. Wireless Commun.*, vol. 11, no. 7, pp. 2585–2595, 2012.

[35] A. Noel and R. Schober, "Convex sensing-reporting optimization for cooperative spectrum sensing," *Wireless Communications, IEEE Transactions on*, vol. 11, no. 5, pp. 1900–1910, 2012.

[36] L. Khalid and A. Anpalagan, "Cooperative sensing with correlated local decisions in cognitive radio networks," *IEEE Trans. Veh. Technol.*, vol. 61, no. 2, pp. 843–849, 2012.

[37] S. Yiu and R. Schober, "Nonorthogonal transmission and noncoherent fusion of censored decisions," *IEEE Trans. Veh. Technol.*, Jan. 2009.

[38] E. Peh, Y.-C. Liang, Y. L. Guan, and Y. Zeng, "Cooperative spectrum sensing in cognitive radio networks with weighted decision fusion schemes," *IEEE Trans. Wireless Commun.*, vol. 9, pp. 3838 –3847, Dec. 2010.

[39] S. Bokharaiee, H. Nguyen, and E. Shwedyk, "Cooperative spectrum sensing in cognitive radio networks with noncoherent transmission," *IEEE Trans. Veh. Technol.*, vol. 61, pp. 2476 – 2489, March 2012.

[40] C.-H. Hwang, G.-L. Lai, and S.-C. Chen, "Spectrum sensing in wideband OFDM cognitive radios," *IEEE Signal Process. Letters*, vol. 58, pp. 709–719, Feb. 2010.

[41] S. Kim, J. Lee, H. Wang, and D. Hong, "Sensing performance of energy detector with correlated multiple antennas," *IEEE Signal Process. Letters*, vol. 16, pp. 671 – 674, Aug. 2009.

[42] J. Lunden, V. Koivunen, A. Huttunen, and H. V. Poor, "Spectrum sensing in cognitive radios based on multiple cyclic frequencies," in *Cognitive Radio Oriented Wireless Networks and Communications*, pp. 37–43, Aug. 2007.

[43] O. Bolkhovskaya and A. Maltsev, "The performance of the GLRT for the spatial signals detection with a small number of observations," *IEEE Signal Process. Letters*, vol. 11, pp. 841–844, Oct. 2004.

[44] M. Novey, T. Adal, and A. Roy, "Circularity and Gaussianity detection using the complex generalized Gaussian distribution," *IEEE Signal Process. Letters*, vol. 16, pp. 993–996, Nov. 2009.

[45] J.-J. van de Beek, M. Sandell, and P. O. Borjesson, "ML estimation of time and frequency offset in ofdm systems," *IEEE Trans. Signal Process.*, vol. 45, pp. 1800 – 1805, July 1997.

[46] J. P. Burg, D. G. Luenberger, and D. L. Wegner, "Estimation of structured covariance matrices," *Proc. IEEE*, vol. 70, pp. 963–974, Sep. 1988.

[47] W. Zeng and G. Bi, "Exploiting the multi-path diversity and multi-user cooperation to detect OFDM signals for cognitive radio in low SNR with noise uncertainty," in *Proc. IEEE Global Telecommun. Conf.*, pp. 1–6, Dec. 2009.

[48] W. Zeng and G. Bi, "Robust detection of OFDM signals for cognitive UWB in low SNR with noise uncertainty," in *Proc. IEEE Int. Symp. Personal, Indoor and Mobile Radio Commun.*, pp. 1–5, Sep. 2008.

[49] D. Tse and P. Viswanath, *Fundamentals of Wireless Communication*. Cambridge University Press, 2005.

[50] D. Duan, L. Yang, and J. C. Principe, "Cooperative diversity of spectrum sensing for cognitive radio systems," *IEEE Trans. Signal Process.*, vol. 58, pp. 3218 –3227, June 2010.

[51] S. Atapattu, C. Tellambura, and H. Jiang, "Energy detection based cooperative spectrum sensing in cognitive radio networks," *Wireless Communications, IEEE Transactions on*, vol. 10, pp. 1232 –1241, April 2011.

[52] W. Han, J. Li, Z. Tian, and Y. Zhang, "Efficient cooperative spectrum sensing with minimum overhead in cognitive radio," *IEEE Trans. Wireless Commun.*, vol. 9, pp. 3006 –3011, Oct. 2010.

[53] Y. Zheng, X. Xie, and L. Yang, "Cooperative spectrum sensing based on SNR comparison in fusion center for cognitive radio," in *International Conference on Advanced Computer Control*, pp. 212 –216, Jan. 2009.

[54] D. Cabric, S. M. Mishra, and R. W. Brodersen, "Implementation issues in spectrum sensing for cognitive radios," in *Thirty-Eighth Asilomar Conference on Signals, Systems and Computers*, pp. 772 – 776, Nov. 2004.

[55] P. Kaligineedi and V. K. Bhargava, "Sensor allocation and quantization schemes for multi-band cognitive radio cooperative sensing system," *IEEE Trans. Wireless Commun.*, vol. 10, pp. 284 –293, Jan. 2011.

[56] S. Appadwedula, V. Veeravalli, and D. Jones, "Decentralized detection with censoring sensors," *IEEE Trans. Signal Process.*, vol. 56, pp. 1362 –1373, April 2008.

[57] Z. Quan, S. Cui, and A. Sayed, "Optimal linear cooperation for spectrum sensing in cognitive radio networks," *IEEE J. Select. Topics in Signal Process.*, vol. 2, pp. 28 –40, Feb. 2008.

[58] W. Zhang, R. Mallik, and K. Letaief, "Optimization of cooperative spectrum sensing with energy detection in cognitive radio networks," *IEEE Trans. Wireless Commun.*, vol. 8, pp. 5761 –5766, Dec. 2009.

[59] R. Jiang and B. Chen, "Fusion of censored decisions in wireless sensor networks," *IEEE Trans. Wireless Commun.*, vol. 4, pp. 2668 – 2673, Nov. 2005.

[60] H. Urkwitz, "Energy detection of unknown deterministic signals," in *Proc. IEEE*, pp. 523–531, April 1967.

[61] C. Shannon, "Communication in the presence of noise," *Proceedings of the IEEE*, vol. 72, pp. 1192 – 1201, Sept. 1984.

[62] H. H. Nguyen and E. Shwedyk, *A First Course in Digital Communications*. Cambridge University Press, 2009.

[63] E. C. Y. Peh, Y.-C. Liang, Y. L. Guan, and Y. Zeng, "Optimization of cooperative sensing in cognitive radio networks: A sensing-throughput tradeoff view," *IEEE Trans. Veh. Technol.*, vol. 58, pp. 5294 –5299, Nov. 2009.

[64] T. Al-Naffouri and B. Hassibi, "On the distribution of indefinite quadratic forms in gaussian random variables," in *IEEE International Symposium on Information Theory*, pp. 1744 –1748, July 2009.

[65] H. H. N. Simin Bokharaiee and E. Shwedyk, "A decoding-based fusion rule for cooperative spectrum sensing with nonorthogonal transmission of local decisions," *EURASIP Journal on Wireless Communications and Networking*, vol. 2013:184 (8 July 2013).

[66] H. Nguyen and E. Shwedyk, "Bandwidth-constrained signature waveforms and Walsh signal space receivers for synchronous CDMA systems," *IEEE Trans. Commun.*, vol. 50, pp. 1137 – 1149, Jul. 2002.

[67] L. Welch, "Lower bounds on the maximum cross correlation of signals," *IEEE Trans. Inform. Theory*, vol. 20, pp. 397–399, May 1974.

[68] P. Viswanath, V. Anantharam, and D. Tse, "Optimal sequences, power control, and user capacity of synchronous CDMA systems with linear MMSE multiuser receivers," *IEEE Trans. Inform. Theory*, vol. 45, pp. 1968 –1983, Sep. 1999.

[69] W. Bolton, Y. Xiao, and M. Guizani, "IEEE 802.20: mobile broadband wireless access," *Wireless Communications, IEEE*, vol. 14, no. 1, pp. 84–95, 2007.

[70] M. E. Sahin, I. Guvenc, and H. Arslan, "Opportunity detection for OFDMA-based cognitive radio systems with timing misalignment," *IEEE Trans. Wireless Commun.*, vol. 8, pp. 5300–5313, Oct. 2009.

[71] R. A. Horn and C. Johnson, *Matrix Analysis*. Cambridge University Press, 1985.